Department of Geomatics Engineering

Development of New Filter and Tracking Schemes for Weak GPS Signal Tracking

(URL: http://www.geomatics.ucalgary.ca/graduatetheses)

by

Pejman Lotfali Kazemi

May 2010

SCHULICH
School of Engineering   UNIVERSITY OF CALGARY

UNIVERSITY OF CALGARY

Development of New Filter and Tracking Schemes for Weak GPS Signal Tracking

by

Pejman Lotfali Kazemi

A THESIS

SUBMITTED TO THE FACULTY OF GRADUATE STUDIES

IN PARTIAL FULFILMENT OF THE REQUIREMENTS FOR THE

DEGREE OF DOCTOR OF PHILOSOPHY

DEPARTMENT OF GEOMATICS ENGINEERING

CALGARY, ALBERTA

May, 2010

Abstract

Various emerging applications require location of users in challenging environments where typical GPS receivers suffer degraded performance or complete failure. Special algorithms and techniques are required to track weak GPS signals, where the signal is typically weaker by 10 to 40 dB compared to the nominal or line-of-sight signal strength. This thesis endeavours to propose solutions that can potentially offer performance improvements over conventional techniques.

Optimum digital tracking filters for loops of first to fourth order, for rate only and phase and rate feedback NCO are derived. It is shown that, contrary to conventional methods, the loops remain stable for high B_LT (the product of loop noise bandwidth and loop update interval) values and for both types of aforementioned NCOs. By using these filters, a significant improvement for high B_LT can be achieved, allowing one to operate in ranges where previous methods cannot operate. As a result, stable loops with longer integration times (update interval) can be easily designed and the tracking sensitivity is improved accordingly.

For the cases when external data aiding is not available, a decision feedback principle is used herein, in which the data bits are estimated through the tracking process itself. An enhanced digital phase locked loop with a frequency rate estimator is also developed. The NCO with phase rate and frequency rate feedback is introduced and based on this NCO and the transfer function of the frequency rate estimator, the tracking loop is optimized in order to minimize the phase noise variance. By utilizing this loop, the performance of low update rate loops in terms of phase mismatch and bit error rate can be improved. A

multistage tracking scheme is also implemented to overcome the problem of tracking weak GPS signals in indoor environments. In this technique several tracking schemes are serially cascaded. It is shown that this technique combined with a developed optimum delay locked loop can be used for seamless outdoor to indoor tracking.

The performance and advantages of these techniques are shown based on a developed software GPS signal simulator, hardware simulated signals, live attenuated GPS signals and live GPS signals in selected indoor environments. The tracking capabilities of these schemes are also compared with a commercially available high sensitivity GPS receiver.

Acknowledgements

Dedication

To my beloved parents Abbas and Zari, my grandmother Aziz and my sister Mojgan.

Table of Contents

List of Tables

List of Figures and Illustrations

List of Abbreviations

AGPS   Assisted GPS
ATAN   Arctangent
AWGN   Additive White Gaussian Noise
BER   Bit Error Rate
$B_L T$ the product between loop noise bandwidth and loop update interval
C/A   Coarse/Acquisition
CDMA   Code Division Multiple Access
C/N_0 Carrier-to-Noise density
DLL   Delay Locked Loop
DPLL   Digital Phase Locked Loop
EKF   Extended Kalman Filter
FEC   Forward Error Correction
FLL   Frequency Locked Loop
GNSS   Global Navigation Satellite Systems
GPS   Global Positioning System
HSGPS   High Sensitivity Global Positioning System
IF   Intermediate Frequency
KF   Kalman Filter
L1   L1 frequency band centered in 1575.42 MHz
LF   Loop Filter
LNA   Low Noise Amplifier
LOS   Line Of Sight
LPF   Low Pass Filter
LS   Least Square
MS   Multi-Stage
MSE   Mean Square Error
NAV   Navigation data
NCO   Numerically Controlled Oscillator
NI   National Instrument
OCXO   Oven Controlled Crystal Oscillator
PLL   Phase Locked Loop
PRN   Pseudo Random Noise
RF   Radio Frequency
RMS   Root Mean Square
SNR   Signal-to-Noise Ratio
TCXO   Temperature Compensated Crystal Oscillator

Chapter One: Introduction

1.1 Background and Motivation

The Global Positioning System (GPS), initialized in 1973 to reduce the proliferation of navigation aids, is a satellite-based radio navigation system that is operated and maintained by the United States Department of Defense (DoD). GPS can provide a solution with accuracy ranging from metre to centimetre given the conditions, measurements, and adopted methods (Misra & Enge 2001). However, the GPS signal is attenuated significantly in an indoor environment, resulting in the failure of signal acquisition and tracking by most conventional receivers. In degraded signal environments GPS receivers usually encounter signal attenuation, self-interference due to stronger GNSS (Global Navigation Satellite System) signals, multipath fading and radio frequency interference. Moreover, during periods of deep signal attenuation, changes in channel characteristics impose rapid phase fluctuations which in turn cause difficulty for conventional carrier phase recovery algorithms. Special algorithms and techniques are required to acquire and track the signal indoors, where the signal is typically weaker by 10 to 35 dB compared to the nominal or line-of-sight signal strength. Typical GNSS signal power in different environments is shown in Figure 1-1.

Various emerging applications require location of users in challenging environments where typical GPS receivers suffer degraded performance or complete failure. The Enhanced 911 Mandate by the Federal Communications Commission (FCC) in the U.S. is one of the most important indoor applications. It requires the wireless carrier to

2

provide automatic location identification (ALI) of the emergency caller, based on which the public-safety answering point (PSAP) then dispatches a rescue team (Wei 2007). Moreover, personal navigation services, which nowadays are available widely on hand held devices such as cellular mobile phones, necessitates seamless GPS tracking both outdoor and indoor.
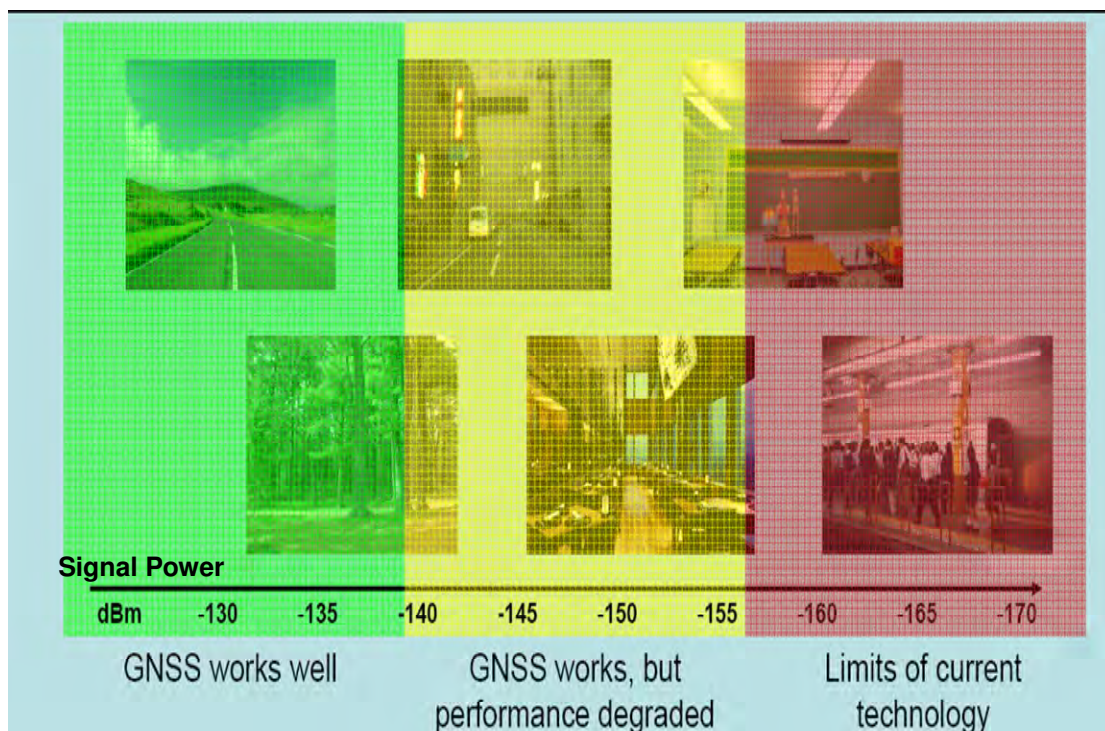
Figure 1-1 Typical GNSS signal power in different environments (Mitelman et al 2006)

This thesis mainly addresses the problem of discrete time carrier phase recovery of a GPS signal in weak signal conditions. In general there are two approaches to build a high sensitivity receiver. One approach involves the use of an aiding unit. The other approach uses a stand-alone receiver unit. Although the first approach can be very effective, it has the drawback of requiring the existence of a reference station and communications

between the reference station and the receiver. In the second approach the GPS receiver alone must have the capability to process and track the weak signal. Both of the above approaches are considered in this thesis. The external assistance includes only navigation data in this thesis. In this way, results can be extended for the pilot channel tracking with the modernized GPS signals.

Most of the designed algorithms in this thesis are implemented in the PLAN Group's GSNRx™ (GNSS Software Navigation Receiver) software developed on a Visual C++ platform. The software-based tracking approach gives more flexibility to use better tracking techniques and consequently enables better performance. There have been few tracking approaches designed for weak signals or for software receivers. Such approaches could enable the use of GPS in wireless applications with lower cost and more accuracy. In the following section some of the previous works related to weak GPS signal tracking and their limitations are reviewed.

1.2 Literature Review and Limitations of Previous Work

HSGPS (High Sensitivity) receivers are a class of receivers that display significantly higher acquisition/tracking sensitivity in comparison to standard receivers. Typical HSGPS receivers are designed for weak signal acquisition/tracking using coherent and non-coherent integration, over periods longer than 20 ms in the latter case. It seems, however, that current technologies cannot completely meet indoor navigation requirements. The limitations of these technologies are discussed below.

Most of the research in the HSGPS field is directed towards acquiring weak signals while weak signal tracking receives less attention. Several detection algorithms have been reported in the literature to address the problem of high sensitivity acquisition under weak GPS signal conditions (e.g. Shanmugam 2008 and references therein). Many field and simulation tests have been carried out using the high sensitivity commercial receivers (e.g. Singh 2006 and references therein).

HSGPS receiver tracking mainly relies on extended integration time to significantly enhance the tracking sensitivity. Unfortunately, the maximum coherent integration time in a GPS receiver can be limited by a variety of factors. For instance, the presence of navigation data modulation typically limits the coherent integration time to less than 20 ms. Modernized GPS solve this problem by adding a pilot channel beside the data channel for L5 and L2C signals. However the presence of navigation data is still a problem for weak L1 GPS signal tracking. In Kumar (1988), a scheme for simultaneous detection and estimation has been proposed. This scheme is based upon first estimating the received signal's local (data dependent) parameters over two consecutive bit periods, followed by the detection of a possible jump in these parameters. The presence of the detected jump signifies a data transition which is then removed from the received signal.

For GPS signal tracking, Tsui (2000), Psiaki & Jung (2002) and Soloviev (2004) proposed weak signal tracking based on navigation data bit prediction. However, the performance of these algorithms based on real GPS signals and in terms of Bit Error Rate (BER) has not been assessed and comparisons between these methods are not available. Assisted GPS is another solution for this problem. Both of the above approaches will be considered in this thesis. However, only navigation data will be considered as an external

assistance. In this way, results could be extended to stand-alone receivers for modernized GPS signals which benefit from a dataless channel. HSGPS techniques for acquiring GPS signal utilizing coherent integration time even up to several seconds have been reported in the literature (e.g. Watson 2005). However, Watson's approach was limited to post-mission mode and critically relied on accurate modeling of second order satellite/receiver dynamic effects. In this case the ephemeris and position of the receiver should be known to estimate the Doppler frequency. Moreover, other factors limit the coherent integration time aside from just the navigation data transition. The main limiting factors are related to conventional tracking architectures such as phase-locked loops and Kalman Filter based tracking.

The phase-locked loop (PLL) is ubiquitous in communications systems, and there exists a vast amount of literature on its application to carrier-phase recovery in coherent receivers (e.g. Gardner 2005). Much research has been done in the field of digital phase locked loops (DPLL) and an excellent survey of theoretical and experimental works accomplished in this area up to 1981 can be found in Lindsey & Chie (1981). Most of this research focuses on different methods for the design of the phase detector and very little effort has been spent in the design of loop filters.

 Since theoretical and practical aspects of continuous phase-locked loops and their performance in different situations is well known, the typical methodology in designing digital loop filters is based on the transformation from the analog domain (Gardner 2005, Stephens 2001, Best 1999, Lindsey & Chie 1981). This technique is widely used for GNSS signal tracking loops (Ward et al 2006, Stephens 2001, Tsui 2000, Spilker 1997). In the controlled-root method proposed by Stephens & Thomas (1995), loop filter

constants are determined specifically for each B_LT (product between loop noise bandwidth and integration time) value. In this way the deficiencies for the loop design for different B_LT are avoided and the digital loop has exactly the desired bandwidth, however the structure of the filter remains the same as the one obtained with the transformation method. In this case the maximum achievable B_LT for a stable loop is limited to 0.4 for rate-only feedback NCOs (Stephens & Thomas 1995). Another method which has been rarely treated in the literature is based on the minimization of a specific cost function. This method was first used in Gupta (1968) using the Z-transform and modified Z-transform for analog-digital phase-locked loops. In this case the phase-locked loop is the same as that for the continuous case except that the filter is replaced by a discrete filter followed by a hold circuit (Gupta 1968). Minimization techniques for the design of digital tracking loops have only been marginally considered in the literature and tracking loops have been essentially designed by means of transformation methods. Loop performance deficiency and stability issue for high B_LT values in GPS signal tracking have been recently discussed by Humphreys et al (2005) and Progri et al (2007) but no solution is proposed to overcome these problems.

Using KF and EKF for carrier tracking goes back to the 70's (Polk & Gupta 1973). Psiaki (2001) and their references consider the design of a KF based carrier tracker for the GPS signal. To enhance this technique in tracking weak signals, Psiaki & Jung (2002) implement the extended KF that is specially designed for tracking weak carrier-suppressed GPS signals. They adopt the Bayesian approach to treat the uncertainty of the data bits. Similar work has been done by Zeidan & Garrison (2004). A tracking threshold of 15 dB-Hz under static conditions and OCXO oscillator is claimed in Psiaki & Jung

(2002) as well as Zeidan & Garrison (2004). However, these works remained at the simulation level. Recent performance of EKF based tracking is discussed in Petovello et al (2008b) for real GPS signal under weak signal conditions where sensitivity of about 20 dB attenuation is reported. This level of attenuation is approximately equal to a C/N_0 (carrier to noise ratio) of 20 dB-Hz (assuming nominal signal level of 40 dB-Hz). As that work shows, there are still severe limitations and lack of methodologies in tracking the GPS signal especially for C/N_0 values less than 24 dB-Hz. The performance of EKF based tracking in extended integrations has not been investigated thoroughly before. Recent work by Petovello et al (2008a) shows that there might be performance degradation for higher integration times for EKF based tracking. This phenomenon is also observed in DPLLs as mentioned before. Investigating the performance of these techniques in longer integration becomes very important for weak signal tracking.

In longer integration, frequency mismatch between the incoming signal and locally generated signal causes correlation loss in each update interval. To overcome this problem, unlike the conventional architecture, the frequency of the locally generated signal should be propagated even in each update interval. The solution of this problem has not been investigated for the closed loop architecture.

1.3 Research Objectives

Given the lack of research directed towards weak GPS signal tracking and carrier phase tracking schemes using long integration time intervals, this thesis expands the work described in the previous section by attempting to investigate and unify existing

architectures utilized by traditional tracking schemes. The main objective of this research is to improve the performance of GPS signal tracking under weak signal conditions. Most importantly it attempts to develop new filters and tracking schemes to enhance the sensitivity of software receivers. To this end the following goals are pursued:

- Analyze and investigate fundamental tracking techniques utilized by traditional GPS signal tracking schemes in terms of sensitivity in order to identify their merits, limitations and scope for weak signal tracking.

- Assess and quantify the benefits of assisted and dataless GPS signals for weak signal tracking and comparison with stand-alone schemes.

- Design and develop new digital tracking loop filters to overcome the stability problems and performance degradation of traditional filters for high integration times.

- Explore and develop novel tracking algorithms that enable efficient GPS signal tracking under weak signal and high dynamic applications.

- Utilize and develop multistage estimation techniques for GPS signal tracking.

1.4 Thesis Outline

This thesis is structured in the following way:

Chapter 1 presented the motivation and the central objectives of the research discussed in the thesis. It also discussed previous research in the relevant area and their limitations.

Chapter 2 covers most of the necessary background knowledge for the subsequent chapters. The basic theory of the carrier phase and frequency estimation is reviewed with an emphasis on the closed loop tracking architecture. Indeed these systems have been studied and described in many papers and books but most of current models and their characteristics are based on the analog loops. The limitations of the traditional tracking loops are discussed and the digital linear model of the phase locked loop, with considering the effect of the integration and dump unit, is derived. Different NCO types are also introduced and their effects on the conventional loops are investigated. The main tracking error sources and their effects on the PLL performance are also discussed.

Chapter 3 focuses on designing digital tracking loops directly in the Z-domain based on the linear model of the DPLL derived in Chapter 2. More specifically a minimization technique is used to determine the filter structure and coefficients. These parameters are determined in order to minimize the variance of the phase error. The effect of the integration time is considered in the linear model to extend the operational range of the filter to larger $B_L T$ values. Instantaneous update of the loop filter (i.e., the absence of computational delay) is assumed. Two kinds of NCOs, namely phase and phase-rate feedback NCO and phase-rate only feedback NCO, are considered. It is shown that the transfer function of the optimum loop filter with the rate-only feedback NCO is different from what is currently used for most GNSS receivers. This

minimization technique for filter design has, to the best of the author's knowledge, never been applied to GNSS software receivers with the two aforementioned kinds of NCOs nor has it been designed up to fourth order loops. The loop filter design curves are given, hence the loop filters can be easily designed without repeating the rigorous mathematical procedure conducted herein especially for high order loops. By this technique it becomes possible to increase the $B_L T$ limit of the tracking loops beyond any other previous methods. Practical considerations in choosing the proper loop and the NCO for different situations are also given. The performance and stability of the designed loops are shown by means of live GPS signals for both static and dynamic situations. Tests are conducted for $B_L T$ values at which conventional loops cannot operate at all. Although the main focus of this chapter is on GNSS tracking loops, the technique used herein could be applied to any other communication systems which require tracking loops.

In Chapter 4, a state variable approach to carrier phase tracking is introduced and a technique of ramping the NCO frequency (instead of using the staircase fashion) to reduce the phase error due to the Doppler rate in a DPLL (Digital Phase Locked Loop) is investigated. A combination of Kalman Filter (KF) and DPLL is used where the KF estimates the frequency rate and feeds this information back to the NCO to change the frequency of the locally generated signal even during each update interval. The output of the loop filter is used as Doppler measurements for the KF. The additional feedback of the frequency rate to the NCO raises stability issues. The NCO transfer function and the effect of the frequency rate estimator in the Z-domain is modeled precisely and the loop filter is designed based on Chapter 3 results to overcome the stability issue raised by high integration time and additional feedback to the loop. The performance of these

approaches is demonstrated with line-of-sight live GPS signals and for coherent integration times of up to one second. It is shown that the phase mismatch between the locally generated signal and the incoming signal is reduced significantly in high integration times; hence the coherent integration time in a closed-loop tracking architecture can be increased without any significant correlation loss.

In Chapter 5 the practical limitations of the techniques presented in previous chapters are investigated and a solution based on the multistage estimation technique is proposed to overcome some of these limitations. The carrier parameters are estimated by an algorithm which has a low threshold on C/N_0 but with possibly higher RMS (Root Mean Square) estimation errors. Then an error signal whose parameters are equal to the difference between the true parameters and the above estimates is processed by another algorithm to estimate these error signal parameters. The first stage algorithm is selected to be a modified least-squares algorithm operating upon the differential signal model. This estimation stage provides relatively coarse estimates of the frequency and its derivatives. The second algorithm is an extended Kalman filter (EKF) which also yields the estimate of the phase along with a more refined estimate of frequency as well. Proper algorithm selection for different stages is also considered. Indoor data is collected in different environments starting from a relatively benign indoor environment, such as a building with large windows to a harsh indoor environment with high attenuation and severe multipath. The results are compared with commercially available high sensitivity receivers.

Chapter 6 concludes the key findings and results of this dissertation. The main limitations of the proposed techniques for weak signal tracking are discussed and recommendations for further improvements are given.

Chapter Two: Fundamentals of Signal Tracking Using Phase-Locked Loops

This Chapter covers most of the necessary background knowledge for the subsequent chapters. The basic theory of carrier phase estimation is reviewed with an emphasis on the closed loop tracking architecture. The limitations of the traditional tracking loops are discussed and the digital linear model of the phase locked loop, with consideration for the effect of the integration and dump unit, is derived. Different NCO types are also introduced and their effects on conventional loops are investigated.

2.1 Introduction to Phase-Locked Loops

The main function of a phase-locked loop is to adjust the frequency of the local oscillator to match the frequency of the input signal. In order to achieve this goal the PLL consists of three basic functional blocks:

1. A phase detector (PD)

2. A loop filter (LF)

3. A voltage-controlled oscillator (VCO).

A phase detector compares the phase of the locally generated signal by the VCO against the incoming signal; as such the output of the PD is an estimate of the phase error. This phase error is then filtered by the loop filter whose output is applied to the VCO as a controlling signal. This control signal changes the frequency of the local oscillator in a way to reduce the phase error between the input signal and the VCO. Obviously, a PLL does not imply zero phase error and both steady phase error (even in noiseless conditions)

and fluctuating phase errors can be present (Gardner 2005). An excessive phase error can cause loss of lock in a PLL. A simple block diagram of the phase-locked loop is shown in Figure 2-1.
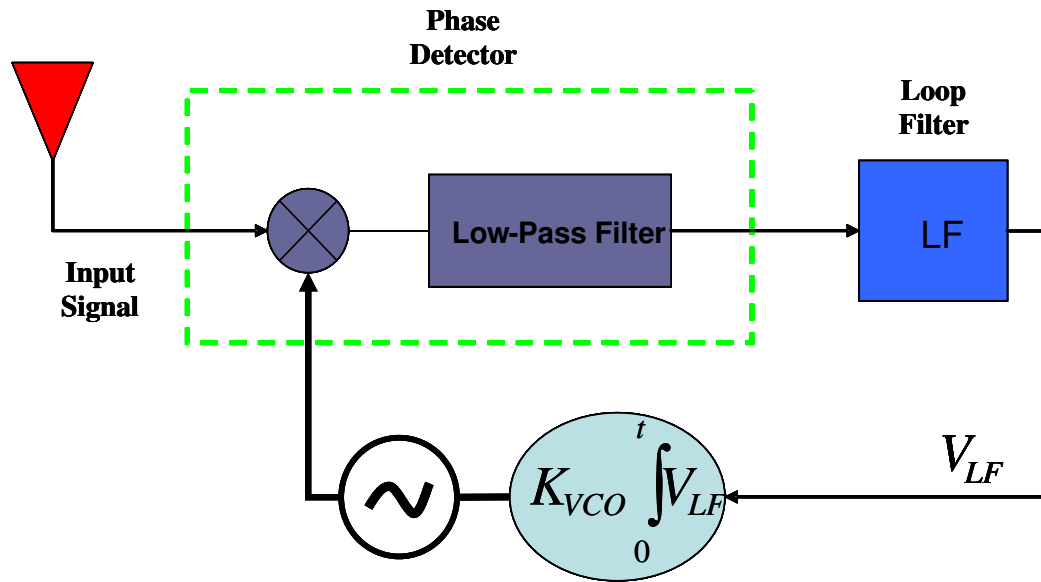
Figure 2-1 Simple phase-locked loop

The output frequency of the VCO is determined by the output signal V_{LF} of the loop filter and can be written as

$$\omega_{VCO} = \omega_0 + K_{VCO}V_{LF} \qquad \text{2-1}$$

where ω_0 is the center frequency of the VCO and K_{VCO} is the VCO gain. The phase angle of the VCO can be obtained as

$$\int_0^t \omega_{VCO}\,dt = \omega_0 t + \int_0^t K_{VCO}V_{LF}\,dt = \omega_0 t + \theta_{VCO}(t). \qquad \text{2-2}$$

Equation 2-2 shows that the VCO performs an integration with respect to the controlling signal.

In Figure 2-1 the phase detector is represented as a mixer. The mixer will produce a frequency summation and frequency difference components. Assuming that the input signal has a power of P, the output of the mixer can be written as

$$\sqrt{2P}\cos(\omega_0 t + \theta(t)) \times 2\sin(\omega_0 t + \int K_{VCO}V_{LF}(t)dt) =$$
$$\sqrt{2P}\sin(\theta(t) - \int K_{VCO}V_{LF}(t)dt) + \sqrt{2P}\sin(2\omega_0 t + \int K_{VCO}V_{LF}(t)dt + \theta(t))$$

2-3

where $\theta(t)$ is the incoming signal phase and $\int K_{VCO}V_{LF}$ is the PLL's estimate of the phase. Of primary interest is the baseband component and the high frequency component will be removed by the low pass filter. Assuming the loop is in lock and the phase error is small, the error signal at the output of the phase detector after linearization can be written as

$$\theta_e(t) = \sqrt{2P}(\theta(t) - \int K_{VCO}V_{LF}dt).$$

2-4

After linearization the block diagram of Figure 2-1 can be simplified as Figure 2-2.
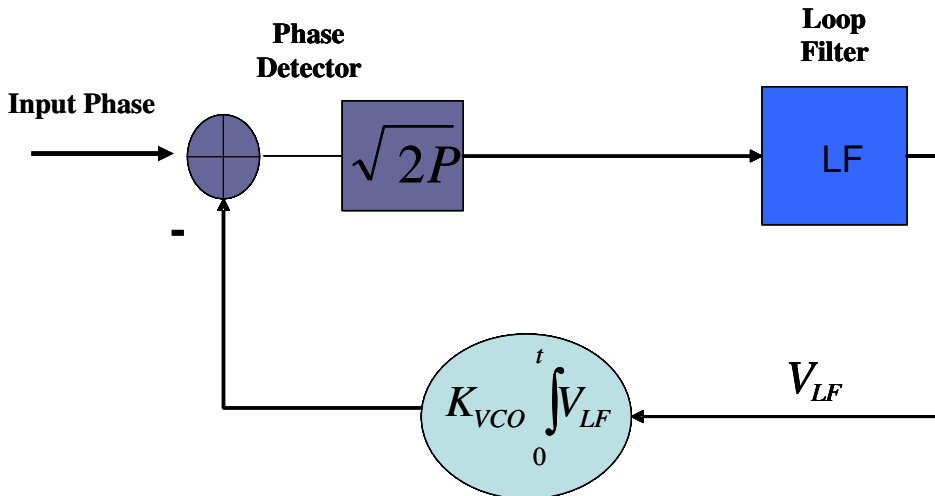
Figure 2-2 Linear phase-locked loop model

For this time-domain analysis a simple case will be considered where the loop filter is only a scalar gain, K_f. This choice of a loop filter will result in a first-order loop. Note that in PLLs the loop filters are not always low pass filters. As stated in Gardner (2005) a better name might have been loop controllers instead of loop filters. The main purpose of these circuits is to establish the dynamics of the feedback loop and to deliver a suitable control signal to the VCO.

By solving for the phase error in Equation 2-4 a mathematical representation of how well the PLL is tracking the input can be derived. The control signal can be written as

$$V_{LF}(t) = K_{LF}\theta_e(t).$$ 2-5

Substituting Equation 2-5 into Equation 2-4 yields

$$\theta_e(t) = \sqrt{2P}(\theta(t) - K_{LF}K_{VCO}\int \theta_e dt).$$ 2-6

The differential form of Equation 2-6 is easier to solve. One can write

$$\dot{\theta}_e(t) + \sqrt{2P}K_{LF}K_{VCO}\theta_e(t) = \sqrt{2P}\dot{\theta}(t).$$ 2-7

Solving Equation 2-7 yields

$$\theta_e(t) = e^{-\sqrt{2P}K_{LF}K_{VCO}t}\int e^{\sqrt{2P}K_{LF}K_{VCO}t}\dot{\theta}(t)dt + \overline{c}e^{-\sqrt{2P}K_{VCO}K_{LF}t}$$ 2-8

where $\overline{c}$ is a constant. For PLL applications the phase input is usually of the form

$$\theta(t) = (a + bt + ct^2 + ...)u(t)$$ 2-9

where a, b and c are some constants and $u(t)$ is the unit step function. Assuming that the input phase is constant, the solution of Equation 2-8 yields

$$\theta_e = ae^{-\sqrt{2P}K_{VCO}K_{LF}t}u(t).$$ 2-10

By taking the limit as $t \rightarrow \infty$ the steady state response can be computed as zero. This indicates that the first order loop can completely adjust the VCO phase to compensate for an input offset phase. However for a constant frequency as an input, the error response can be computed as

$$\theta_e(t) = (\frac{b}{\sqrt{2P}K_{VCO}K_{LF}} - \frac{b}{\sqrt{2P}K_{VCO}K_{LF}} e^{-\sqrt{2P}K_{VCO}K_{LF}})u(t) \qquad\qquad 2\text{-}11$$

and the steady state error response is

$$\lim_{t \rightarrow \infty} \theta_e = \frac{b}{\sqrt{2P}K_{VCO}K_{LF}} u(t). \qquad\qquad 2\text{-}12$$

Equation 2-12 indicates that the first-order phase-locked loop has a constant error for tracking a constant frequency. Note that the loop gains are in the denominator of Equation 2-12, as such by increasing the gains in the loop the steady state error can be decreased. As will be shown later, this increase in the loop gain is equivalent to increasing the loop noise bandwidth. Equation 2-11 shows that the error function is exponentially affected by the amplitude, $\sqrt{2P}$, of the received signal. The varying amplitude value of the incoming signal must be controlled, otherwise it will change the time response of the system. Often an Automatic Gain Control (AGC) circuit is used or a limiter is placed ahead of the phase detector (Stephens 2002).

It can also be shown that, for a frequency ramp as an input, the first-order phase-locked loop has an increasing phase error. If this accelerating input lasts only for a short time this error might not cause loss of lock or degradation of the PLL system. However if this Doppler input lasts for a long time, as with the satellite communications, then this error is unacceptable and higher order loops should be utilized. Figure 2.3 shows the error

response of the first-order loop for three different inputs. These three inputs are important considerations for PLL design. In order to track phase ramp or frequency ramp properly, higher order loops are required. As a result improvement must be made to the loop filter (loop controller) to accommodate these input signals.
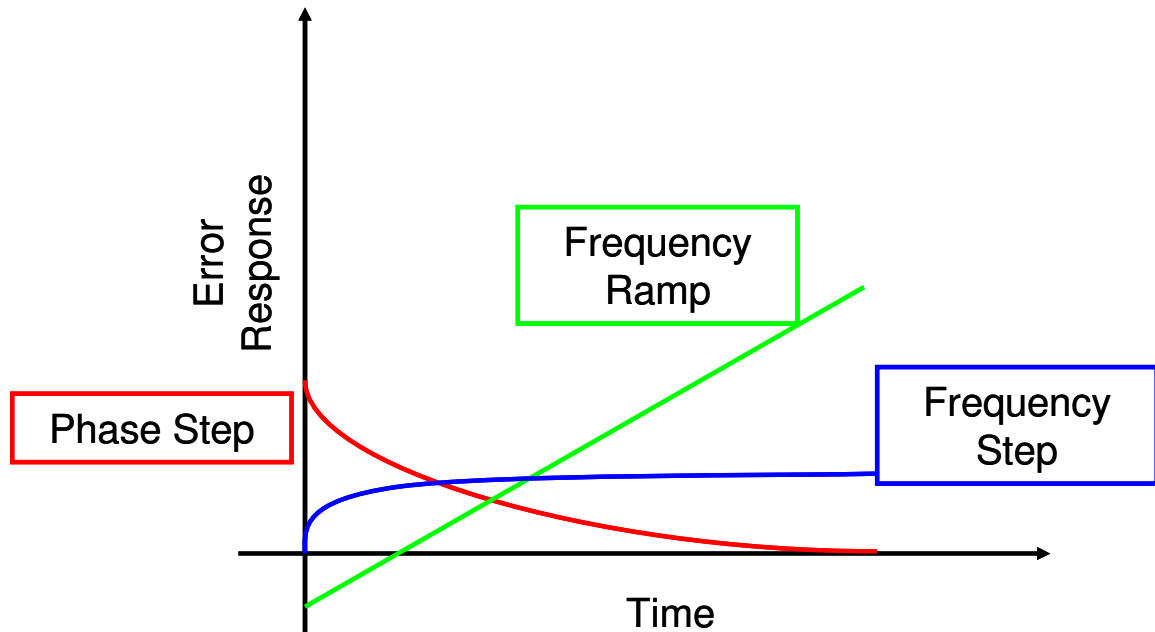
Figure 2-3 First-order loop response for different phase inputs

Time domain analysis of higher order loops results in difficult differential equations. Obtaining the equivalent of Equation 2-8 for higher order loops requires performing convolutions and solving difficult differential equations. To simplify the analysis of the phase-locked loops, frequency domain analysis can be used.

2.1.1 Frequency Domain Analysis

Although PLLs are inherently nonlinear systems their main operations can be approximated by linear models. When the loop is locked, the phase error is small and the linear model will be applicable. Analysis of a linear control system can be performed by means of its transfer function $H(s)$. The transfer function relates the input and output signals of the system. If the input and output signals are presented by $i(t)$ and $o(t)$, respectively, then $H(s)$ is given by

$$H(s) = \frac{O(s)}{I(s)} \qquad\qquad 2\text{-}13$$

where $I(s)$ and $O(s)$ are the Laplace transforms of $i(t)$ and $o(t)$ respectively. In the case of the PLL the input and output signals are assumed to be phase signals. As a result $H(s)$ is a transfer function of a phase estimator.

This kind of analysis hides the subtleties of time-domain performance and operation, especially for digital control loops where time delay is a fundamental processing element (Stephens 2002). However this is an inevitable choice in order to simplify the problem. Figure 2-4 represents the phase-locked loop in the Laplace domain. Note that the phase detector is simply modeled as the difference between the incoming phase and the estimated phase by the VCO. The possible gain of the phase detector is also considered in the loop filter transfer function.

$$H(s)$$
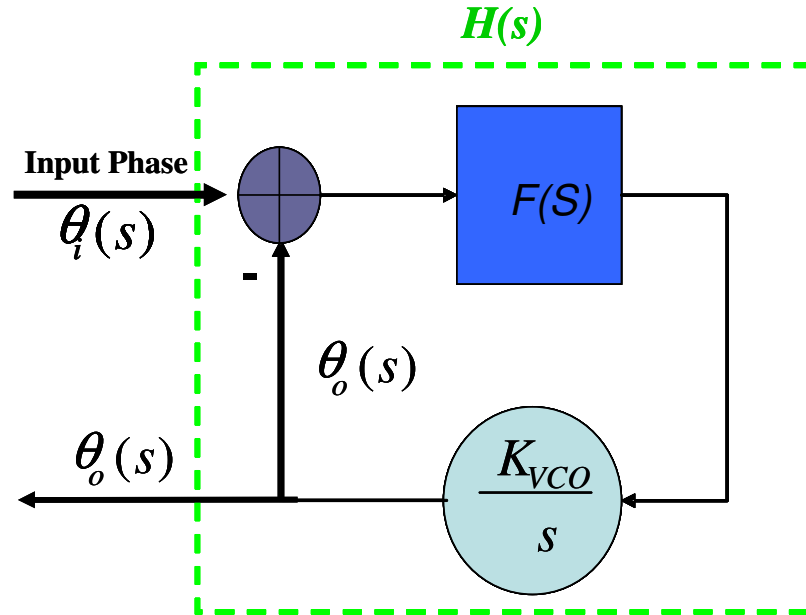
Figure 2-4 Typical PLL model in frequency domain

From Figure 2-4 the transfer function $H(s)$ of the loop can be written as

$$H(s) = \frac{\theta_0(s)}{\theta_i(s)} = \frac{K_{VCO}F(s)}{s + K_{VCO}F(s)}. \qquad\qquad 2\text{-}14$$

The error transfer function is defined as

$$H_e(s) = \frac{\theta_e(s)}{\theta_i(s)} = 1 - H(s) = \frac{s}{s + K_{VCO}F(s)}. \qquad\qquad 2\text{-}15$$

The highest order of s in the denominator of $H(s)$ is the order of PLL. For instance if the highest order is n, then the PLL can track n terms of Equation 2-9, with zero steady-state phase error.

In order to design a second-order PLL the following transfer function for the loop filter can be used:

$$F(s) = K_{LF} \frac{s\tau_1 + 1}{s}.$$

2-16

By defining the total loop gain as $K = K_{LF} K_{VCO}$ and from Equation 2-14, the closed loop

transfer function of the second order PLL can be derived as

$$H(s) = \frac{K + K\tau_1 s}{s^2 + K\tau_1 s + K} \equiv \frac{2\xi w_n s + w_n^2}{s^2 + 2\xi w_n s + w_n^2}$$

2-17

where w_n is the natural frequency, expressed as

$$w_n = \sqrt{K}$$

2-18

and ξ is the damping factor which is equal to

$$\xi = \frac{w_n \tau_1}{2}.$$

2-19

The error transfer function can be obtained from Equation 2-15 as

$$H_e(s) = H(s) - 1 = \frac{s^2}{s^2 + 2\xi w_n s + w_n^2}.$$

2-20

The final value theorem allows the computation of the steady-state response for different

inputs. In contrast to the first order loop the steady state error is zero for the phase ramp

as an input (for bt, the second term in Equation 2-9) .

$$\lim_{t\to\infty} \theta_e(t) = \lim_{s\to 0} s\theta_e(s) = \lim_{s\to 0} s\theta_i(s)H_e(s) = \lim_{s\to 0} s\frac{b}{s^2} \frac{s^2}{s^2 + 2\xi w_n s + w_n^2} = 0.$$

2-21

The limitation of the second-order loop is in tracking the frequency ramp input. The

steady state error response for, $\theta(t) = ct^2$ can be obtained as

$$\lim_{t\to\infty} \theta_e(t) = \frac{2c}{w_n^2}.$$

2-22

This error for loops with small w_n can be significant. In this case, similar to Equation 2-12, increasing the loop gain can reduce the steady state error.

One of the important parameters in PLL design is the loop noise bandwidth which is defined as (Gardner 2005, Stephens 2002, Tsui 2000, Best 1999, Stephens & Thomas 1995, Thomas 1989)

$$B_L = \frac{1}{|H(0)|^2} \int_0^\infty |H(j\omega)|^2 \, df.$$

2-23

The loop noise bandwidth will be discussed in greater detail in analyzing the digital phase-locked loop. The normalization by |H(0)| in Equation 2-23 is commonly omitted in the literature, but, since the closed loop transfer function of a PLL has unity gain at DC this normalization is implicit. This normalization term is omitted in the remainder of this thesis. An alternative normalization is also possible, for example Lindsey (1966) uses normalization by the maximum absolute value of the transfer function. It is interesting to note that, in this case the noise bandwidth often corresponds closely to the 3 dB cut-off frequency. There is no such correspondence for the case of normalization by the DC gain. However, the latter is more common in the PLL literature, and is therefore the one used in the remainder of this thesis. As Gardner (2005) stated *"Ordinary filters are commonly specified in terms of their 3-dB bandwidth. Bandwidth of phase lock loops could also be so specified, but that is rarely useful and there is no apparent significance to such values."*

From Equation 2-17 the noise bandwidth of the second order loop can be derived as

$$B_L = \int_0^\infty |H(j\omega)|^2 \, df = \frac{w_n}{2\pi} \int_0^\infty \frac{1 + (2\xi\frac{\omega}{w_n})^2}{(1 - (\frac{\omega}{w_n})^2)^2 + (2\xi\frac{\omega}{w_n})^2} \, d\omega = \frac{w_n}{2}(\xi + \frac{1}{4\xi}). \qquad \text{2-24}$$

The damping factor and noise bandwidth are considered as independent design parameters. Note that changing the zero location of the loop filter effectively alters the damping factor.

The closed loop responses for different damping factors are plotted in Figure 2-5 and the error transfer function from Equation 2-20 is shown in Figure 2-6.
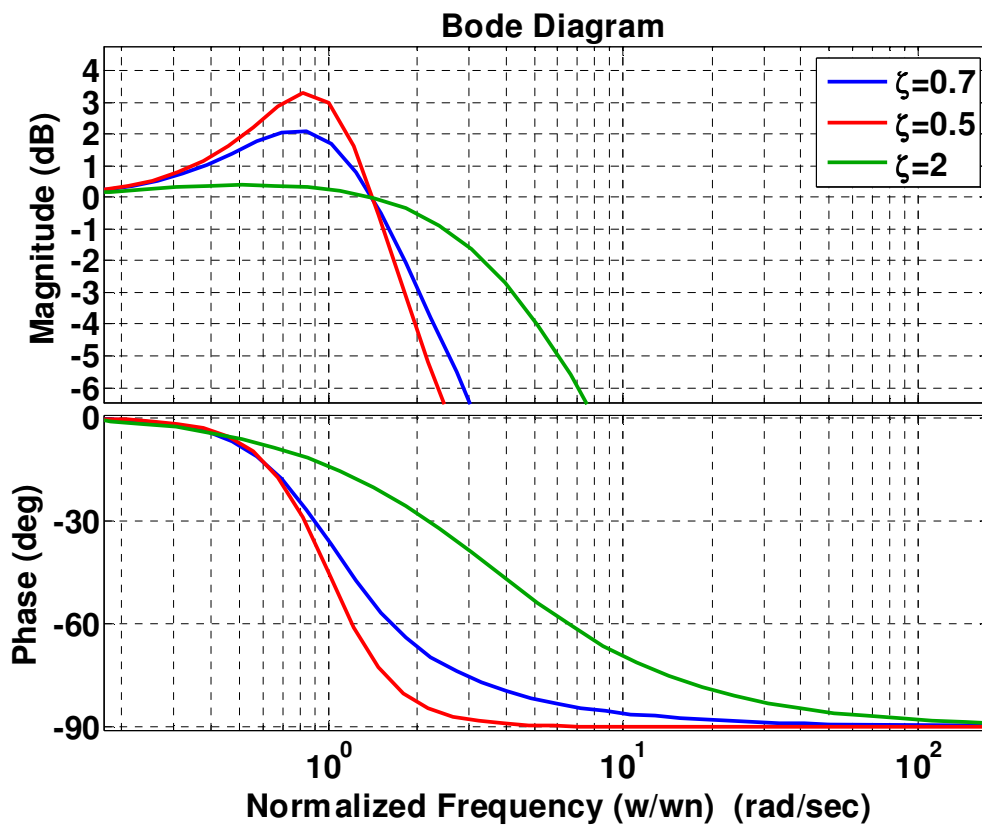
Figure 2-5 Closed-loop responses of the second-order loop
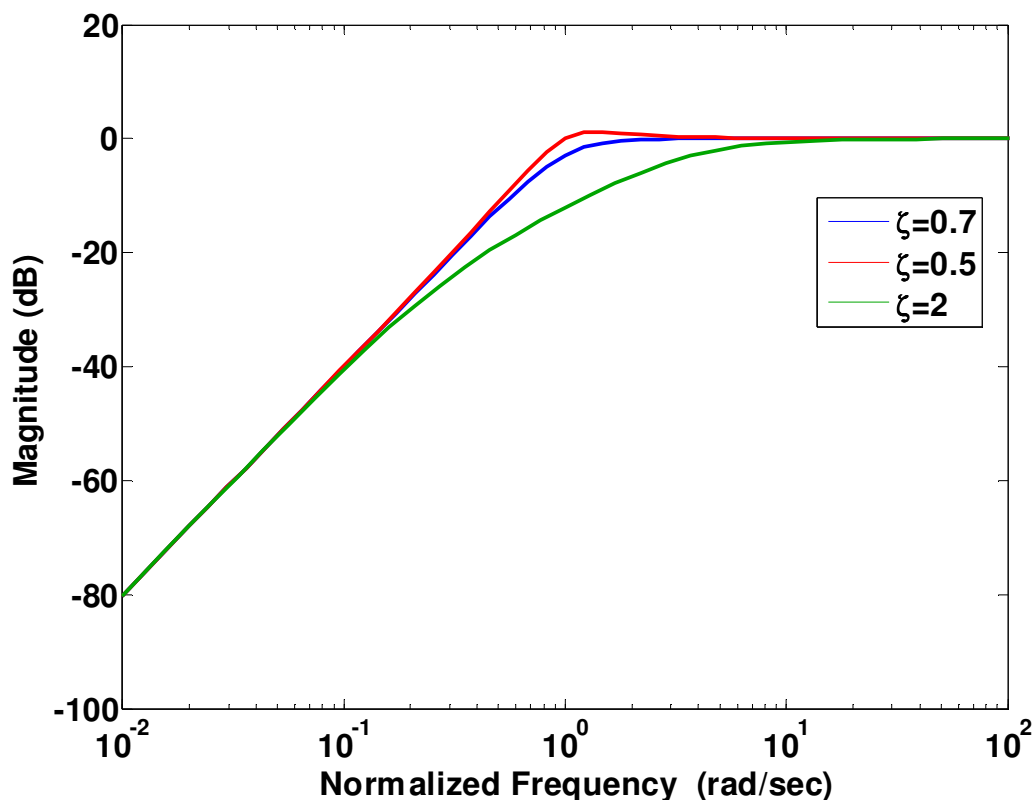
Figure 2-6 Frequency response of the phase error transfer function

Figure 2-5 indicates that the filtering characteristic of the PLL corresponds to the low-pass characteristic of the loop's transfer function. This figure also shows that the input phase modulation which is within the loop bandwidth will be tracked and the phase modulation that is outside the bandwidth cannot be tracked. The input phase modulation outside the loop bandwidth is attenuated and only phase modulation within the loop bandwidth is transferred to the VCO's phase output.

The error response is necessarily complementary: input modulation outside the loop bandwidth is hardly tracked at all, resulting in almost 100% tracking error, whereas input phase modulation within the loop bandwidth is tracked with a small error (Gardner 2005).

2.1.2 Root-Locus Analysis

The characteristics of the transient response are closely related to the location of the closed-loop poles. The location of the closed-loop poles can be determined by the value of the loop gain chosen. It is important, therefore, to know how the closed-loop poles move as the loop gain is varied.

One simple gain adjustment may move the poles to the desired locations. As mentioned earlier, increasing the loop gain reduces the steady state error and makes the loop more responsive to dynamics by increasing the bandwidth. However excessive gain might make the system unstable. Assuming the input is bounded, the system is stable if the output is also bounded. A linear system is stable only if the integral of the absolute value of the impulse function is finite. In the frequency-domain it is necessary for the real component of the poles to be negative or equivalently the poles should reside in the left hand side of the S-plane.

The root-locus method is a powerful graphical technique to investigate the effects of the variation of a system parameter on the location of the closed-loop poles (Ogata 2001). Poles change their locations as the loop gain is changed. The path that the closed-loop poles trace out in the frequency-space (S-plane or Z-plane), by changing the loop gain, are called root loci. The locations of closed-loop poles start on locations of the open-loop poles, for a zero loop gain, and terminate on the open-loop zeros for infinite gain. The open-loop transfer function for a PLL is given by $\frac{KF(s)}{s}$, thus at least one pole is always located at $s = 0$. Note that the loop filter determines the open-loop zeros location. Root

loci of the second order PLL is shown in Figure 2-7. As it is depicted for all of the gain values, the root loci of the closed-loop poles are on the left-hand side of the S-plane and the loop is stable.

Root Locus

System: oloop
Gain: 121
Pole: -17.5
Damping: 1
Overshoot (%): 0
Frequency (rad/sec): 17.5

System: oloop
Gain: 1.71
Pole: -0.855 - 4.99i
Damping: 0.169
Overshoot (%): 58.4
Frequency (rad/sec): 5.06
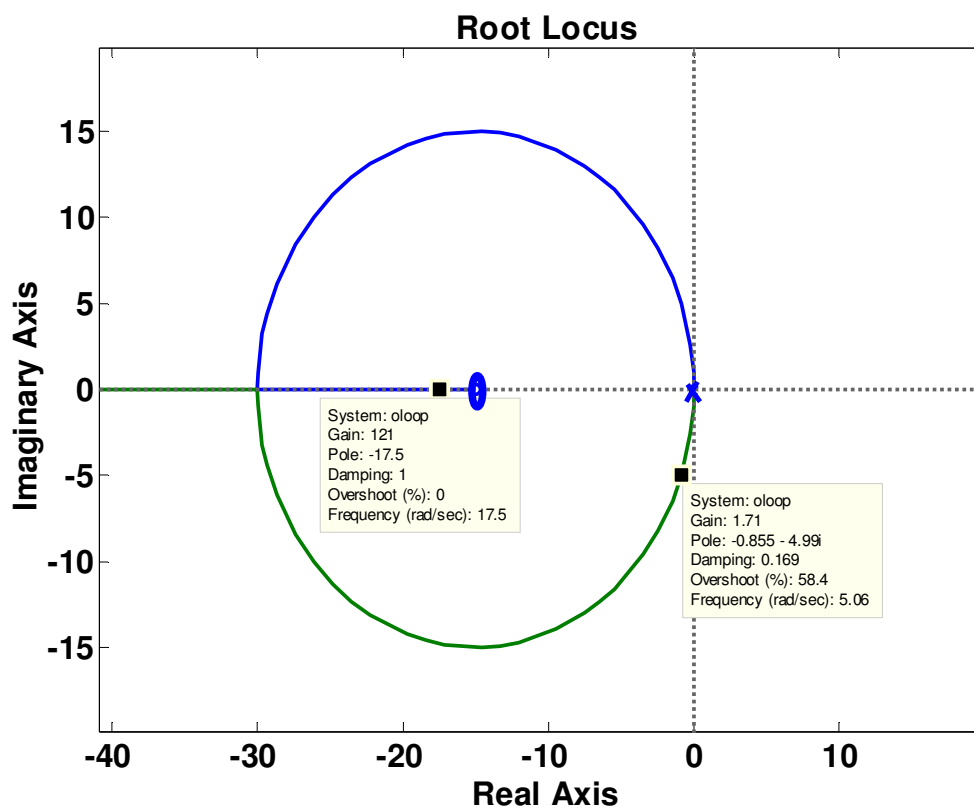
Figure 2-7 Root locus for second order loop

2.2 Digital Phase-locked loops

Nowadays more and more PLLs are being implemented in digital versions. This trend is a result of the rapid evolution of digital microelectronics. The main benefits of such an implementation are lower costs, drift-free components, easier implementation and

absence of tolerance problems (Gardner 2005). Especially for software receivers this is an inevitable choice. Digital PLLs (DPLL) are widely used in GNSS for high accuracy positioning.

2.2.1 Digital Transformations

The typical methodology in designing digital loops is based on the transformation from the analog domain (Gardner 2005, Stephens 2002, Tsui 2000, Best 1999, Lindsey & Chie 1981). Stephens (2002) stated three important factors about choosing this method which are quoted below:

- *"The art of PLL design is highly advanced and, since useful results can be achieved, it is advantageous to utilize the design procedures already developed for PLL.*

- *Many useful analog design methods have relatively simple closed form design formulas. Therefore, digital PLL design methods based on such analog design formulas are rather simple to implement.*

- *In many applications it is of interest to use a digital PLL to simulate the performance of an analog PLL."*

There are different transformations possible, the most noteworthy are the boxcar and bilinear transforms. Considering the first-order loop, the phase error rate $\dot{\theta}_e(t)$ in Equation 2-7 at $t = nT$ can be approximated by

$$\dot{\theta}_e(nT) = \frac{\theta_e(nT) - \theta_e((n-1)T)}{T}.$$

2-25

By using Equation 2-25 the sampled equivalent of Equation 2-7 is obtained as

$$\frac{\theta_e(nT) - \theta_e((n-1)T)}{T} + K\theta_e(nT) = \frac{\theta(nT) - \theta((n-1)T)}{T} \Rightarrow$$

$$\theta_e(nT) = \frac{(\theta_e(nT) - \theta_e((n-1)T)) + \theta_e((n-1)T)}{1 + KT}$$

2-26

Taking the Z-transform from Equation 2-26 results in

$$\theta_e(z)(1 + KT - z^{-1}) = \theta(z)(1 - z^{-1}).$$

2-27

From Equation 2-27 the transfer function of the digital loop can be obtained as

$$H_e(z) = \frac{\theta_e(z)}{\theta(z)} = \frac{1}{1 + KT} \frac{z - 1}{z - \frac{1}{1 + KT}}.$$

2-28

Whereas from Equation 2-15 the transfer function of the continuous-time counterpart PLL is

$$H_e(s) = \frac{s}{s + K}.$$

2-29

By comparing Equations 2-29 and 2-28 the boxcar equivalent of a S-domain transfer function is obtained by the following substitution:

$$H(s) \xrightarrow{s = \frac{1 - z^{-1}}{T}} H(z).$$

2-30

This equation is based on the backward difference approximation of a derivative and if the time function changes slowly over the interval T, it is a good approximation. In other

words as the sampled data become farther apart (as the sampling rate decreases), the

mapping form S-domain to Z-domain becomes distorted.

The bilinear transform is based on the following approximation:

$$\theta_e(nT) = \theta_e((n-1)T) + \frac{T}{2}(\dot{\theta}_e(nT) - \dot{\theta}_e((n-1)T)).$$ 2-31

In this case it can be shown that in general the digital transfer function can be derived

from

$$H(s) \xrightarrow{s=\frac{2}{T}\frac{1-z^{-1}}{1+z^{-1}}} H(z).$$ 2-32

This transform is based on approximating the integrals with a trapezoidal approximation.

In comparison with the boxcar transform it has a different mapping form the analog

domain. Unlike the backward difference, the bilinear transform maps the entire left-hand

S-plane into the unit circle. Whereas, the boxcar difference mapping does not utilize all

of the Z-plane's unit circle. In this case all of the left-hand S-plane is mapped into a small

circle in the right-hand side of the unit circle. Figure 2-8 shows the mapping from the S-

domain to the Z-domain with bilinear and boxcar transforms.

Z-Plane

S-Plane

Bilinear

Backward
Difference
(Boxcar)
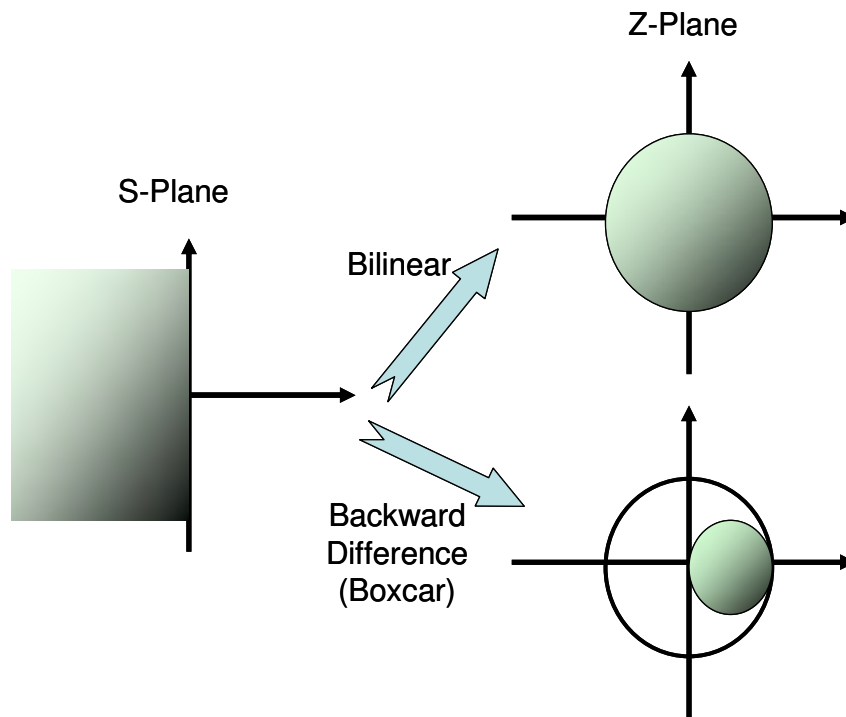
Figure 2-8 Mapping of S-domain to Z-domain

For a stable digital system, the system must have a bounded impulse response function. This condition can be determined by examining the position of the closed-loop transfer function poles. If all the poles are in the unit circle then the system is stable. As Figure 2-8 shows any stable analog transfer function is mapped to a stable digital function.

It can be seen that an infinite area in the S-plane is mapped to a unit circle which is a non-linear mapping of frequency. The bilinear transform from Equation 2-32 is

$$s = \frac{2}{T}\frac{1 - z^{-1}}{1 + z^{-1}}.$$ 2-33

Assuming $s = j\Omega$ and $z = e^{j\omega T}$, and by substituting into the above equation the relation

between continuous frequency and discrete frequency can be obtained as

$$j\Omega = \frac{2}{T}\frac{1-e^{-j\omega T}}{1+e^{-j\omega T}} \ .$$ 2-34

Algebraic simplification yields

$$\Omega = \frac{2}{T}\tan(\frac{\omega T}{2}) \ .$$ 2-35

For $\theta \langle\langle 1$, $\tan(\theta) \approx \theta$, and as long as the product of $\omega T \langle\langle 1$, then there is approximately a

linear frequency mapping between the S-plane and the Z-plane. When the loop frequency

approaches the sampling frequency it implies nonlinear mapping. In this case the

frequency breakpoint of the analog and digital transfer functions will be different.

Usually to obtain the desired digital frequency breakpoint, the analog filter's transfer

function is pre-warped (Stephens 2002). The transformation technique is widely used to

design the digital loop filters, however as will be shown later, the $\omega T \langle\langle 1$ constraint could

be a severe limitation.

2.2.2 DPLL Modeling

 Similar to analog PLLs, the input signal whose phase is to be tracked is sampled and

mixed with a locally generated signal by the VCO and the resulting signal is then

accumulated over an update interval of length T to perform low-pass filtering. The VCO

in the digital loop is called an NCO (Numerically Controlled Oscillator) since it has

discrete inputs and outputs. The phase difference between the incoming and locally generated signal is detected by the phase detector and this phase error is further filtered by the loop filter to generate the control signal for the NCO.

There is a fundamental difference between the analog PLL and DPLL since there is an inherent delay in the DPLL. Note that in order to generate the error signal $\theta_e(nT)$, the loop must have already computed the NCO output phase $\theta_o(nT)$ which obviously depends on $\theta_e(nT)$ (Stephens 2002).

In order to solve this dilemma a delay is considered in the DPLL model. This means a DPLL can be considered as a predictor, since $\theta_o(nT)$ is estimated based on $\theta_e((n-1)T)$. The loop filter combines present and past values of the residual phase, θ_e, to generate the control signal for the NCO. The control signal is considered as the estimated phase rate. More specifically it is noted that the estimated phase rate for the n+1 interval is the loop filter output at the nth interval.

Similar to the analog PLL, the phase detector is usually a nonlinear function of the phase error. However in lock conditions when the phase error is small it can be modeled as the difference between the average incoming phase and the average generated phase by the NCO at each accumulation interval (update interval). This assumption results in a linear model of DPLL as depicted in Figure 2-9.
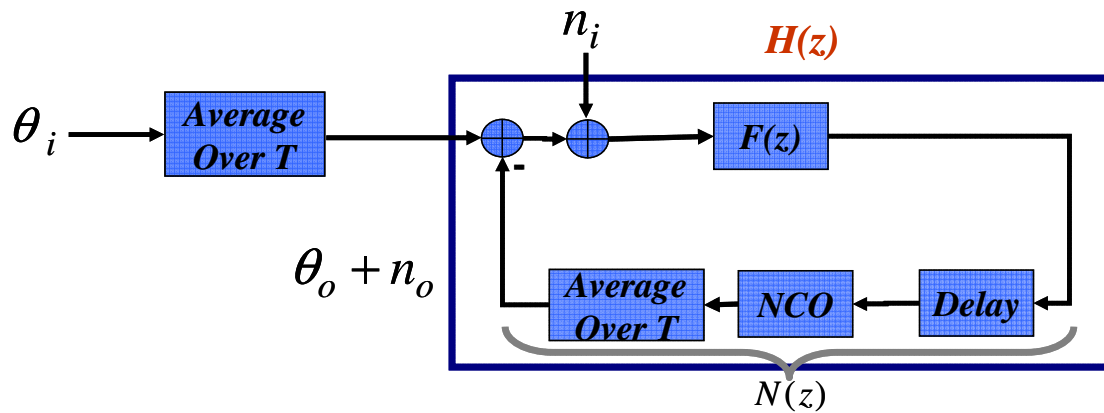
Figure 2-9 Linear DPLL model

Note that this model is essentially different from the available model in standard PLL literature (Lindsey & Chie 1987, Stephens 2002) as the effect of averaging is considered in this model. In Figure 2-9 *F(z)* represents the transfer function of the loop filter and *N(z)* is the transfer function of the NCO when the averaging effect due to the integrate and dump block is accounted for. The input of the loop is assumed to be a phase signal affected by white Gaussian noise. The random component of the NCO phase, due to the input noise is denoted by n_0 and θ_0 represents the deterministic component of the NCO phase (Kazemi 2008). From Figure 2-9 the close loop transfer function can be written as

$$H(z) = \frac{F(z)N(z)}{1 + F(z)N(z)}.$$
2-36

2.2.3 NCO Modeling

As can be seen from Equation 2-36 the model of the NCO has a significant impact on the transfer function of the phase estimator and it should be accurately modeled. Recall from the analog PLL that the VCO is a simple integrator. In the digital-domain this can be approximated by the accumulators, or using the mapping functions as discussed previously. In the standard PLL literature, the NCO is commonly modeled as $\frac{T}{z-1}$ (Lindsey & Chie 1981, Tsui 2000, Stephens 2002). This is not a valid model for long integration intervals and the effect of averaging should be taken into account for performance analysis in these regions

In conventional NCOs (denoted as rate-only feedback NCOs), which are most commonly used in phase-locked loops, the estimate of phase rate from the loop filter is used to update the NCO rate for the next integration interval. By considering sufficiently short integration intervals the phase rate of the received signal can be assumed to be constant during this interval. In this case the average generated phase by the NCO in each interval is equivalent to the generated phase in the middle of the interval.

In this case the locally generated signal at nth update interval by the NCO is

$$e^{-j\varphi} = e^{-j(\Delta\varphi_n t + \varphi_n^s)}.$$

2-37

where $\Delta\varphi_n$ is an estimated phase rate and φ_n^s is the initial phase at the nth epoch. The average generated phase at the nth epoch can be computed as

$$\varphi_n = \frac{1}{T}\int_0^T (\Delta\varphi_n t + \varphi_{in\_n})dt = \frac{T}{2}\Delta\varphi_n + \varphi_n^s.$$

2-38

where T is the update interval. Similarly for the next epoch the average generated phase can be computed as

$$\varphi_{n+1} = \frac{1}{T} \int_0^T (\Delta\varphi_{n+1} t + \varphi_{n+1}^s) dt = \frac{T}{2} \Delta\varphi_{n+1} + \varphi_{n+1}^s .$$

2-39

and from Equation 2-38 the initial phase at the n+1th epoch is

$$\varphi_{n+1}^s = \varphi_n^s + \Delta\varphi_n T .$$

2-40

Substituting Equation 2-40 into Equation 2-39 and by subtracting Equation 2-38 from Equation 2-40 the difference equation relating the average phase in the n+1th interval with that of the nth interval can be found as

$$\varphi_{n+1} = \varphi_n + \frac{T}{2}(\Delta\varphi_n + \Delta\varphi_{n+1}) .$$

2-41

This relation can be also easily inferred from Figure 2-10. As shown in Figure 2-10, there is no discontinuity in propagating the NCO phase.
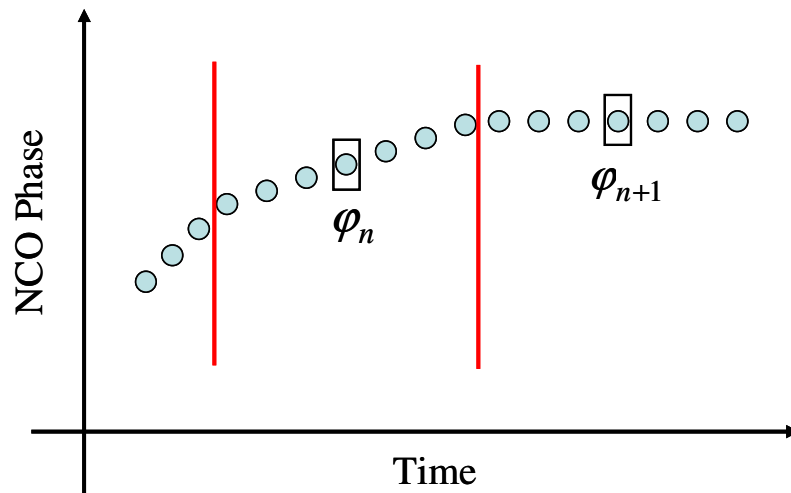
Figure 2-10 Schematic illustration of the NCO phase for the rate-only feedback NCO

Since the required parameters for generating the local signal for the n+1th interval come from the nth interval there is an inherent delay in the DPLL. More specifically, it is noted that the estimated phase rate for the n+1th interval is the loop filter output at the nth interval. By taking the Z-transform of Equation 2-41 and considering the effect of this delay, it is possible to obtain the NCO transfer function considering the averaging effect as

$$N_r(z) = \frac{T(z+1)}{2z(z-1)}.$$

2-42

Recently, more work has been done regarding the proper modelling of a DPLL. For instance, Legrand (2002) derives a multirate model of the DPLL including the effect of integration and dump. This model simplifies to the model used herein under the assumption that the predetection bandwidth is small compared to the sampling frequency. In (Humphreys et al 2005), a simple approximation is used to take into account the effect of the integration and dump unit. Interestingly, multiplication of the integration unit transfer function by the NCO transfer function is also equivalent to the model.

Another scheme for the NCO is to update both phase and phase rate of the locally generated signal at the start of each integration interval (Thomas 1989). In this case the NCO phase function is no longer a continuous function. The command to the NCO still consists of a phase rate only, however, the NCO applies a phase discontinuity at each update. These discontinuities are designed so as to have the following relation between the average generated phases of the NCO in two consecutive intervals:

$$\varphi_{n+1} = \varphi_n + T \cdot \Delta\varphi_{n+1}$$

2-43

As Equation 2-43 shows, the average generated phase at the n+1th epoch benefits from the most recent estimate of the phase rate, contrary to Equation 2-41. The starting phase at each sum interval can be found by propagating the average generated phase half of the interval backward:

$$\varphi_{n+1}^s = \varphi_{n+1} - \frac{T}{2}\Delta\varphi_{n+1}.$$

2-44

Practically it has been determined that propagating the starting phase is more robust against numerical errors (Kazemi 2008). In this case the starting phase for the next epoch can be found as

$$\varphi_{n+1}^s = \varphi_n^s + \frac{T}{2}(\Delta\varphi_n + \Delta\varphi_{n+1}).$$

2-45

This scheme is depicted in Figure 2-11. Defining the φ_{n+1}^s as in Equation 2-45 and Subtracting Equation 2-38 from Equation 2-39 will result in Equation 2-43.

Note that all the information that is required to determine the start phase for the n+1th epoch is available at the nth epoch. By considering the effect of delay and taking the Z-transform of Equation 2-43 into account, the transfer function of the NCO with phase and phase rate feedback can be derived as

$$N_p(z) = \frac{T}{(z-1)}.$$

2-46
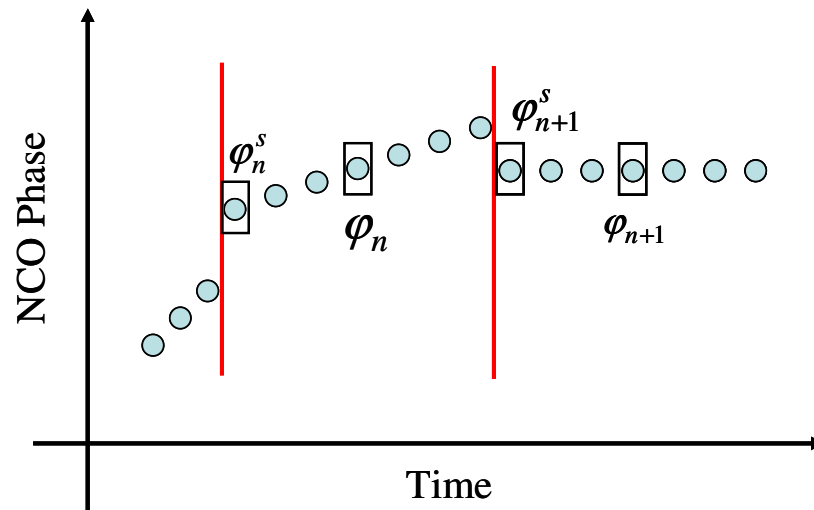
Figure 2-11 Schematic illustration of the NCO phase for the phase and phase rate

feedback NCO

As shown in Equation 2-46, the discontinuity in phase results in a different transfer function from Equation 2-42. As will be shown in Chapter 3, this difference in transfer function will result in different optimum filter structures. However, as will be shown later, the optimum filter for these two kinds of NCOs will yield the same closed loop transfer function; hence the two are equivalent from the point of view of linear tracking loop theory. However, there are practical differences which will be discussed in Chapter 3.

2.2.4 Noise bandwidth of DPLL

One of the important parameters in predicting the performance of the DPLL is the noise bandwidth. Figure 2-12 shows a bandpass filter followed by a DPLL. An input signal is

assumed to be sinusoidal with a power spectral density of $\frac{P}{2}\delta(f+f_0)+\frac{P}{2}\delta(f-f_0)$ as

shown in Figure 2-12.
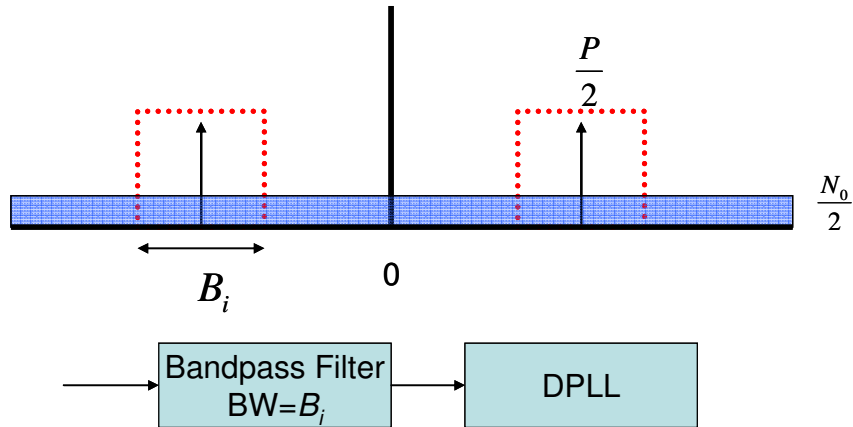
Figure 2-12 Bandpass noise into a DPLL

The bandpass filter is assumed to have a bandwidth B_i. Assuming the input noise is

white with constant power spectral density of $\Phi_{n_i n_i}=\frac{N_0}{2}$, the input signal to noise ratio

into the loop is then

$$\rho = \frac{P}{B_i N_0}.$$

2-47

The filtering characteristics of the DPLL will reduce the noise further. The output noise

power spectrum of the DPLL can be obtained as (Oppenheim et al 1999)

$$\Phi_{n_0 n_0}(z) = |H(z)|^2 \Phi_{n_i n_i}^s(z)$$

2-48

where $\Phi_{n_i n_i}^s$ is the power spectrum of the input sampled white noise sequence. The total

noise power can be derived as

$$\sigma_n^2 = \frac{1}{2\pi j} \oint \Phi_{n_o n_o} z^{-1} dz .$$

2-49

Substituting Equation 2-48 into Equation 2-49 yields

$$\sigma_n^2 = \frac{1}{j2\pi} \oint H(z)H(z^{-1})\Phi_{n_i n_i}^s (z)z^{-1} dz .$$

2-50

In Equation 2-50, since the integral is along the unit circle the conjugate z^* can be replaced by z^{-1}. The one sided normalized loop noise bandwidth is defined to be

$$2B = \frac{1}{j2\pi} \oint H(z)H(z^{-1})z^{-1} dz$$

2-51

and is related to the one sided loop noise bandwidth as

$$B_L = \frac{B}{T} .$$

2-52

The integral in Equation 2-47 can be computed by expressing B in terms of the coefficients of $H(z)$ and either using the integral tables (Jury 1964) or computing the residues within the unit circle as

$$2B = \sum_i \lim_{z \to z_i} (z - z_i)H(z)H(z^{-1})z^{-1}$$

2-53

where z_i are the first order poles of the integrand within the unit circle. As Equation 2-50 shows, increasing the noise bandwidth will increase the output noise power. However, as previously mentioned, it is required to increase the noise bandwidth to make the loop more responsive to dynamics.

2.2.5 Loop Filters

As mentioned earlier, the loop filter combines the present and past values of the phase error to estimate the phase rate and produce the command signal for the NCO. The transformation method is widely used for designing loop filters, especially for GNSS signal tracking loops. The transformation method implements simply the discrete version of loop filters that have been previously designed for analog loops. However this approach neglects both the inherent delay in the digital loop and variation in the open loop gain by changing the loop update interval (Kazemi et al 2009).

As was shown previously, as long as the product of $\omega T \langle\langle 1$, then there is approximately a linear frequency mapping between the S-plane and the Z-plane. Equation 2-24 shows that the noise bandwidth is directly related to the natural frequency as such in this method the digital loops will imitate the continuous-time loop only if $B_L T$ is close to zero (Lindsey & Chie 1987, Kaplan 2006). As the product $B_L T$ increases, the effective loop noise bandwidth and closed loop pole locations deviate from the desired ones and eventually the loop becomes unstable. In this case the maximum achievable $B_L T$ value depends on the type of the transform function and the original continuous-time filter characteristics (Kazemi et al 2009).

To clarify the above points, a third order loop designed by this technique is analyzed further. For tracking an accelerating frequency input a third-order loop is required. Especially note that GPS receivers have significant Doppler induced by the satellite moving or user motion. As a result usually a third-order loop is required to track the GPS signal.

The typical structure of the filter for the third order loop is shown in Figure 2-13. Various methods are available for determining the filter coefficients (Spilker 1997, Ward 2006, Stephen 2002). The configuration in Ward (2006) is chosen here for more analysis because of its popularity in designing GNSS tracking loops. In this case the filter coefficients can be determined based on the bandwidth consideration as follows:

$$
\begin{aligned}
B_L^d &= 0.7845\omega_n \\
A &= \omega_n^3 \\
B &= 1.1\omega_n^2 \\
C &= 2.4\omega_n
\end{aligned}
\qquad\qquad 2\text{-}54
$$

where B_L^d is the desired noise bandwidth and ω_n is the natural frequency.
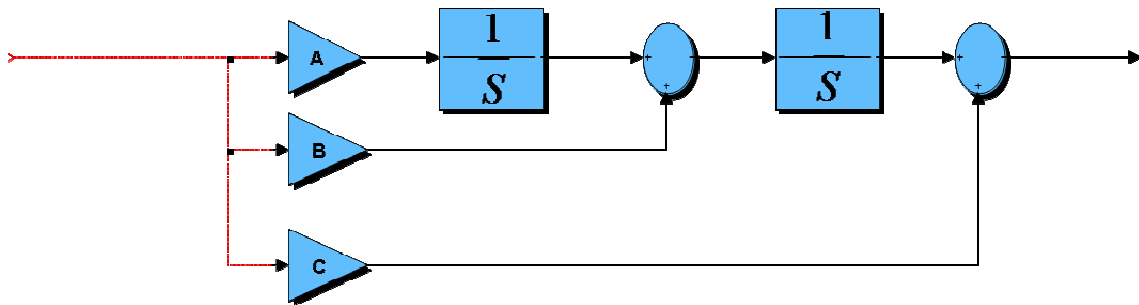
Figure 2-13 Traditional third order loop filter

After deriving the filter coefficients, the filter should be mapped from the S-domain to the Z-domain. Various transformations, such as impulse invariant, step invariant and bilinear transformation, are available, each of which with its unique characteristics. These mapping functions are as follows:

$$\frac{1}{s} \Rightarrow \begin{cases} \dfrac{T(z+1)}{2(z-1)} & \text{Trapzoidal integrator (Bilinear)} \\[2mm] \dfrac{Tz}{(z-1)} & \text{Backward Euler integrator (Boxcar)} \\[2mm] \dfrac{T}{z-1} & \text{Forward Euler integrator} \end{cases} \qquad . \qquad \text{2-55}$$

For instance by choosing the boxcar transform in 2-55 and from Figure 2-13, the filter transfer function can be written as

$$F(z) = \frac{(AT^2 + BT + C)z^2 + (-2C - BT)z + C}{(z-1)^2}. \qquad \text{2-56}$$

Equation 2-56 shows that by changing the update rate of the filter (integration time), the zeros' locations and the total gain of the filter will change. As a consequence, the location of the closed loop poles will alter by changing the integration time. These effects are negligible only when $B_L T$ is near zero (Kazemi et al 2009).

Pole displacement and loop gain alteration has a significant effect on the loop performance. The pole displacements significantly change the noise bandwidth from its desired value and the actual noise bandwidth becomes higher than its desired value by increasing the integration time. This increase in the desired bandwidth should be taken into account in assessing the loop performance. One should expect degradation in loop noise performance. On the other hand the dynamic loop performance will not be improved significantly since this increase is mainly due to the higher undesirable peak value in the magnitude response, rather than a higher 3 dB cut-off frequency.

Figure 2-14 depicts the loop transfer function of a standard third-order loop with an equivalent continuous-time bandwidth (desired bandwidth) of 15 Hz that is updated at

different integration times. It can be inferred from this figure that the update rate of the loop significantly impacts the frequency response. In fact, increasing the integration time causes the loop to lose its low-pass filtering characteristics and as the frequency response shows for high integration times (in this case 100 ms), the loop becomes unstable. This issue is further discussed in Chapter 3.
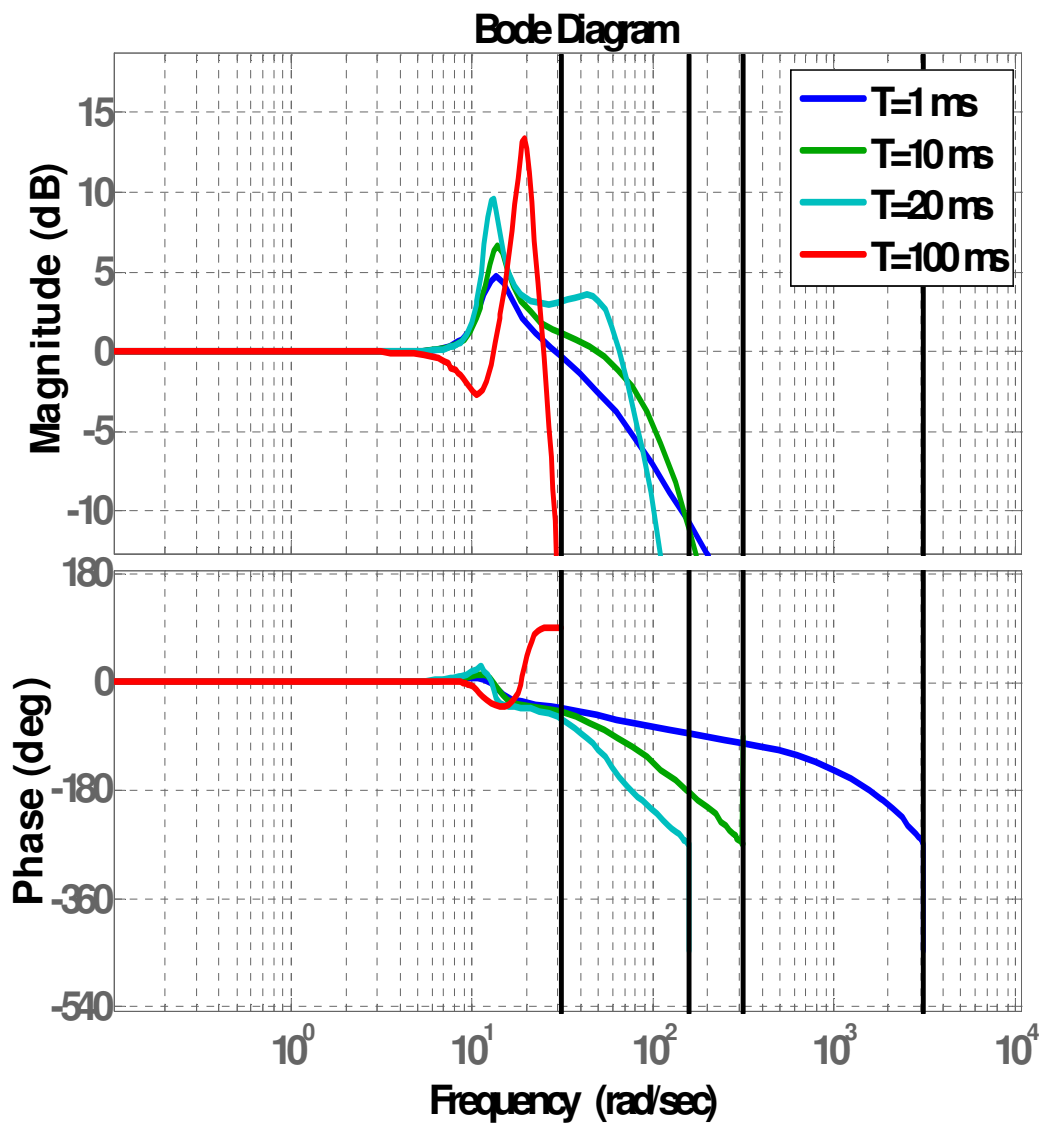
Figure 2-14 Loop noise transfer function of a standard 3rd-order loop with an

equivalent continuous-time bandwidth of 15 Hz updated at different integration

times.

The performance degradation caused by increasing the normalized bandwidth depends on

the type of mapping function, type of NCO and the original continuous-time filter. The

increase in bandwidth from its desired value by increasing the integration time is shown in Figure 2-15 for different kinds of NCOs and mapping functions. Since the continuous-time NCO can be simply modeled as an integrator, in the standard PLL literature, it is stated that the digital NCO can be modeled by any kind of digital integrator. In most cases a boxcar integrator is used to model the NCO. However, as was shown in previous sections, this is not a correct model for common conventional NCOs (rate-only feedback NCOs) and these NCOs should be modeled as bilinear integrators.
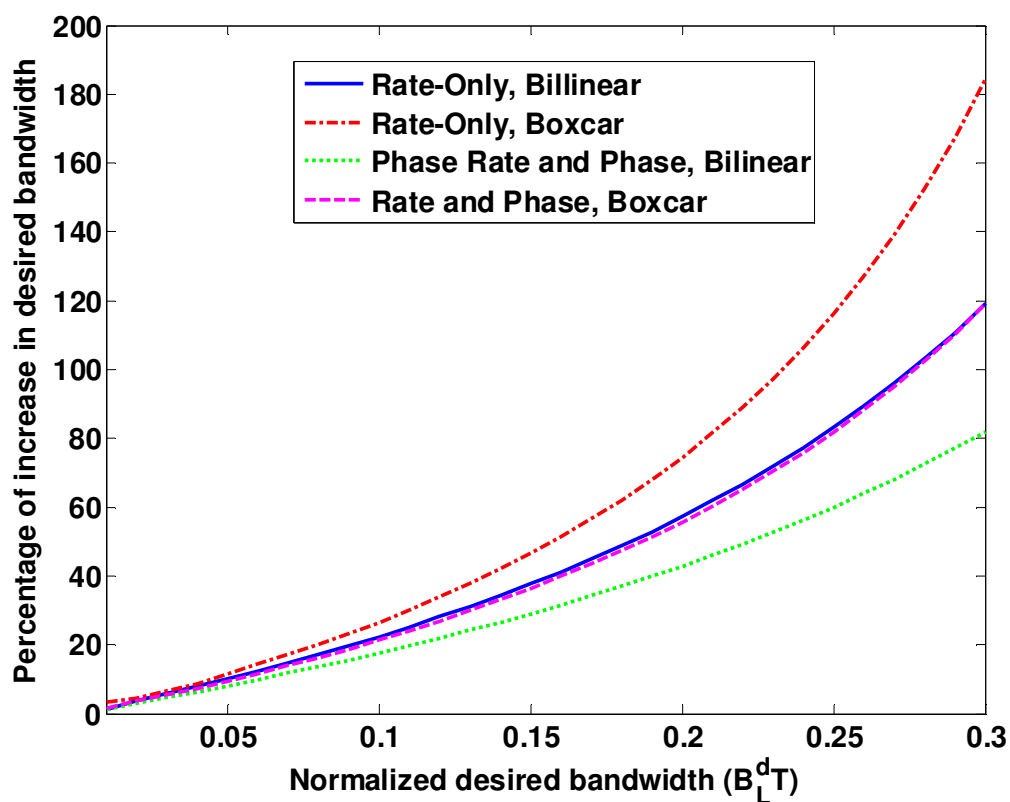
Figure 2-15 Increase in desired bandwidth for different configurations by utilizing transformation method

The deviation of the closed loop poles by increasing the integration time for a fixed 15 Hz desired bandwidth is shown in Figure 2-16. For a stable loop, all of the closed loop

poles should reside inside the unit circle. For the choice of the bilinear transform and phase rate-only feedback NCO, the closed loop poles reside outside the unit circle once a design point normalized bandwidth higher than 0.55 is chosen. As a result one should choose a B_LT less than 0.55, which severely limits the maximum allowable integration time or bandwidth (Kazemi et al 2009).
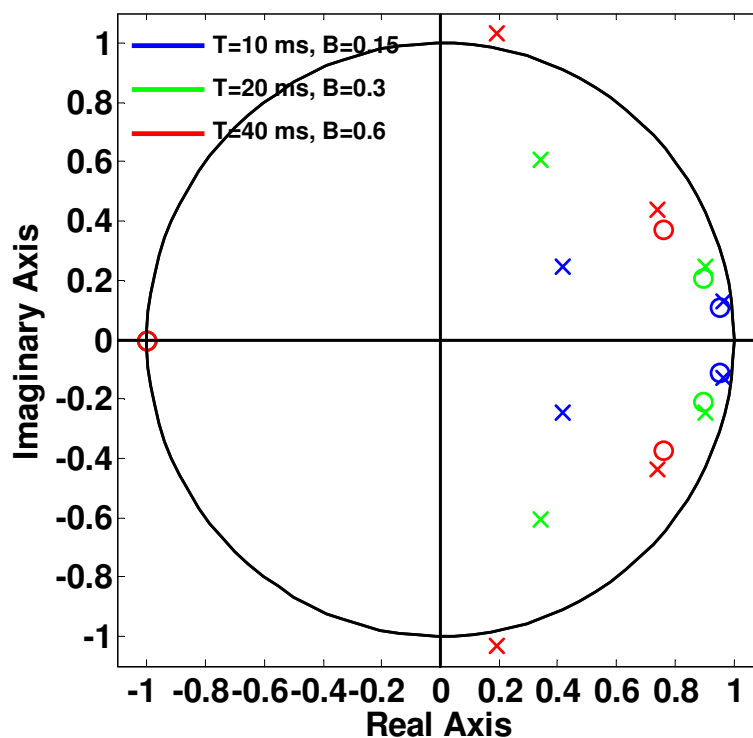
Figure 2-16 Closed loop Poles and zeros locations for a fixed 15 Hz bandwidth and different integration times

One might try to reduce the loop gain to compensate for the increased bandwidth and even make the loop stable. For some cases, reducing the gain might help in reducing the bandwidth as depicted in Figure 2-17. However, as shown in Figure 2-18 for high B_LT

values and because of the improper location of the loop filter's zeros, poles of the closed-loop system will reside outside of the unit circle for all of the gain values. As the cyan and magenta paths show in Figure 2-18 two poles will always reside outside the circle unit, regardless of the loop gain value.
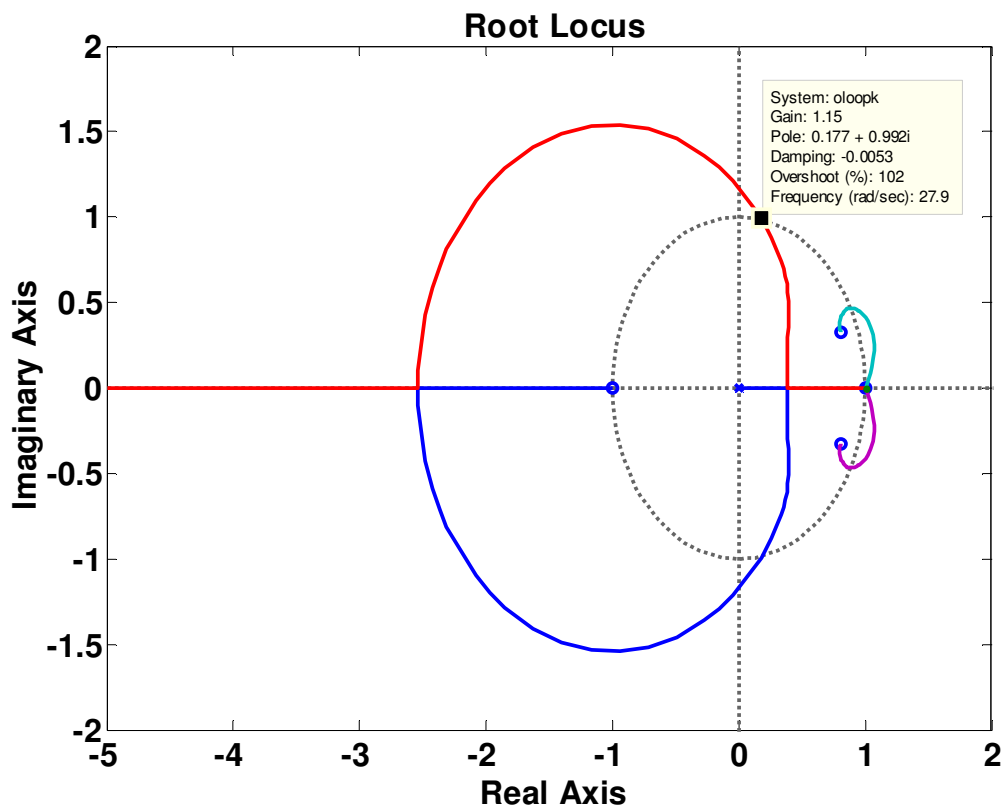
Figure 2-17 Root Locus for B$_L$T=0.5
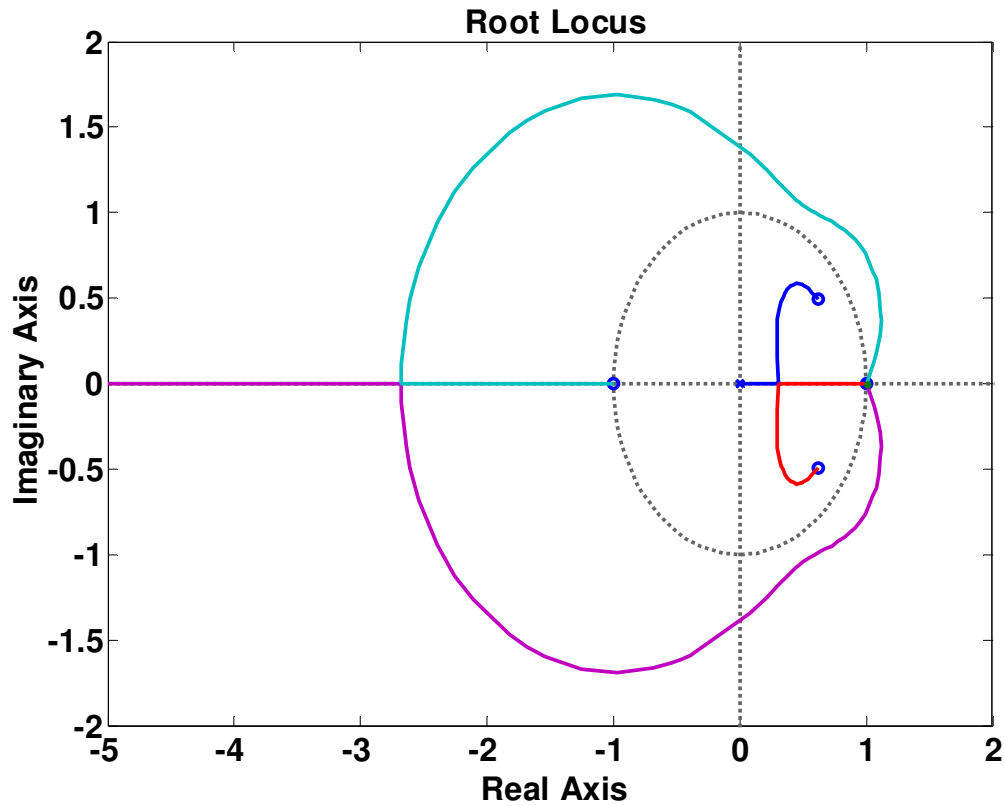
Figure 2-18 Root locus for B$_L$T=0.9

The model adopted here agrees very well with the practical results. Different configurations for live GPS carrier tracking are shown in Figure 2-19. Loss of lock can be seen to occur when a normalized bandwidth of 0.6 is chosen, which supports the theoretical analysis. Assuming that a bandwidth of 15 Hz is required, an integration time of 40 ms results in an unstable loop and loss of lock occurs, hence a lower integration time should be chosen to ensure stability. Similarly, if the integration time is fixed to 20 ms, then a 30 Hz bandwidth results in an unstable loop and lower bandwidth should be chosen. However, for high dynamic applications, large bandwidths are required and for

weak signal tracking applications high integration time are required, whereas this method cannot meet these requirements. Therefore, other techniques which are more robust against low update rate (long integration times) or high bandwidths should be used (Kazemi & O'Driscoll 2008).
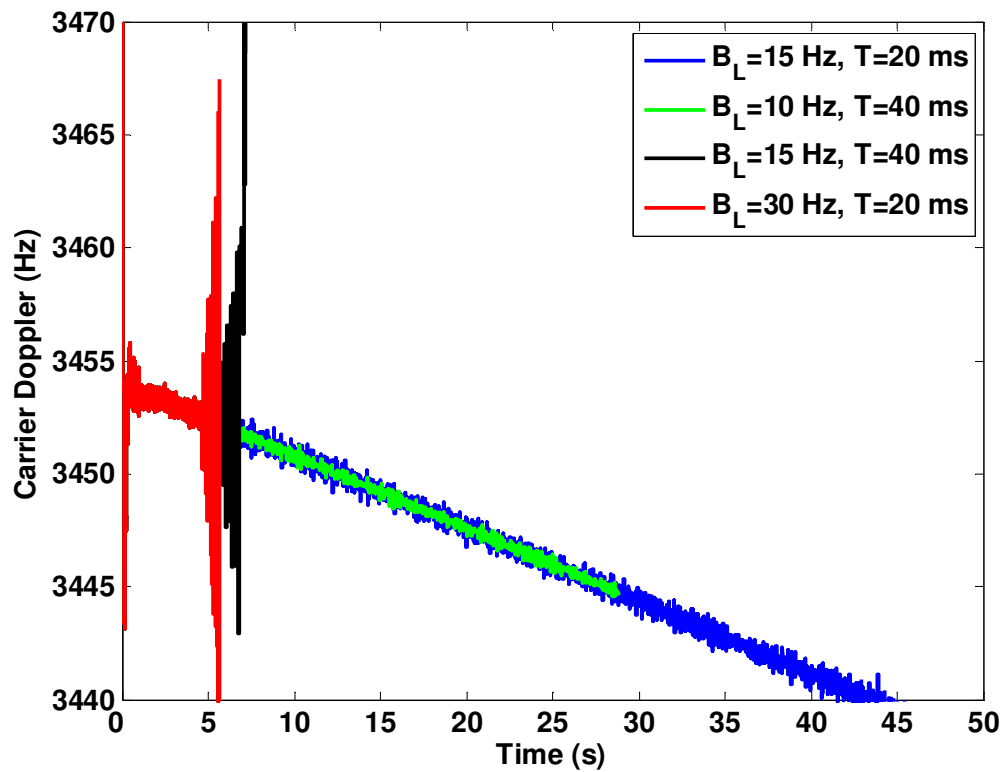
Figure 2-19 Live GPS signal tracking results shows instability of the loop for high normalized bandwidth

Another method which is more robust against normalized bandwidth variations is the controlled-root method (Stephens & Thomas 1995). In this method loop filter coefficients are determined from loop roots that can each be selectively placed in the s-plane on the basis of a direct physical meaning in terms of loop noise bandwidth, root-specific decay

rate, or root-specific damping (Stephens & Thomas 1995). This method effectively solves the deviation caused by the transform from analog domain to digital domain because filter coefficients are derived specifically for each B_LT value. However the structure of the filter is assumed to be based on boxcar integrators (as shown in Figure 2-13 for third order loop) where only the coefficients are determined based on both B_L and T.

Since the structure of the filter remains identical among different NCO transfer functions, the operational range of the loop cannot be increased for all kinds of NCOs (it is assumed that other effects in the loop are modeled in the NCO transfer function). For instance, using this method the B_LT should be kept lower than 0.4 for third order loops with rate-only feedback NCO, which is again a severe limiting factor. However, in comparison with the transformation method, the B_LT limit can be increased significantly for phase and phase rate feedback NCOs.

In Figure 2-20 the frequency response of a tracking loop designed with controlled-root method for $B_LT=0.3$ is compared with the loop designed with the transformation method. The controlled-root method imitates a low-pass filter characteristic relatively better than the transformation method and as shown in Figure 2-21, it has a better transient response with faster settling time and less overshoot.
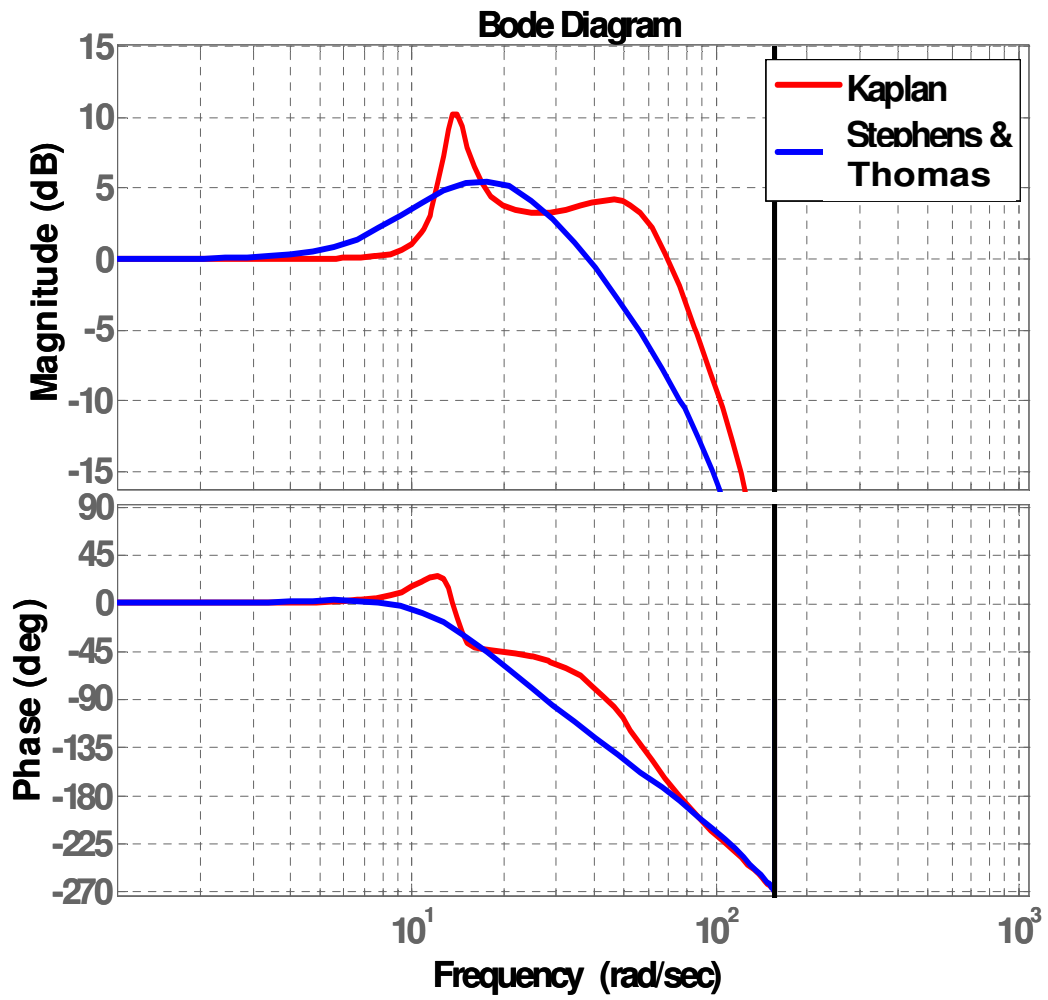
Figure 2-20 Frequency response comparison for B$_L$T=0.3
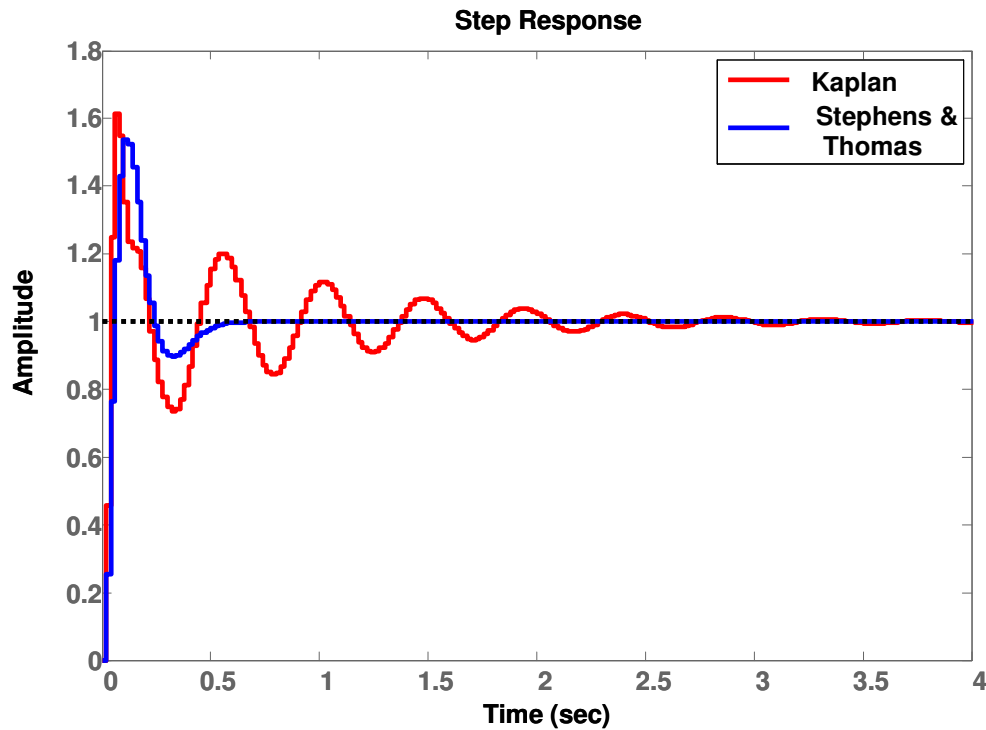
Figure 2-21 Transient response comparison

For the case of normalization by the DC gain, Stephens and Thomas (1995) have shown that superior tracking performance, in terms of cycle slips can be achieved with larger B_LT values. In addition, as it is shown in the next chapter, an increase in B_L for a fixed update interval also results in smaller steady state tracking error. For these reasons the development of phase locked loops with large B_LT values is one of the major goals of this work.

To increase the operational range of the loops and consequently improve the weak signal tracking performance (by increasing T) and dynamic tracking performance (by increasing B_L), the optimum loop structures for the two aforementioned NCOs and first to fourth order loops are derived in the following Chapters.

2.3 Summary

Most of the necessary background knowledge for the PLL operation was covered in this Chapter. The basic theory of carrier phase estimation was reviewed with an emphasis on the closed loop tracking architecture. Proper and simple DPLL modeling in order to predict the DPLL performance in high B_LT values was introduced. It was shown that simple modeling of the transformation from analog domain to digital domain is not sufficient to analyze the DPLL stability. The model adopted herein is based on the average generated phase of the NCO and eventually it will result in a same model as more complicated analysis methods as in Legrand (2002). Different NCO types are also introduced and their effects on the conventional loops are investigated. Specifically, phase and phase-rate feedback NCOs based on Thomas (1989) were introduced for GNSS applications and some of its advantages for medium range integration times were discussed.

The limitations of the traditional tracking loops were discussed and it was shown that basically it is impossible to achieve a B_LT value higher than about 0.6 with traditional design methods and for a third order loop (The exact value depends on the type of the transformation method used).

Chapter Three: New Enhanced GNSS Tracking loops

In this Chapter, the basic architecture for GPS signal tracking is briefly reviewed and its main limitations in weak signal conditions are discussed. By considering the effect of integration and dump in the linear model of the digital phase-locked loop, optimum tracking filters for loops of first to fourth order, for rate only feedback NCO and phase and rate feedback NCO are derived. Optimization is based on the minimization of the loop phase jitter. It is shown that, by using these new filters, a significant improvement for high $B_L T$ can be achieved, allowing one to operate in ranges where previous methods cannot operate. As a result, stable loops with higher bandwidths and/or longer integration time can be easily designed and consequently the sensitivity of the loops can be improved significantly. In order to wipe off the navigation data, for the cases when external data aiding is not available, a decision feedback principle is proposed herein, in which the data bits are estimated through the tracking process itself. New loop filters are implemented in a GPS software receiver and their performance for large $B_L T$ evaluated by using true GPS signals.

3.1 GPS Signal Tracking

GPS signals are spread spectrum signals resulting from the modulation of a sinusoidal carrier by a spreading code and navigation data. The general expression of the received signal at the input of the antenna from a single satellite is

$$r(t) = \sqrt{2P}C(t)D(t)\cos(2\pi f t + \varphi_0) + n(t) \qquad \text{3-1}$$

where P is the signal power, $C(t)$ is the spreading code, D(t) represent the data modulation, f is the carrier frequency including the Doppler effects and φ_0 is the carrier phase and $n(t)$ is an additive white Gaussian noise. The acquisition module gives the initial estimates of the Doppler and code offset, then control will be handed over to tracking loops to track the variations of carrier phase and code offset due to the line of sight movement between satellites and the receiver.

To track an incoming GPS signal, both carrier phase and C/A code need to be matched by the locally generated counterparts. As a result, it requires two loops to track a GPS signal. One loop is to track the C/A code and the other one is to track the carrier frequency. These two loops must be coupled together as shown in Figure 3-1. Usually a Delay locked loop is used for tracking the C/A code and more details about DLLs can be found in Spilker (1997).

Once one of these loops loses lock, the others will lose lock as well. The carrier loop filter output is adjusted by a scale factor and is added to the code loop filter output as aiding. Generally, the carrier loop is a weaker loop because the carrier wavelength is much shorter than the chip length and the carrier loop needs to track all dynamics while the code loop needs only to track the dynamic difference between the carrier loop and code loop when carrier aiding is applied to the code.
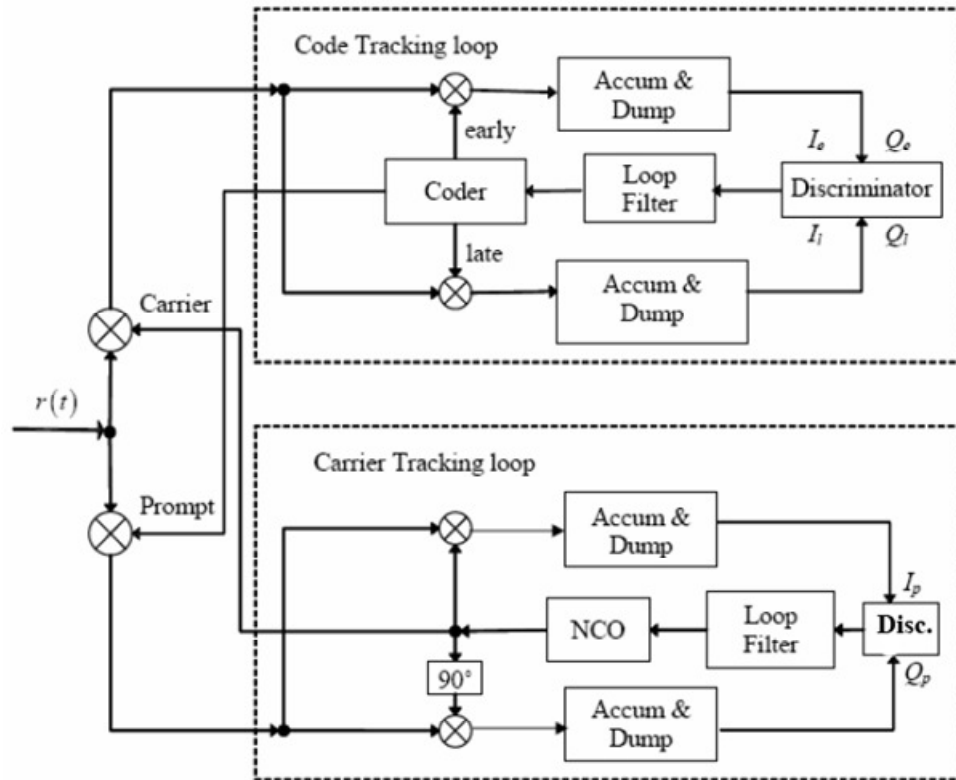
Figure 3-1 Carrier and code tracking loops (Tsui 2000)

Because of the presence of the navigation data a Costas loop which is insensitive to the data modulation should be used. A Costas or squaring loop removes the dependence upon the data values. The basic operation is the same as the digital phase locked loop described in the previous chapter. The input signal whose phase is to be tracked is sampled in quadrature and is mixed with a locally generated signal by the NCO. The resulting complex signal is then accumulated over an update interval of length T to generate the accumulated in-phase (I) and quadrature (Q) components. The phase difference between the incoming and locally generated signal is detected by the discriminator using I and Q components and this phase error is further filtered by the loop filter to generate the control signal for the NCO. The upper arm of the Costas Loop, sometimes called the I

arm (In-phase arm), produces the demodulated data symbol. Without modulation, the quadrature arm produces an error voltage similar to a simple phase-locked loop. Typical phase discriminators for a Costas loop are described in Table 3-1. As shown in Humphreys et al (2005) and Wei (2007), the decision directed discriminator shows relatively superior performance in weak signal conditions.

Table 3-1 Common Costas loop discriminators (Ward 2006)

Discriminator	Output phase error	Remarks
Sign(I)×Q	$\sin(\delta\phi)$	• Decision directed Costas • Near optimal for high SNR • Least computational burden
I×Q	$\sin(2\delta\phi)$	• Classic Costas analog discriminator • Near optimal for low SNR • Moderate computational burden
Q/I	$\tan(\delta\phi)$	• Suboptimal, but works well for Low and high SNR • Higher computational burden
atan(Q/I)	$\delta\phi$	• Two-quadrant arctangent • Optimal (Maximum-likelihood estimator) for both low and high SNR • Highest computational burden

After wiping off the signal carrier and down converting the signal to baseband, then it is passed through the accumulation and dump filter. The normalized version of I and Q samples, which are more convenient for performance analysis, are given by

$$I_i = \frac{\sin(\pi \Delta f T)}{\pi \Delta f T} \sqrt{2 \frac{S}{N_o} T} R(\tau_i) D_i \cos(\Delta \Phi_i) + \eta_{I_i}$$

$$Q_i = \frac{\sin(\pi \Delta f T)}{\pi \Delta f T} \sqrt{2 \frac{S}{N_o} T} R(\tau_i) D_i \sin(\Delta \Phi_i) + \eta_{Q_i}$$

$$E(\eta_{I_i}^2) = E(\eta_{Q_i}^2) = 1$$

$C(t) = PRN\ code\ modulation$;

$D(t) = 50\ bps\ data\ modulation$;

$\Delta f = Frequency\ misalignment\ between\ the\ incoming$ 3-2

$samples\ and\ the\ local\ carrier\ replica$;

$\Delta \Phi = Phase\ misalignment$;

$\dfrac{S}{N_o} = Signal\ to\ noise\ density$;

$T = Coherent\ integration\ time$;

$\eta_{I_i} = Normalized\ In - phase\ noise\ component\ with\ N(0,1)\ distribution$;

$\eta_{Q_i} = Normalized\ In - phase\ noise\ component\ with\ N(0,1)\ distribution$;

The performance of the ATAN discriminator for different SNRs and an integration time of 1 ms is shown in Figure 3-2. Monte Carlo simulations have been performed for this analysis. This figure proves that the discriminator leads to a bias in measuring the phase under low SNR conditions. In such circumstances, the response of the discriminator reduces to a quasi-sine pattern. In this case, since the discriminator does not feedback the correct phase error to the loop, the loop will lose lock.
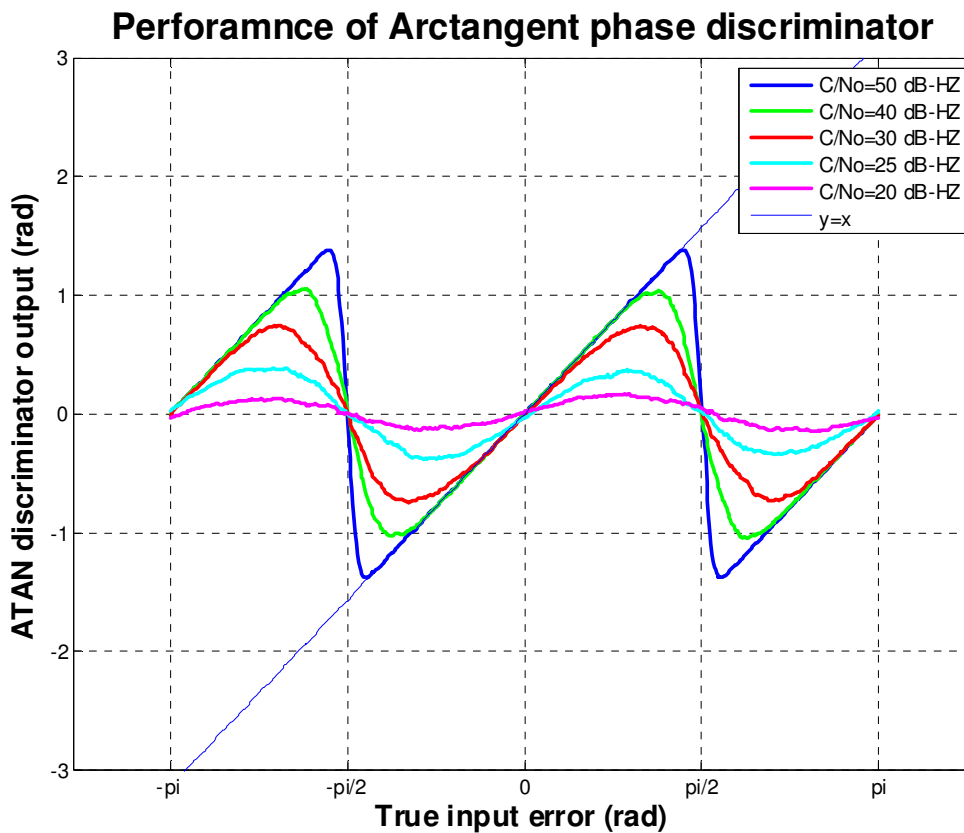
Figure 3-2 Performance of ATAN discriminator for T=1 ms

Figure 3-3 shows the effect of increasing the integration time on the phase discriminator output. As Figure 3-3 indicates it is possible to enhance the SNR by increasing the coherent integration and prevent loss of lock in weak signal conditions.
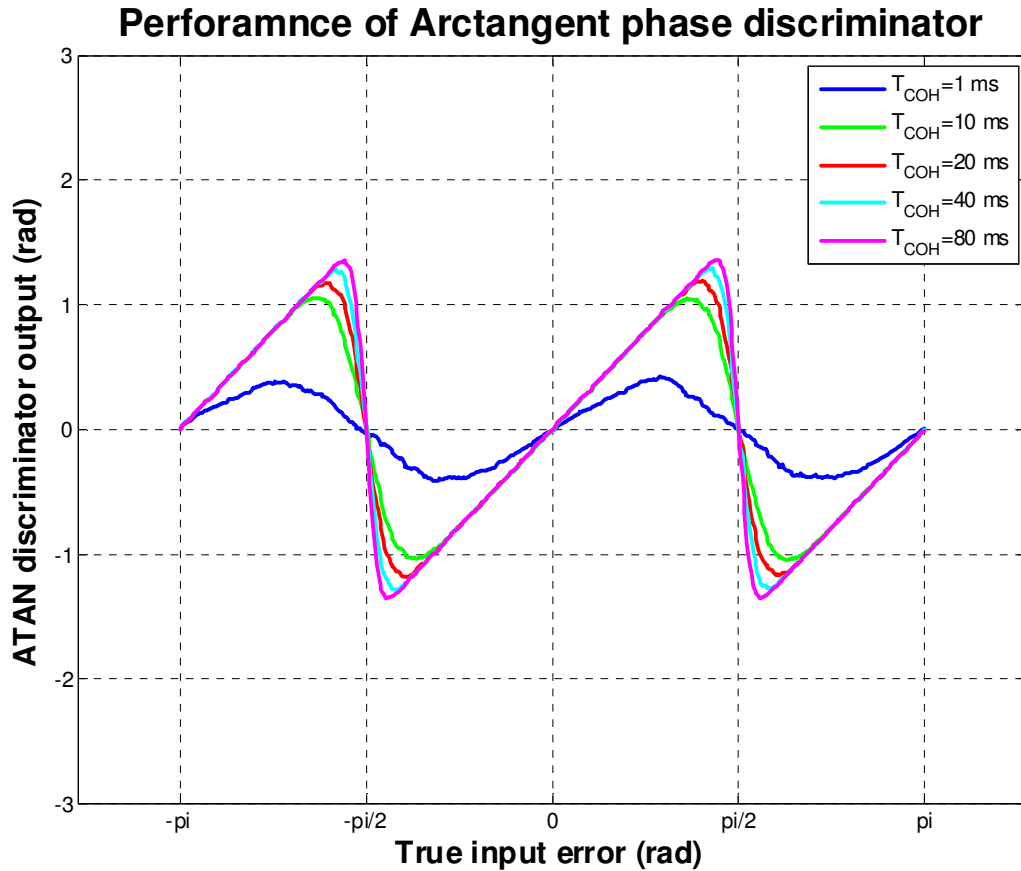
Figure 3-3 Effect of increasing integration time on phase discriminator performance

for C/N$_0$ =26 dB-Hz

For increasing the integration time, bit synchronization should first be performed. After initial C/A-code acquisition, databit timing is subject to navigation bit offset ambiguity. This ambiguity is due to a lack of knowledge in the databit timing, namely the offset of the databits transmitted. The beginning of each C/A-code period is known, but it is not known where the navigation bit data, which is composed of 20 C/A-code periods, begins. For bit synchronization the histogram method could be utilized (Van Dierendonck 1997). The histogram method partitions the assumed databit period into C/A-code periods. The 20 ms databit length is separated into 20, 1 ms C/A-code periods. The algorithm senses

sign changes between successive code periods and records these sign changes by incrementing the count in the bin corresponding to that particular code period. This technique is discussed by Van Dierendonck (1997). This method doesn't have good performance in lower SNRs since it relies on the 1 ms of accumulated data. As a result, usually it is required to first initialize the receiver in strong signal conditions. After bit synchronization the integration time can be increased as shown in Figure 3-4. The accumulation and dump filter outputs for different integration times are shown in Figure 3-5. Note that the maximum allowable integration by this technique is limited to the duration of navigation data (20 ms for L1 signal).
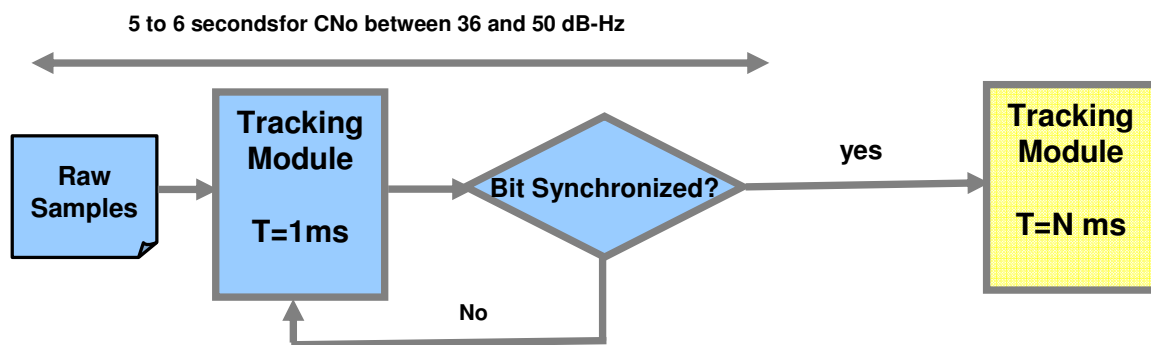
Figure 3-4 Initialization of the software receiver
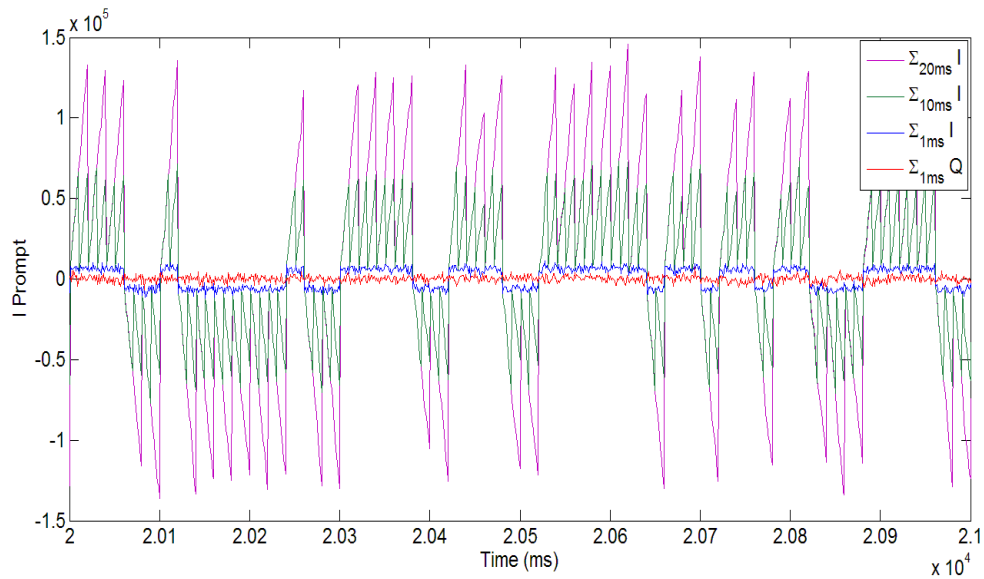
Figure 3-5 Accumulators output for different integration times

The noise reduction effect of the integration time at the outputs of the PLL and DLL discriminators based on the live GPS signal is shown in Figure 3-6. As the average phase error estimation becomes more accurate, consequently less noisy Doppler estimation is achieved. This effect is shown in Figure 3-7. One-sigma jitter of PLL and DLL discriminators for different SNRs and integration times is summarized in Table 3-2.
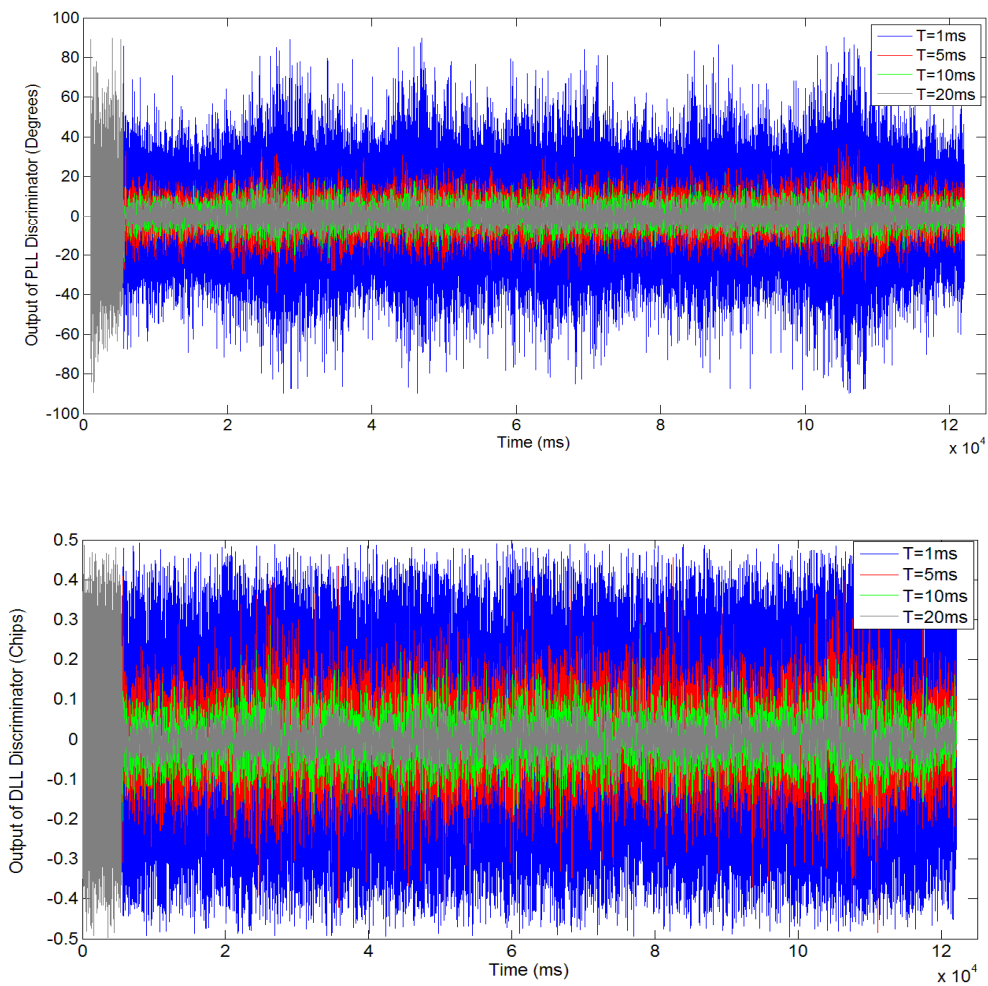
Figure 3-6 Noise reduction effect by increasing the integration time at the output of the PLL and DLL discriminators
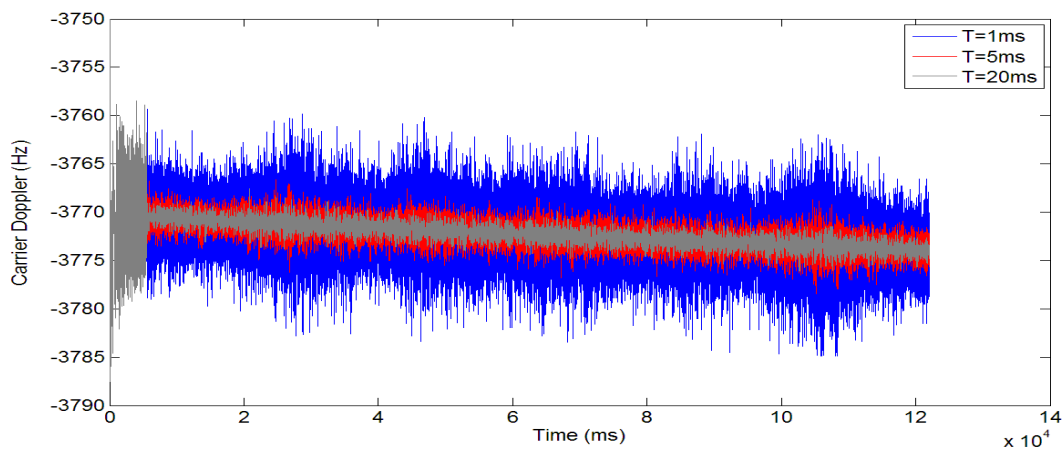
Figure 3-7 Carrier Doppler

Table 3-2 1-Sigma Jitter of PLL and DLL discriminators for different integration times

	PRN 6 ,CNo=50 dB-Hz		PRN 16 ,CNo=42 dB-Hz		PRN 30, CNo=37 dB-Hz	
	1-Sigma PLL Jitter (Deg.)	1-Sigma DLL Jitter (Chips)	1-Sigma PLL Jitter (Deg.)	1-Sigma DLL Jitter (Chips)	1-Sigma PLL Jitter (Deg.)	1-Sigma DLL Jitter (Chips)
T=1 ms	4.41	0.05	11.73	0.13	18.33	0.16
T=5 ms	1.97	0.02	5.26	0.06	8.16	0.09
T=10 ms	1.55	0.01	4.05	0.04	5.88	0.06
T=20 ms	1.50	0.01	3.90	0.03	5.59	0.04

Integration time is a compromise design parameter and must be as long as possible to operate under weak or RF interference signal conditions. On the other hand, it must be as short as possible to operate under high dynamic stress signal conditions. There are three main challenges in increasing the coherent integration time:

- If the coherent integration periods include a data bit boundary, the possible phase reversal may negate the positive effects of extended integration. In the case of L1 GPS signal where the data bit rate is 50 Hz the maximum allowable coherent integration time becomes 20 ms.

- Even in the absence of data transitions, the extension of coherent integration time proportionally reduces the tolerable frequency error due to the sinc pattern in signal after the accumulation and dump process. This effect is depicted in Figure 3-8.
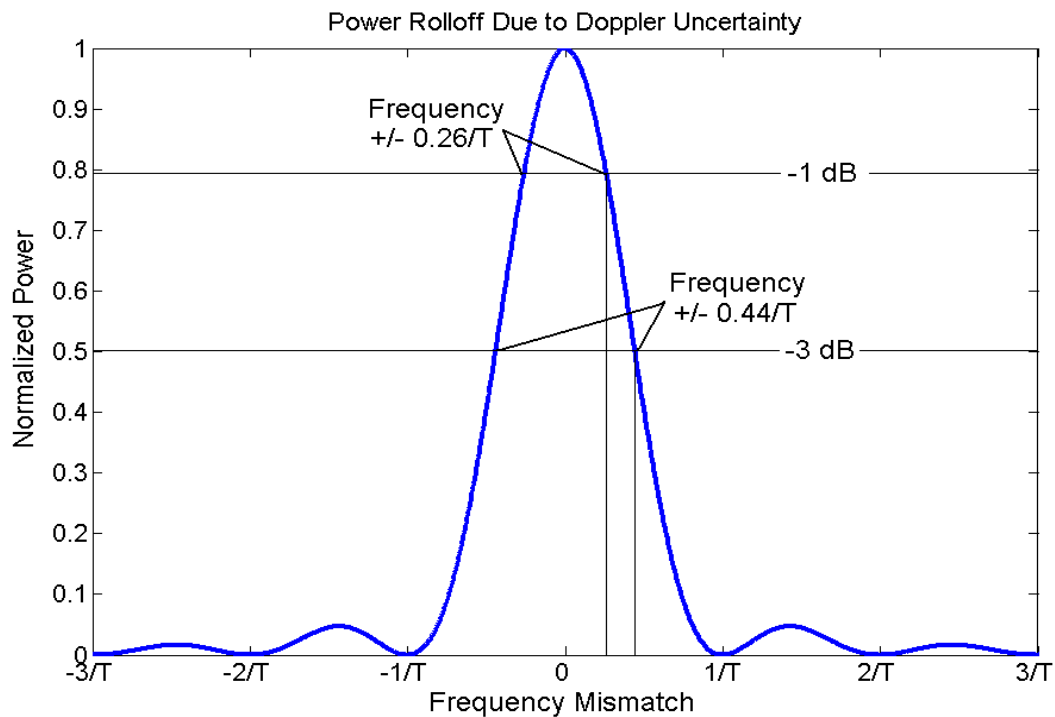
Figure 3-8 Effect of frequency error on SNR

- As was shown in the previous Chapter, traditional GPS tracking loops are based on digital approximations of analog loops and these approximations break down as integration time increases. The product between loop noise bandwidth and integration time ($B_L T$) should remain near zero.

3.2 Decision Feedback Stand-alone Technique

The presence of navigation data modulation typically limits the coherent integration time to less than 20 ms. Modernized GPS solve this problem by adding a pilot channel beside the data channel for L5 and L2C signals. However the presence of navigation data is still a problem for weak L1 GPS signal tracking. In order to integrate beyond the navigation data boundaries, Assisted GPS (AGPS) can be utilized as a possible solution for this problem. Assistance data would include items such as satellite ephemeris or almanac, timing, position and frequency information and navigation data. Assistance data can be delivered via different wireless networks which use wireless standards such as the Global System for Mobile Communications (GSM) or CDMA among others (Singh 2006). However, establishment of a wireless network might not be possible everywhere. Only navigation data is considered as an external assistance in this thesis. In this way, results could be extended to stand-alone receivers for modernized GPS signals which benefit from a dataless channel.

For the cases when external data aiding is not available, a simple method based on the decision feedback principle is proposed here, in which the data bits are estimated through the tracking process itself. By using a DPLL and assuming low residual phase

errors, a sign detector can be used as an optimum solution for the data message (Proakis 2000). In this case the sign of the 20 ms prompt in-phase accumulator is used as an estimator to detect the data and compensate for the data transition in order to integrate for longer than 20 ms. This scheme is shown in Figure 3-9. Besides 20 ms integrators, T ms integrators are also introduced. After each 20 ms the possible phase reversal caused by the navigation data is detected and the T ms integrators output are corrected accordingly.
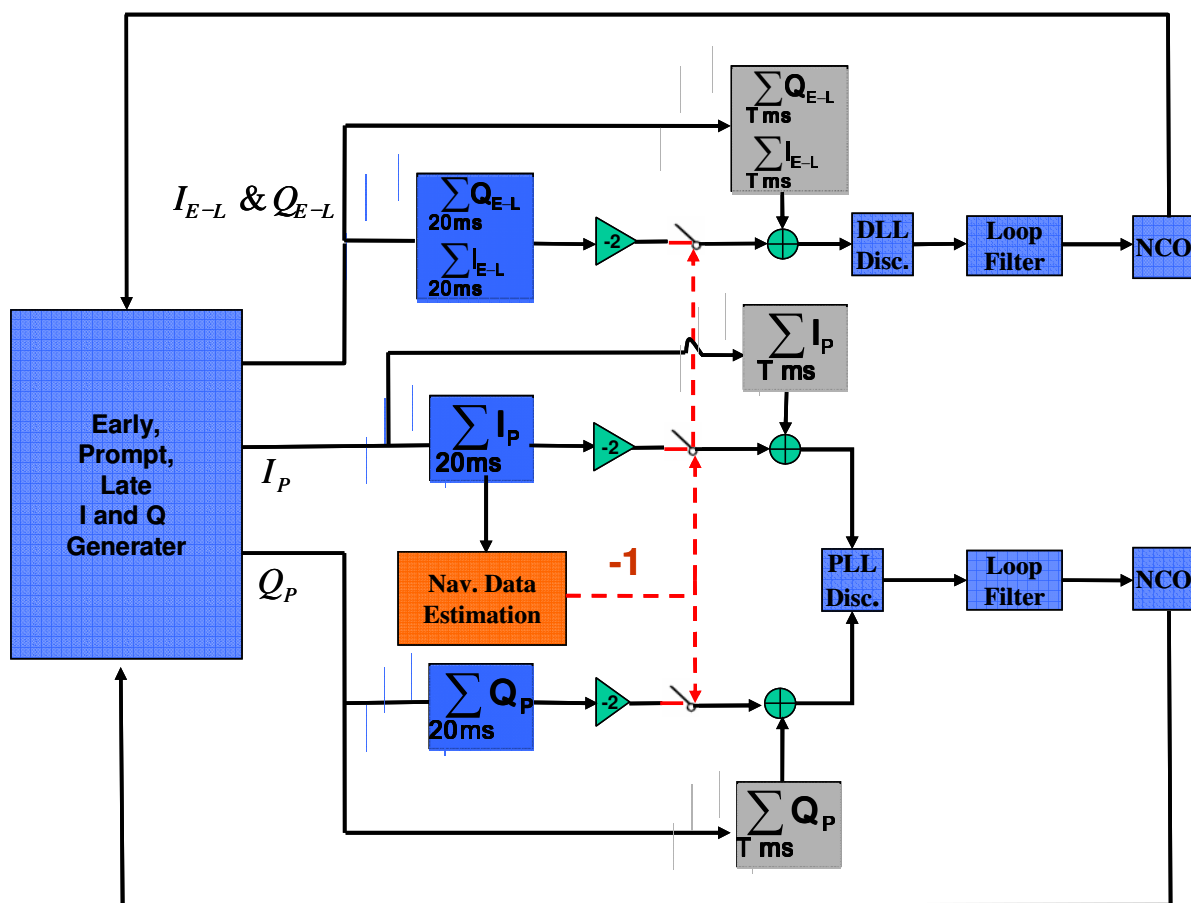
Figure 3-9 Stand-alone GPS tracking loops

The performance of this technique depends on the BER performance of the loop. The conditional BER for the BPSK with phase error is given by (Proakis 1989)

$$P_e = \frac{1}{2} erfc(\sqrt{SNR} \cos(\varphi_e))$$
3-3

where *erfc(.)* is the complementary error function and SNR is the signal to noise ratio (SNR) per bit of the received signal and φ_e is the phase error.

As shown later using live GPS signals, the proposed technique in Figure 3-9 can reduce the noise significantly for C/N_0 higher than 20 dB-Hz. Since it does not increase the computation burden significantly, this technique is recommended in order to integrate beyond 20 ms and increase the raw measurements accuracy of the tracking loops.

Due to the BER performance of the BPSK modulation it is recommended to use external assistance to wipe off the navigation data for C/N_0 values less than 20 dB-Hz (where the BER is lower than about 0.01). Unfortunately the Hamming coding on L1 GPS signal does not allow for bit error correction (it allows only for error detection). However for modernized GPS signals, the available FEC (Forward Error Correction) convolutional coding allows for error correction as well. As a result the performance of the proposed technique herein can be improved.

Other techniques such as an energy-based detector (Soloviev et al 2004) are mainly useful when there is a imbalance between I and Q channels and the signal power is distributed between the I and Q channels (for instance in FLL). This detector searches for

the bit combination which gives the maximum energy over the integration interval. However, these techniques increase the computation burden significantly.

One of the advantages of using long integration times is in reducing the processing time and the required computations since the loop will be updated less frequently. The sign detector does not increase the computation count in comparison with conventional methods since the presence of 20 ms accumulators is required in classical loops as well. As a result the receiver can benefit from faster processing time (Kazemi & O'Driscoll 2008).

3.3 Optimum Digital Filters for GNSS Tracking Loops

Even after wiping off the navigation data the maximum achievable B_LT for a stable loop is limited to 0.4 for rate-only feedback NCOs (Stephens & Thomas 1995). For most communication applications, this condition is satisfied since B_LT remains close to zero. However for some GNSS applications, such as weak signal tracking and for extremely high dynamic applications, larger B_LT values are required. Configurations with a 20 ms integration time and a 60 Hz bandwidth ($B_LT = 1.2$) or with a 500 ms integration time and a 3 Hz bandwidth ($B_LT = 1.5$) are impossible with these conventional methods.

A method which has been rarely treated in the literature is the minimization method. This method was first used in Gupta (1968) using the Z-transform and modified Z-transform for analog-digital phase-locked loops. In this case the phase-locked loop is the same as for the continuous case except that the filter is replaced by a discrete filter followed by a hold circuit.

The main focus of this part is the design of digital tracking loops directly in the Z-domain based on the linear model of the DPLL. More specifically a minimization technique is used to determine the filter structure and coefficients. These parameters are determined in order to minimize the variance of the phase error. The effect of the integration time is considered in the linear model to extend the operational range of the filter to larger $B_L T$ values. Instantaneous update of the loop filter (i.e., the absence of computational delay) is assumed. Two kinds of NCOs, namely phase and phase-rate feedback NCO and phase-rate only feedback NCO, are considered. This minimization technique for filter design has, to the best of the author's knowledge, never been applied to GNSS software receivers with the two aforementioned kinds of NCOs nor has it been designed up to fourth order loops. As will be shown later, it becomes possible to increase the $B_L T$ limit of the tracking loops beyond any other previous methods (Kazemi 2008) using this technique.

3.3.1 General Design Methodology

The design of the optimum digital filter is based on the minimization of the following function:

$$Q = \overline{n_0^{\,2}(k)} + \lambda \sum_k \varepsilon^2(k) \qquad\qquad 3\text{-}4$$

where the random component of the NCO phase, due to the input noise is denoted by n_0 and $\varepsilon(k) = \theta(k) - \theta_0(k)$ is the deterministic component of the phase difference between incoming and generated phase. The parameter λ is determined on the basis of noise

bandwidth considerations. While minimizing Equation 3-4 the overall transfer function of the loop can be found as a function of λ. For any desired noise bandwidth, a specific λ exists which can be substituted in the transfer function. The first term on the right hand side of the Equation 3-4 can be expressed in terms of the closed loop transfer function *H(z)* as follows:

$$\overline{n_0^{\,2}(k)} = \frac{1}{2\pi j}\int_\Gamma \Phi_{n_0 n_0}(z)\frac{dz}{z} \qquad\qquad 3\text{-}5$$

where Γ represents the unit circle, $\Phi_{n_0 n_0}$ is the noise spectral density of n_0 and is related to the input noise spectral density by

$$\Phi_{n_0 n_0}(z) = H(z)H(z^{-1})\Phi_{n_i n_i}(z). \qquad\qquad 3\text{-}6$$

Denoting the Z transforms of $\varepsilon(k)$ and $\theta(k)$ by *E(z)* and $\Theta(z)$ respectively, the second term of Equation 3-4 from Parseval's theorem (Proakis 2000) can be written as

$$\sum_k \varepsilon^2(k) = \frac{1}{2\pi j}\int_\Gamma E(z)E(z^{-1})\frac{dz}{z}$$
$$= \frac{1}{2\pi j}\int_\Gamma (1 - H(z))(1 - H(z^{-1}))\Phi_{\theta\theta}\frac{dz}{z} \qquad\qquad 3\text{-}7$$

where

$$\Phi_{\theta\theta} = \Theta(z)\Theta(z^{-1}). \qquad\qquad 3\text{-}8$$

From Equations 3-5 and 3-7, the cost function can be written as

$$Q = \frac{1}{2\pi j}\int_\Gamma [(1 - W(z)N(z) - W(z^{-1})N(z^{-1}))\lambda\Phi_{\theta\theta}$$
$$+ P(z)W(z)W(z^{-1})]\frac{dz}{z} \qquad\qquad 3\text{-}9$$

where

$$W(z) = \frac{H(z)}{N(z)}$$

3-10

and

$$P(z) = [\rho + \lambda\Phi_{\theta\theta}(z)]N(z)N(z^{-1})$$

3-11

where ρ is the power spectral density of the noise. By applying the standard minimization procedure to Q, the optimum solution for $W(z)$ and thus $F(z)$ can be found as (Jury 1964)

$$W_0(z) = \frac{z[\dfrac{\lambda N(z^{-1})\Phi_{\theta\theta}(z)}{zP^-(z)}]_+}{P^+(z)}$$

3-12

where

$$P(z) = P^+(z)P^-(z).$$

3-13

In the above, contrary to the minus part $P^+(z)$ is the part of $P(z)$ whose poles and zeros lay inside the unit circle and $[\ ]_+$ represents the part of the partial fraction expansion of its argument whose poles are inside the unit circle. Finally from Equations 2-36, 3-10 and 3-12 the optimum digital filter transfer function is found as

$$F(z) = \frac{W_0(z)}{1 - W_0(z)N(z)}.$$

3-14

The optimum filter in Equation 3-4 is a function of λ and, as mentioned earlier, this parameter is determined from noise bandwidth considerations which can be computed by Equation 2-51.

In the following two different transfer functions of the aforementioned NCOs with four different inputs (resulting in first to fourth order loops) will be considered. The material presented here mainly follows the work of Kazemi et al (2009).

3.3.2 Loop Filter Design for Phase Step

In this case $\theta(t) = u(t)$, where $u(t)$ the step function, and Equation 3-8 becomes

$$\Phi_{\theta\theta} = \frac{z}{(z-1)} \cdot \frac{z^{-1}}{(z^{-1}-1)}. \qquad \text{3-15}$$

3.3.2.1 Phase and Phase rate Feedback NCO

The transfer function of the phase and phase-rate NCO is given by Equation 2-46 and, from Equation 3-11, $P(z)$ can be written as

$$P(z) = \frac{\rho T^2 z(-z^2 + (2+h_1)z - 1)}{(z-1)^4} =$$

$$\left\{ \frac{\rho T^2 (az^2 + bz)}{(z-1)^2} \right\} \cdot \left\{ \frac{az^{-2} + bz^{-1}}{(z^{-1}-1)^2} \right\} \qquad \text{3-16}$$

where

$$h_1 = \frac{\lambda}{\rho}. \qquad \text{3-17}$$

The terms in the brackets of Equation 3-16 represent $P(z)^+$ and $P^-(z)$, respectively. By equating the coefficients of equal powers of z in Equation 3-16, the following set of equations are obtained:

$$\begin{cases} ab = -1 \\ a^2 + b^2 = 2 + h_1 \end{cases}.$$

3-18

From the available solutions of Equation 3-18, the one which has the root of $az+b$ inside

the unit circle is acceptable. From Equations 2-42, 3-15 and 3-16, the argument of the [

]+ operator in Equation 3-12 can be written as

$$\frac{\lambda N(z^{-1})\Phi_{\theta\theta}(z)}{zP^{-}(z)} = \frac{\lambda Tz}{(z-1)(bz+a)}.$$

3-19

By considering the fact that the roots of $bz+a$ are outside the unit circle (note this is part

of the $P^{-}(z)$, which has all of its poles and zeros outside the unit circle) and writing the

partial expansion of 3-19, $W_0(z)$ can be found as

$$W_0(z) = \frac{\lambda(z-1)}{T\rho(a+b)(az+b)}.$$

3-20

From Equation 3-18 it can be easily derived that $(a+b)^2 = h_1$. Utilizing this fact in

Equation 3-20, $W_0(z)$ can be simplified to

$$W_0(z) = \frac{(z-1)(a+b)}{T(az+b)}.$$

3-21

Finally from Equations 2-42, 3-14 and 3-21, the optimum filter can be found as

$$F_p(z) = \frac{(a+b)}{Ta} = \frac{K}{T}$$

3-22

where K is the loop optimum gain. As Equation 3-22 shows, the optimum filter for the

first order loop with phase and phase rate feedback NCO only consists of an optimum

gain. In order to find the coefficients of the filter for different noise bandwidths, Equation

3-18 should be solved for a range of values of h_1. From these coefficients, the filter gain

in Equation 3-22 can be computed. Finally from Equations 2-36 and 2-47 the normalized

bandwidth is obtained. Figure 3-10 shows the typical value of h_1 required to obtain the

normalized bandwidth in a large B_LT region. The optimum gain of the filter as a function

of a normalized bandwidth is shown in Figure 3-11.
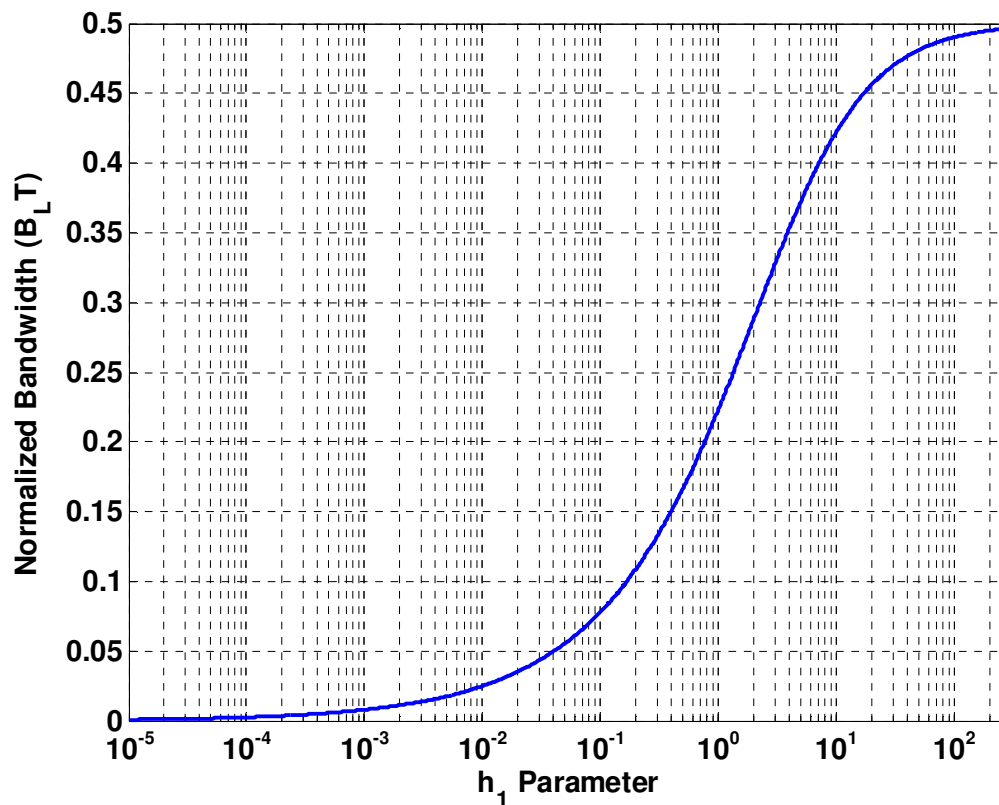
Figure 3-10 One-sided Normalized Bandwidth versus the h_1 parameter.
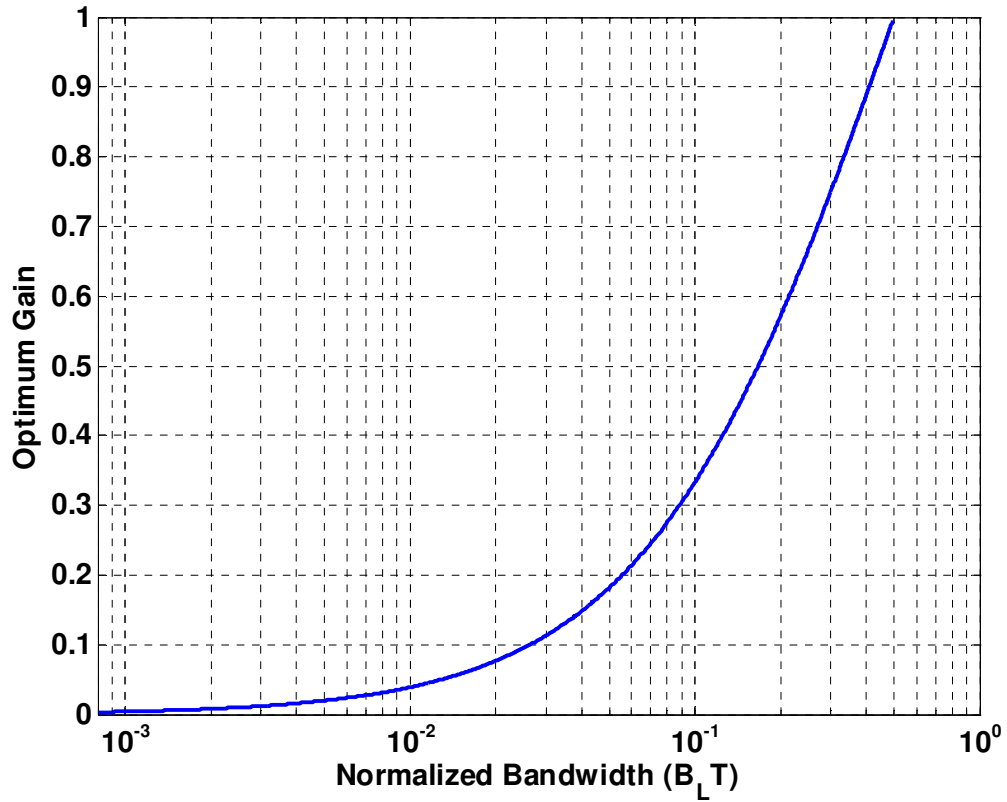
Figure 3-11 Optimum gain versus Normalized Bandwidth for first order loop

3.3.2.2 Phase Rate-only Feedback NCO

In this case the transfer function of the NCO is given by (3) and $P(z)$ becomes

$$P(z) = \frac{\rho T^2 (z+1)^2 (-z^2 + (2+h_1)z - 1)}{4(z-1)^4} =$$

$$\left\{ \frac{\rho T^2 (\bar{a}z^2 + \bar{b}z + \bar{c})}{4(z-1)^2} \right\} \cdot \left\{ \frac{\bar{a}z^{-2} + \bar{b}z^{-1} + \bar{c}}{(z^{-1}-1)^2} \right\}.$$

3-23

By equating the coefficients of equal powers of z in Equation 3-23, the following set of equations are obtained:

$$\begin{cases} \overline{a}\,\overline{c} = -1 \\ \overline{a}\,\overline{b} + \overline{b}\,\overline{c} = h_1 \\ \overline{a}^2 + \overline{b}^2 + \overline{c}^2 = 2 + 2h_1 \end{cases}$$

3-24

Note that Equation 3-24 has one extra unknown in comparison with Equation 3-18. From Equations 3-12 and 3-23 and the fact that $(\overline{a} + \overline{b} + \overline{c})^2 = 4h_1$, $W_0(z)$ can be derived as

$$W_0(z) = \frac{z(z-1)(\overline{a} + \overline{b} + \overline{c})}{T(\overline{a}z^2 + \overline{b}z + \overline{c})}.$$

3-25

Finally the optimum filter for the phase rate only feedback NCO can be obtained as

$$F_r(z) = \frac{2(\overline{a} + \overline{b} + \overline{c})z}{T(2\overline{a}z + \overline{b} - \overline{c} + \overline{a})}.$$

3-26

As Equation 3-26 shows, even for the first order loop, the filter structure does not consist of only a gain. This fact cannot be predicted by conventional loop design techniques. By computing the pole location of Equation 3-26 for different values of h_1, it turns out that the filter's pole lies at z=-1. Also for the same h_1 value the optimum gain of the filter is twice the gain in Equation 3-22.

These facts suggest the same optimum open loop transfer functions for these two kinds of NCOs:

$$N_p(z)F_p(z) = N_r(z)F_r(z)$$

3-27

and from Equations 2-38 and 2-42, one obtains

$$F_r(z) = \frac{2z}{(z+1)}F_p(z)$$

3-28

Note that Equation 3-27 is also valid for higher order loops, hence it is enough to derive the optimum filter structure only for one of the aforementioned NCOs and to use Equation 3-28 to derive the other one. However, this optimum open loop transfer function cannot be used for all kinds of NCOs. For instance, in the presence of additional computational delay in the transfer function of the NCO the optimum solution will result in a different open loop transfer function.

As mentioned earlier the presence of the pole at z=-1 and zero at z=0 cannot be predicted by conventional methods. The presence of these terms in the filter structure is the key in increasing the operational range of the loop (operating in high normalized bandwidth values). Contrary to the controlled-root method in which the maximum normalized bandwidth is limited to 0.3333 for the first order loop with phase rate-only feedback NCO, this value can be increased up to 0.5 when the optimum structure derived here is used. Note that from Equation 3-27, the same loop performance is expected in theory, regardless of the NCO type used. However, in practice the imperfect cancellation of the filter pole at z=-1 with the zero of the NCO at z=-1 might cause instability problems. Therefore the location of this pole should be modified. These issues are further discussed in section 3.5.

3.3.3 Loop Filter Design for Phase Ramp

The designed loops for this case are equivalent to their second order continuous time counterparts. In this case $\theta(t) = tu(t)$, and Equation 3-8 becomes

$$\Phi_{\theta\theta} = \frac{Tz}{(z-1)^2} \cdot \frac{Tz^{-1}}{(z^{-1}-1)^2}.$$

3-29

The design procedure is demonstrated using a phase and phase rate feedback NCO and then Equation 3-27 is used to obtain the filter structure for phase rate only feedback NCO. However, for the latter case the filter structure could be also be derived directly as it was done for the first order loop.

From Equations 2-42 and 3-11 $P(z)$ can be written as

$$P(z) = \frac{-\rho T^3 z(z^4 - 4z^3 + (6+h_2)z^2 - 4z + 1)}{(z-1)^6} =$$
$$\left\{ \frac{\rho T^3 (az^3 + bz^2 + cz)}{(z-1)^3} \right\} \cdot \left\{ \frac{az^{-3} + bz^{-2} + cz^{-1}}{(z^{-1}-1)^3} \right\}$$

3-30

where

$$h_2 = \frac{\lambda T^2}{\rho}.$$

3-31

By equating the coefficients of equal powers of z in Equation 3-30, the following set of equations are obtained:

$$\begin{cases} ac = 1 \\ ab + bc = -4 \\ a^2 + b^2 + c^2 = 6 + h_2 \end{cases}$$

3-32

The acceptable solution from the above equation is the one which causes the roots of $az^2 + bz + c$ to lie inside the unit circle. By considering the facts that the roots of $a + bz + cz^2$ are outside the unit circle and $(a+b+c)^2 = h_2$, $W_0(z)$ can be computed as

$$W_0(z) = \frac{((2a+b)z - a + c)(z-1)}{T(az^2 + bz + c)}.$$

3-33

Finally from Equations 2-42, 3-14 and 3-33 the optimum filter can be found as

$$F_p(z) = \frac{(2a+b)z + c - a}{Ta(z-1)} = \frac{K(z - z_z)}{T(z-1)}$$

3-34

where K is the optimum open loop gain and z_z is the optimum zero location of the filter. These values are depicted in Figure 3-12 respectively for different normalized noise bandwidths. The required h_2 values for different normalized noise bandwidths are shown in Figure 3-13.
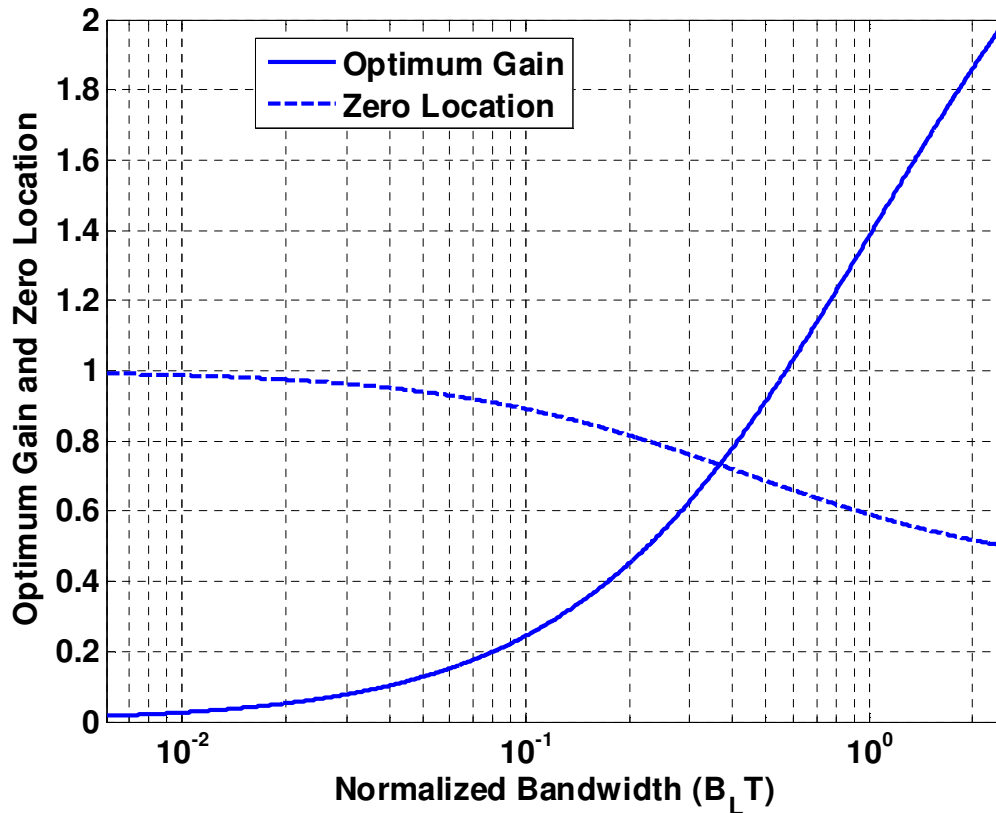
Figure 3-12 Optimum gain and zero location versus Normalized Bandwidth for a second order loop
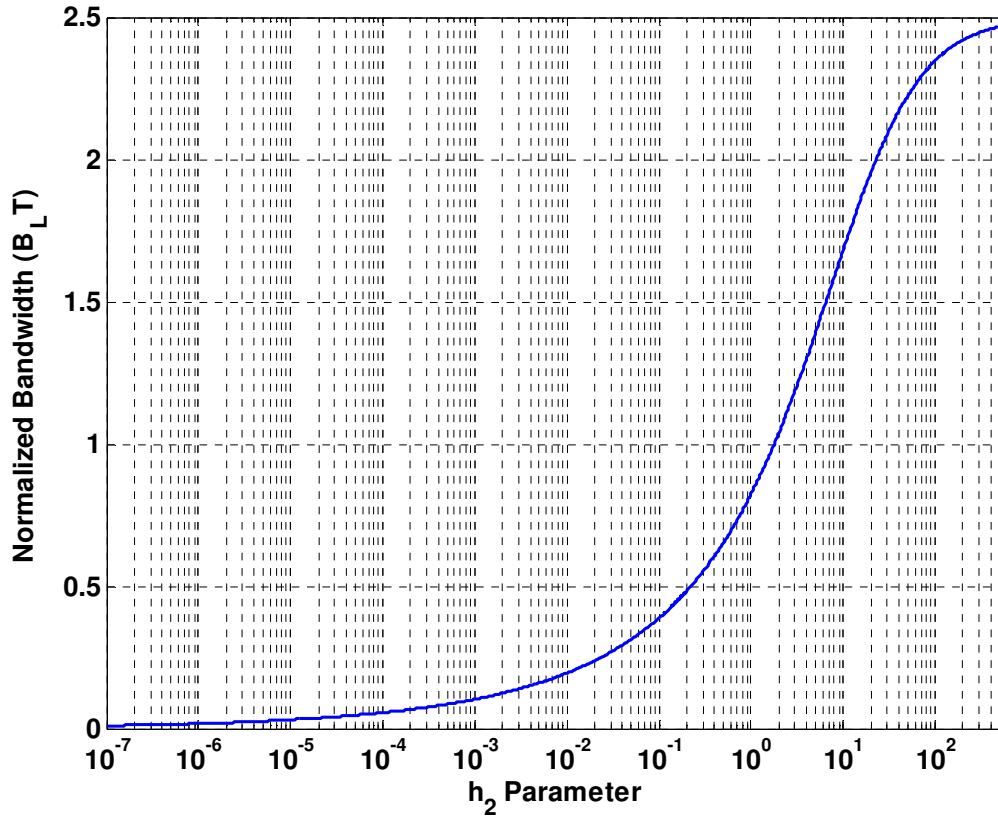
Figure 3-13 One-sided Normalized Bandwidth versus the h₂ parameter.

3.3.4 Loop Filter Design for Frequency Ramp (phase acceleration)

In this case $\theta(t) = t^2 u(t)$, and Equation 3-8 becomes

$$\Phi_{\theta\theta} = \frac{T^2 z(z+1)}{(z-1)^3} \cdot \frac{T^2 z^{-1}(z^{-1}+1)}{(z^{-1}-1)^3}.$$

3-35

The same procedure as that of the two previous cases can be done to derive the optimum

filter for the phase and phase rate feedback NCO as

$$F_p = \frac{(A_n z^2 + B_n z + C_n)}{T(A_d z^2 + B_d z + C_d)}$$

3-36

where

$$\begin{cases} A_n = d^2 + (\text{-}10b\text{-}22a\text{-}2c)d + 14ab\text{-}2ac + 2bc + 5b^2 + c^2 + 13a^2 \\ B_n = \text{-}2d^2 + (28b + 8c + 56a)d\text{-}2b^2 + 20ac + 8bc\text{-}8ab\text{-}14a^2 + 2c^2 \\ C_n = 5d^2 + (\text{-}10b\text{-}26a + 2c)d + 2ab\text{-}2bc\text{-}10ac + b^2 + c^2 + 5a^2 \\ A_d = 4ab + 4ad + 4ac + 4a^2 \\ B_d = \text{-}d^2 + (2c + 14b + 26a)d\text{-}9a^2 + 6ac\text{-}6ab + 2bc\text{-}b^2\text{-}c^2 \\ C_d = d^2 + (\text{-}30a\text{-}14b\text{-}2c)d + 2ab\text{-}2bc\text{-}10ac + b^2 + c^2 + 5a^2 \end{cases}$$

3-37

and *a, b, c, d* can be found by solving the following set of nonlinear equations with a

constraint of having roots of $az^3 + bz^2 + cz + d$ inside the unit circle:

$$\begin{cases} ad = -1 \\ ac + bd = 6 \\ ab + bc + cd = h_3 - 15 \\ a^2 + b^2 + c^2 + d^2 = 2h_3 + 20 \end{cases}.$$

3-38

where $h_3 = \dfrac{\lambda T^4}{\rho}$. By finding poles and zeros location of Equation 3-36 the filter structure

can be further simplified as

$$F_p(z) = \frac{K(z - z_z)(z - \bar{z}_z)}{T(z-1)^2}.$$

3-39

where $\bar{z}_z$ the complex conjugate of the optimum zero location. This case is the most

applicable loop for satellite signal tracking since the relative satellite and receiver motion

cause the receiver to observe an accelerating frequency input.

The required h_3 values for different normalized noise bandwidths are shown in Figure 3-14. Optimum zero location and gain values are depicted in Figures 3-15 and 3-16 respectively, for different normalized noise bandwidths.
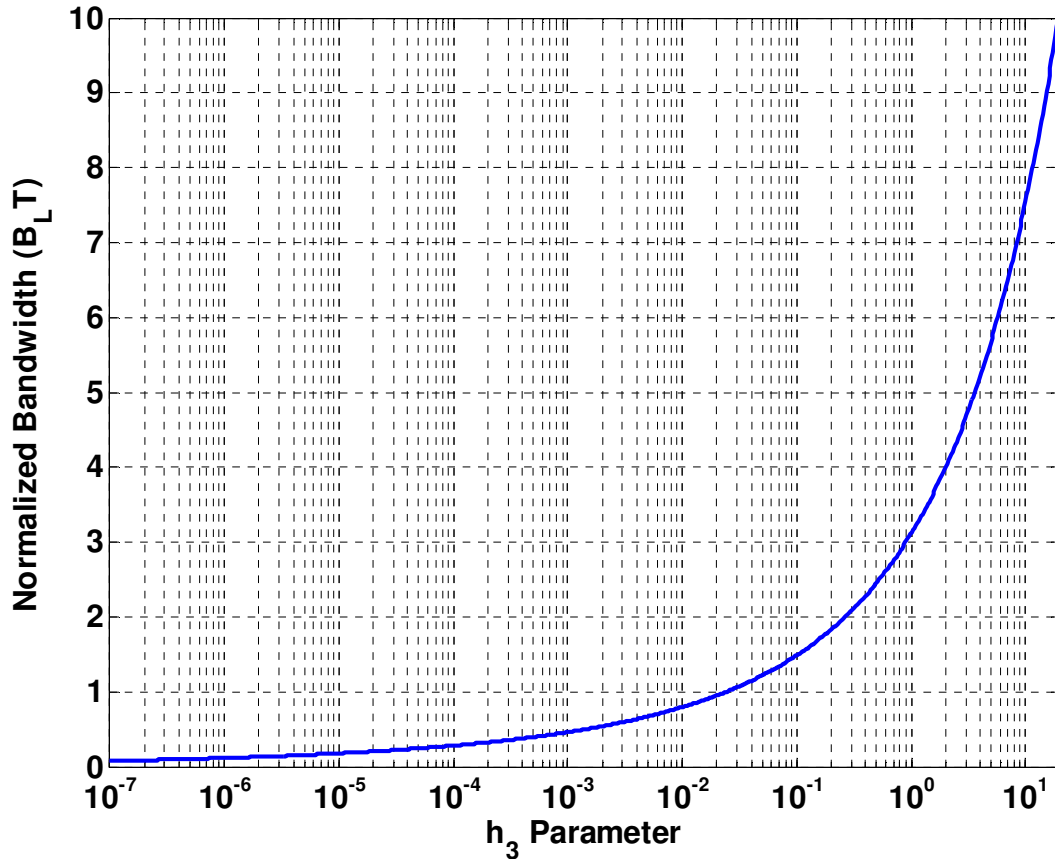
Figure 3-14 One-sided Normalized Bandwidth versus the h3 parameter.
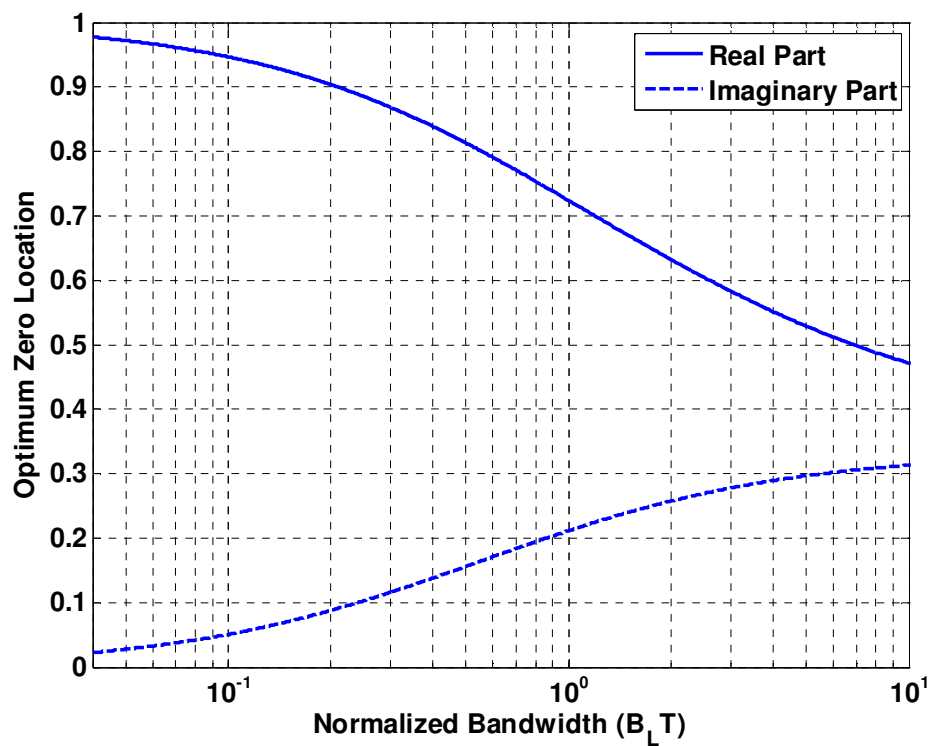
Figure 3-15 Optimum zero location versus Normalized Bandwidth for third order loop
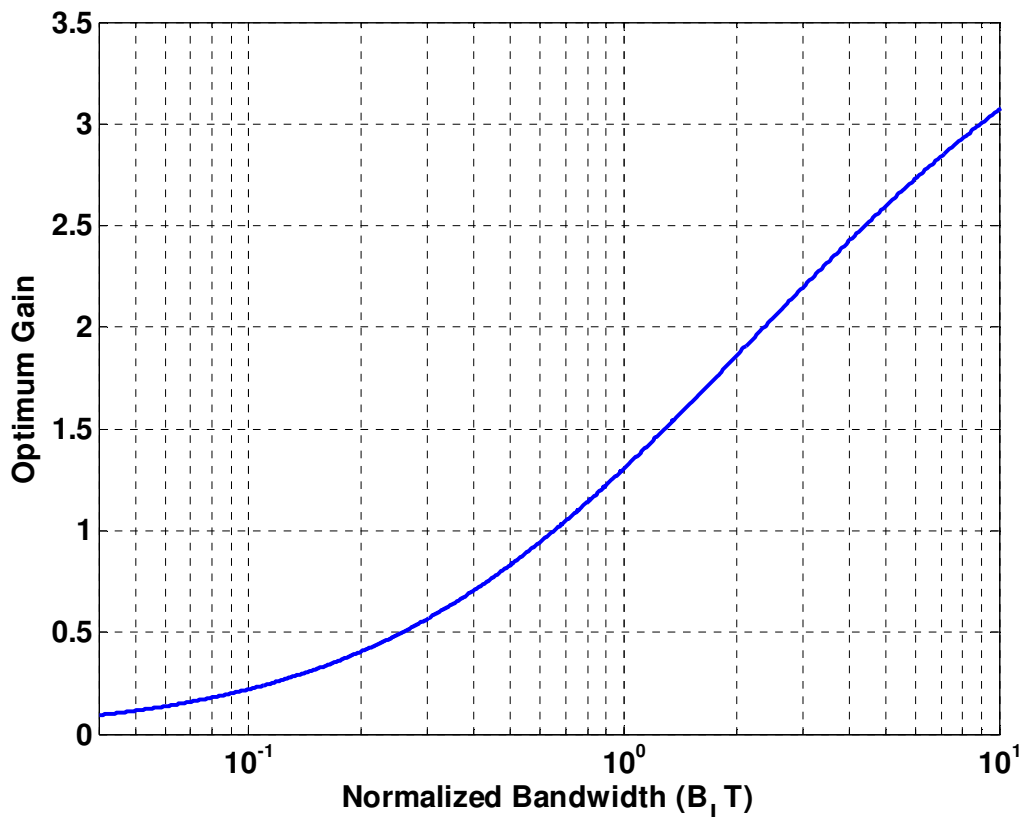
Figure 3-16 Optimum gain versus Normalized Bandwidth for third order loop

3.3.5 Loop Filter Design for Phase Jerk

Receivers designed for high dynamics should use high order loops to avoid loss of lock due to the large accelerations encountered. It is well known that a type III loop has zero, constant and infinite phase errors for phase acceleration, jerk, and higher dynamics, respectively. In order to reduce the constant phase error, higher bandwidth is required which in turn degrades the noise performance of the loop. Type IV loops inherently have a zero steady state phase error for phase jerk, which makes them more robust against

dynamics. In GNSS signal tracking applications, loop bandwidth can be set to a smaller value for a fourth order loop than for a third order loop, hence lower signal strength can be tracked. For a type IV loop, the desired input is $\theta(t) = t^3 u(t)$ and $\Theta(z)$ can be written as

$$\Theta(z) = \frac{T^3 z(z^2 + 4z + 1)}{(z-1)^4}.$$

3-40

Following the same procedure as the previous cases the filter structure can be derived as

$$F_p = \frac{(A_n z^3 + B_n z^2 + C_n z + D_n)}{T(A_d z^3 + B_d z^2 + C_d z + D_d)}$$

3-41

where

$A_n = -c^2d + 61ae^2 - 5a^2c + 30be^2 + de^2 + 15a^3 + 26a^2b - e^3 + 5b^3 + c^3 - 38bce + 14bde + 6abc - 50abd - 136abe - 4acd + 46ade - 6bcd - 42ace + 19ab^2 - 115a^2e + 15ad^2 + 5ac^2 - 51a^2d + 5b^2c - 14b^2d + 5bd^2 - 45b^2e + cd^2 + 11ce^2 - 11c^2e + 4bc^2 - d^2e$

$B_n = 9c^2d - 210ae^2 + 45a^2c - 105be^2 - 3de^2 - 26a^3 - 33a^2b + 4e^3 - 5b^3 + c^3 + d^3 + 102bce - 60bde - 6cde + 30abc + 168abd + 390abe + 18acd - 174ade + 30bcd + 102ace - 21ab^2 + 336a^2e - 51ad^2 + 165a^2d + 6b^2c + 51b^2d - 15bd^2 + 129b^2e - 39ce^2 + 30c^2e + 3bc^2 + 3d^2e$

$C_n = 249ae^2 - 45a^2c + 129be^2 + 6de^2 + 19a^3 + 21a^2b - 5e^3 + 4b^3 + c^3 + d^3 - 60bce + 102bde + 30cde - 24abc - 138abd - 330abe + 18acd + 240ade - 6bcd - 42ace + 15ab^2 - 303a^2e + 75ad^2 + 9ac^2 - 150a^2d - 3b^2c - 39b^2d + 30bd^2 - 105b^2e + 9cd^2 + 51ce^2 - 15c^2e + 3bc^2 + 3d^2e$

$D_n = c^2d - 91ae^2 + 14a^2c - 45be^2 + 5de^2 - 5a^3 - 5a^2b + 5e^3 - b^3 + d^3 + 14bce - 38bde - 6cde + 6abc + 38abd + 94abe - 14acd - 94ade - 4ab^2 + 91a^2e - 30ad^2 - 5ac^2 + 45a^2d + b^2c + 11b^2d - 11bd^2 + 30b^2e - cd^2 - 14ce^2 + 5c^2e - bc^2 + 4d^2e$

$\qquad\qquad\qquad\qquad\qquad\qquad\qquad\qquad\qquad\qquad\qquad\qquad\qquad$ 3-42

$A_d = 6abe + 6abd + 6a^2d + 6a^2c + 6abc + 3ab^2 + 3ac^2 + 3ad^2 + 6a^2e + 3ae^2 + 6ace + 6ade + 6acd + 3a^3 + 6a^2b$

$B_d = c^2d - 58ae^2 + 11a^2c - 27be^2 - de^2 - 12a^3 - 17a^2b + e^3 - 2b^3 - c^3 + 44bce - 8bde + 6abc + 62abd + 148abe + 10acd - 40ade + 12bcd + 48ace - 10ab^2 + 121a^2e - 12ad^2 - 2ac^2 + 57a^2d + b^2c + 20b^2d - 2bd^2 + 51b^2e - cd^2 - 11ce^2 + 11c^2e - bc^2 + d^2e$

$C_d = -2c^2d + 152ae^2 - 31a^2c + 78be^2 + 2de^2 + 14a^3 + 16a^2b - 3e^3 + 3b^3 + c^3 - d^3 - 52bce + 52bde + 12cde - 18abc - 106abd - 242abe - 2acd + 134ade - 12bcd - 48ace + 11ab^2 - 215a^2e + 39ad^2 + 4ac^2 - 108a^2d - 2b^2c - 31b^2d + 13bd^2 - 78b^2e + 2cd^2 + 31ce^2 - 13c^2e + 2bc^2 - 2d^2e$

$D_d = c^2d - 97ae^2 + 14a^2c - 51be^2 - de^2 - 5a^3 - 5a^2b + 2e^3 - b^3 + d^3 + 8bce - 44bde - 12cde + 6abc + 38abd + 88abe - 14acd - 100ade - 6ace - 4ab^2 + 88a^2e - 30ad^2 - 5ac^2 + 45a^2d + b^2c + 11b^2d - 11bd^2 + 27b^2e - cd^2 - 20ce^2 + 2c^2e - bc^2 + d^2e$

and *a, b, c, d* and *e* can be found by solving the following set of nonlinear equations with

a constraint of having roots of $az^4 + bz^3 + cz^2 + dz + e$ inside the unit circle:

$$\begin{cases} ae = 1 \\ ad + be = -8 \\ bd + ce + ac = h_4 + 28 \\ cd + de + ab + bc = 8h_4 - 56 \\ a^2 + b^2 + c^2 + d^2 + e^2 = 18h_4 + 70 \end{cases}$$ 3-43

where

$$h_4 = \frac{\lambda T^6}{\rho}.$$ 3-44

By finding the poles and zeros location of Equation 3-41, the filter structure can be further simplified as

$$F_p(z) = \frac{K(z - z_z)(z - \bar{z}_z)(z - z_r)}{T(z-1)^3}.$$ 3-45

In Figures 3-17 and 3-18 the optimum zeros location and gain for the fourth order loop are given for different normalized noise bandwidths. The required h_4 values to achieve different normalized noise bandwidths are depicted in Figure 3-19. These figures enable one to design the required filter easily without repeating the required rigorous math for designing high order loops.
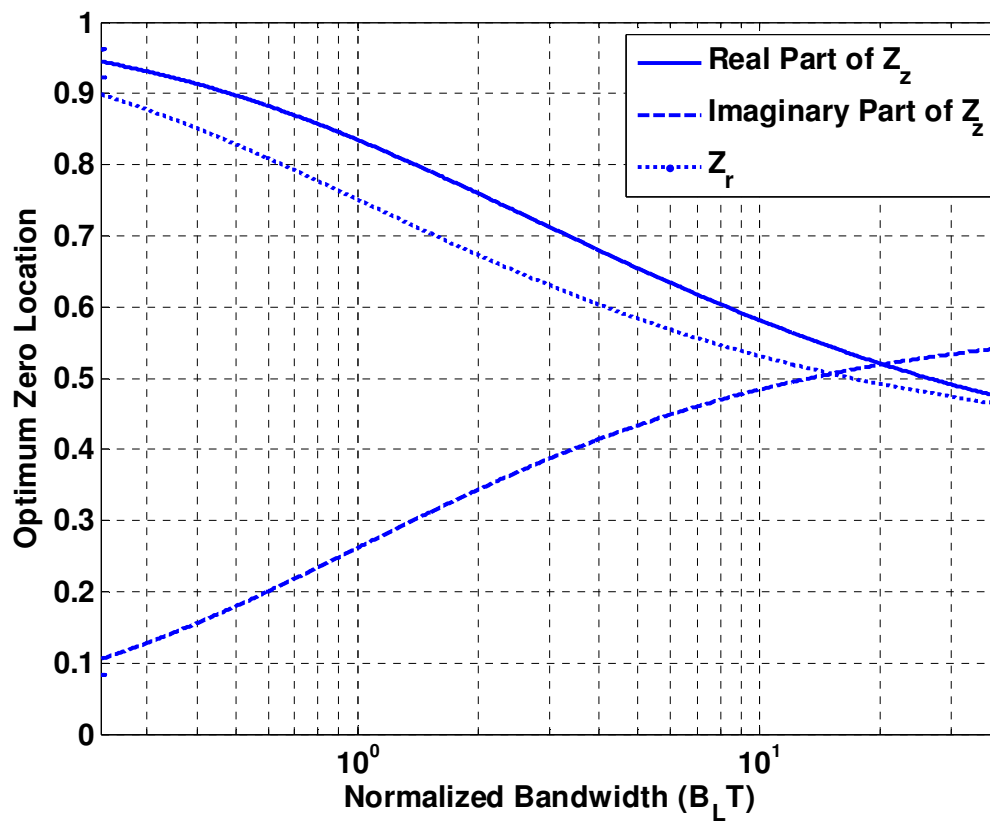
Figure 3-17 Optimum zeros location versus Normalized Bandwidth for a fourth order loop
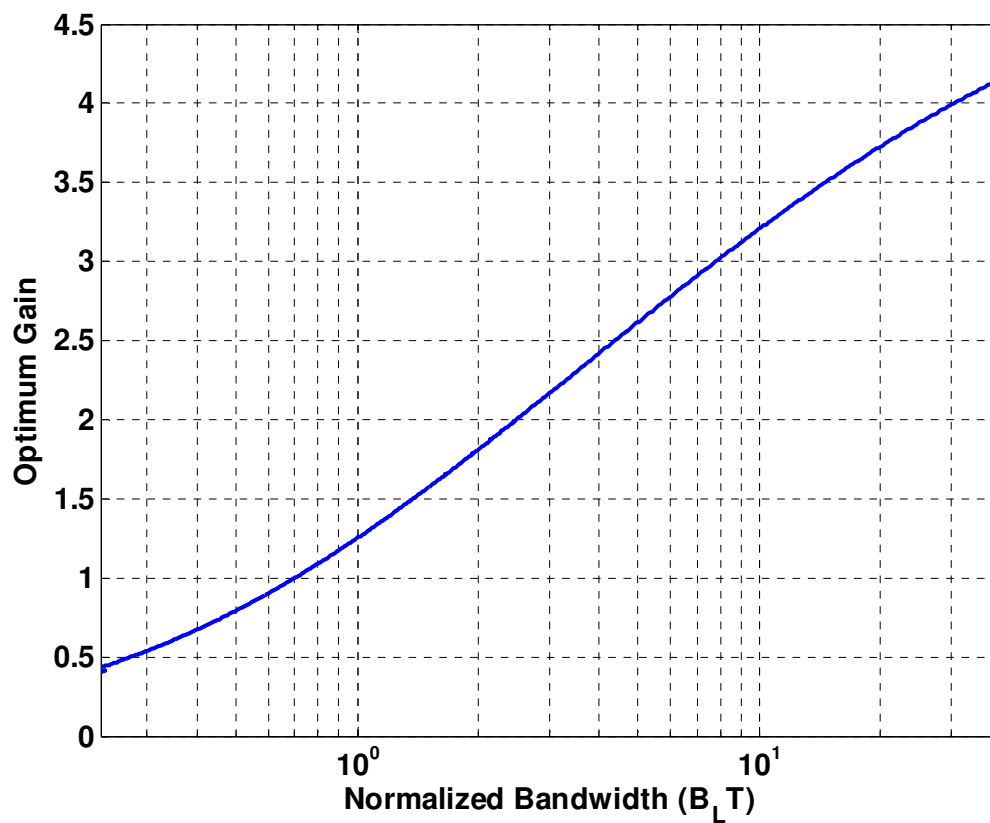
Figure 3-18 Optimum gain versus Normalized Bandwidth for a fourth order loop
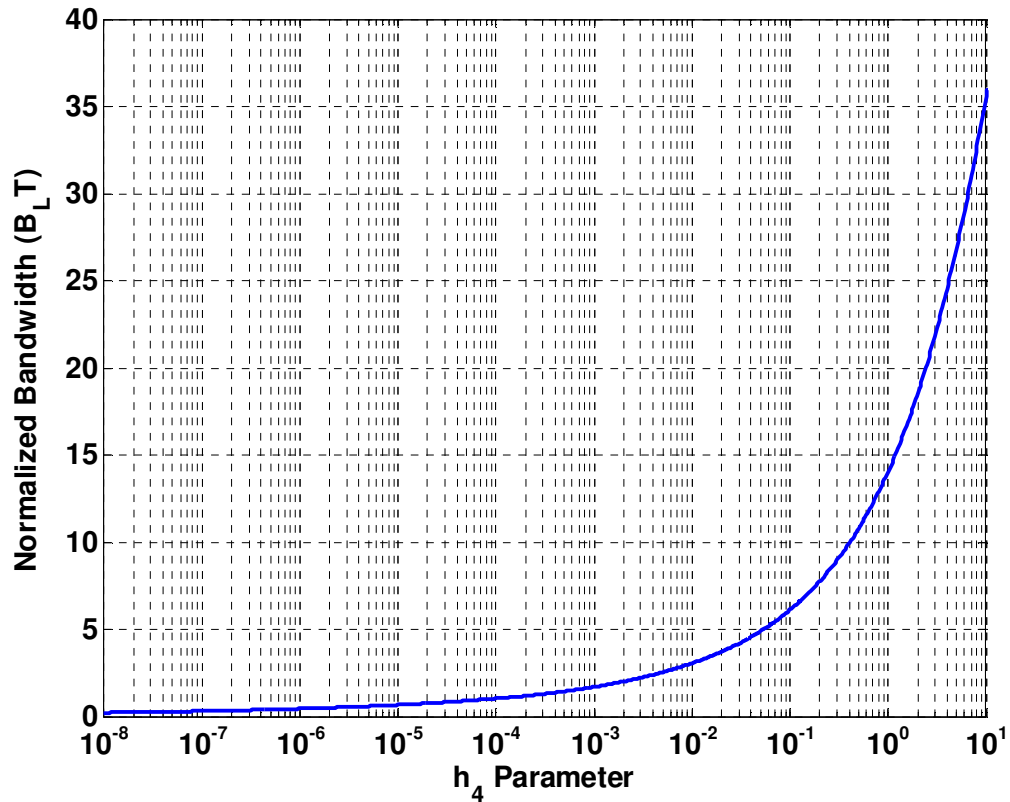
Figure 3-19 One-sided Normalized Bandwidth versus the h4 parameter

3.4 Steady State Error due to Higher Order Dynamics

Under the assumption of linearity, the steady state phase error, φ_s, for constant dynamics can be computed using the final value theorem as

$$\varphi_s = \underset{z \to 1}{Lim}(\frac{z-1}{z})(1-H(z))\Theta(z). \qquad 3\text{-}46$$

In Equation 3-46 the input signal will depend on the type of the loop. For instance it is well known that with type II loop a phase ramp will be tracked with zero phase error, phase acceleration will generate a constant (non-zero) phase error and finally phase jerk

or higher order dynamics will introduce a infinite phase error. Similarly, a type III loop has zero, constant and infinite phase errors for phase acceleration, jerk, and higher dynamics, respectively. Thus, the dynamics of interest are phase acceleration for a type II loop and phase jerk for type III loop (Kazemi et al 2009).

A normalization of the phase error coefficients defined in Equation 3-46, can be introduced as

$$C_i = (\varphi_s)^{1/i} B_L \qquad\qquad 3\text{-}47$$

where i is the magnitude of the highest order nonzero derivative of the input signal. These coefficients exhibit slower variation with B_L than do those of Equation 3-46. Figure 3-20 shows the phase coefficients as functions of normalized bandwidths for different loop types. Note that the radian phase error for different cases can be derived from this figure. For instance, for the type II loop, the phase radian error is $(\dfrac{\omega_0 a}{c})(\dfrac{C_2}{B_L})^2$ where ω_0 is radian center frequency, a is acceleration in m/s^2 and c is the speed of light. The reader should note that Figure 3-20 does not imply that a fourth order loop has a higher steady state error since as mentioned before, the input signal for deriving the steady state error coefficient is different for different loop orders.
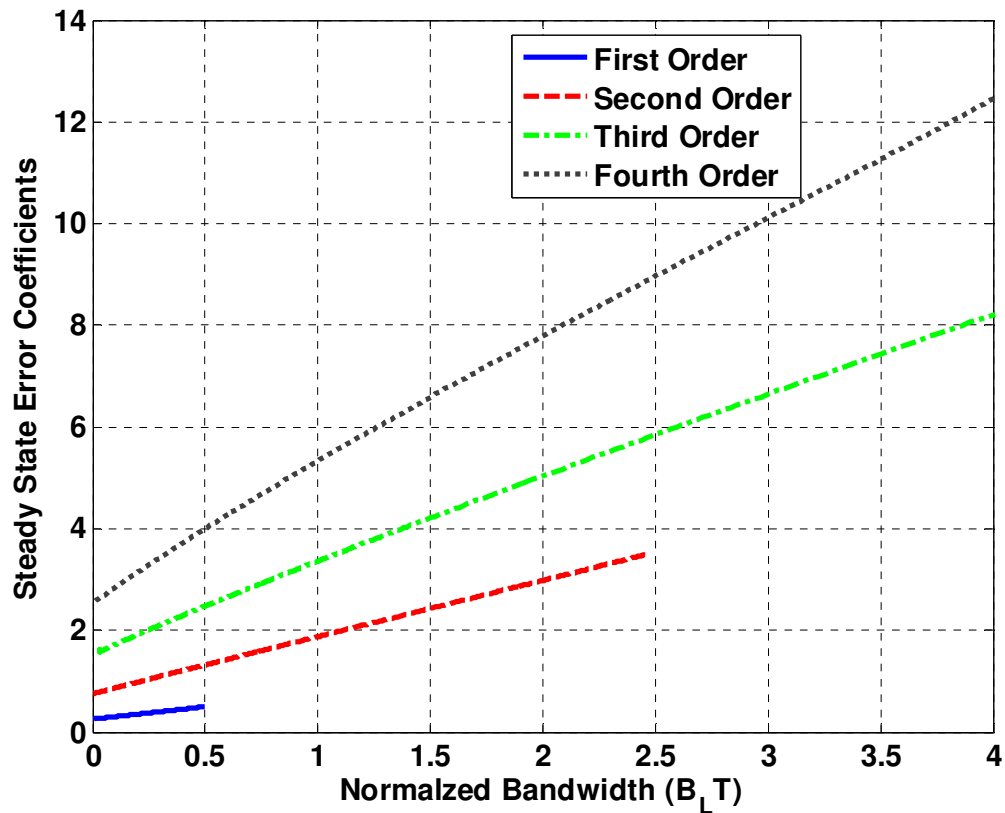
Figure 3-20 One-sided Normalized Bandwidth versus the steady state error coefficients for first to fourth order loops

3.5 Practical Considerations

The two filter structures presented here for the two aforementioned NCOs will result in the same closed loop transfer function with their corresponding NCO transfer functions. Hence, in theory the same loop performances are expected for the two loops.

As Equation 3-28 shows, there is a pole at z=-1 in the filter structure for phase rate-only feedback NCO. Although this pole has been obtained as a result of an optimization

procedure, in practice it would cause stability problems. This pole has oscillatory effects and it should be displaced to a point near -1. In general, the presence of this pole in the filter structure produces a nosier loop filter output with respect to the conventional filter structures that do not have this pole. This displacement will introduce sub-optimality but it is necessary to ensure stability (Kazemi 2008). This effect can be evaluated by separating the pole at -1 from Equation 3-28 and taking the inverse Z-transform:

$$F(z) = F'(z) \cdot \frac{z}{z+1} \xrightarrow{z^{-1}} Z^{-1}\{F'(z)\} * (-1)^n \qquad \text{3-48}$$

Multiplication in frequency is equivalent to convolution in the time domain so the output of the $F'(z)$ is convolved with the $(-1)^n$. In Figure 3-21 it is assumed that the output of the $F'(z)$ term is a ramp function with 100 samples. It can be seen that the output of the system does not decay to zero and the system becomes unstable. However, by changing the place of this pole to a place near -1, it is possible to make the system stable.
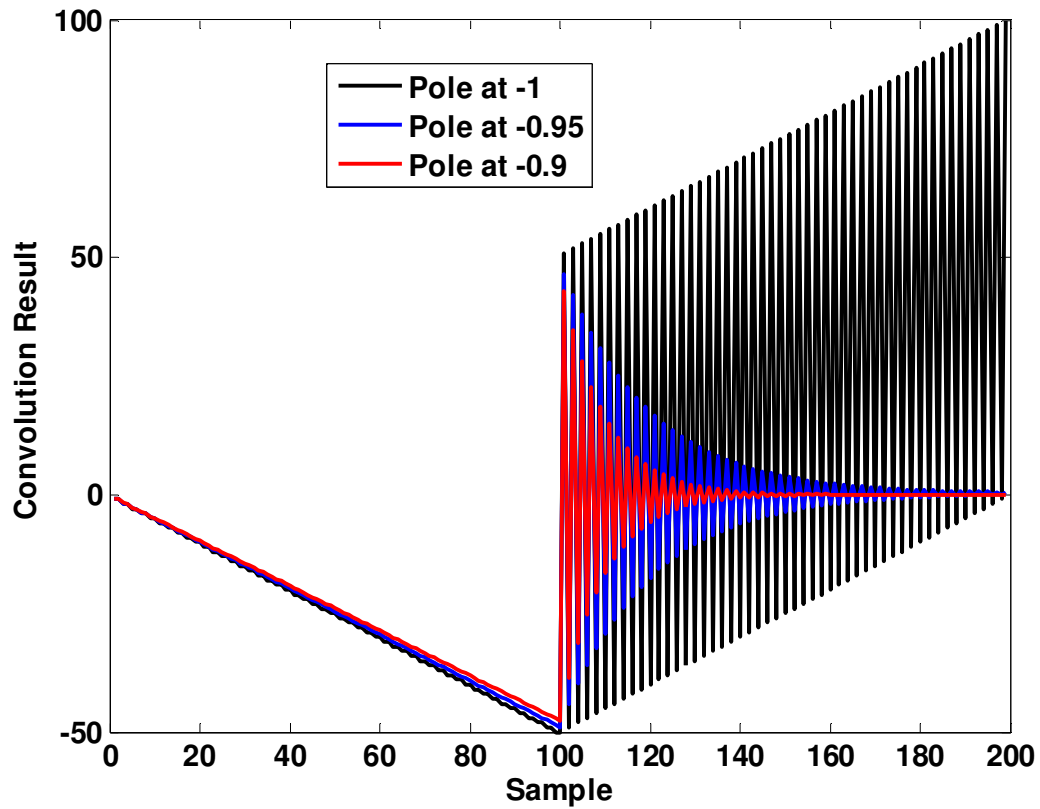
Figure 3-21 Effect of the real left side pole on the ramp function

The presence of this pole is necessary to increase the operational range of the loop and it should be kept near -1 for loops operating with high B_LT values. As the pole becomes closer to the origin, its oscillatory effect will be reduced. However it cannot be placed far away from -1 since this will distort the root locus of the loop. While this pole is near -1 it will create an extra root locus branch from -1 to its location, with negligible effect on the rest of the branches. Shifting this pole to say -0.9 will ensure stability and low oscillatory effect.

These effects are also shown for live GPS L1 signal in Figure 3-22. It is obvious that the pole at z=-1 increases the noise significantly in the Doppler estimate and loss of lock will occur eventually. As shown in Figure 3-22 by moving the pole at -1 to the -0.9, the increased noise effect can be significantly reduced. The effects of this pole are negligible especially for long integration times (low update rate loops).
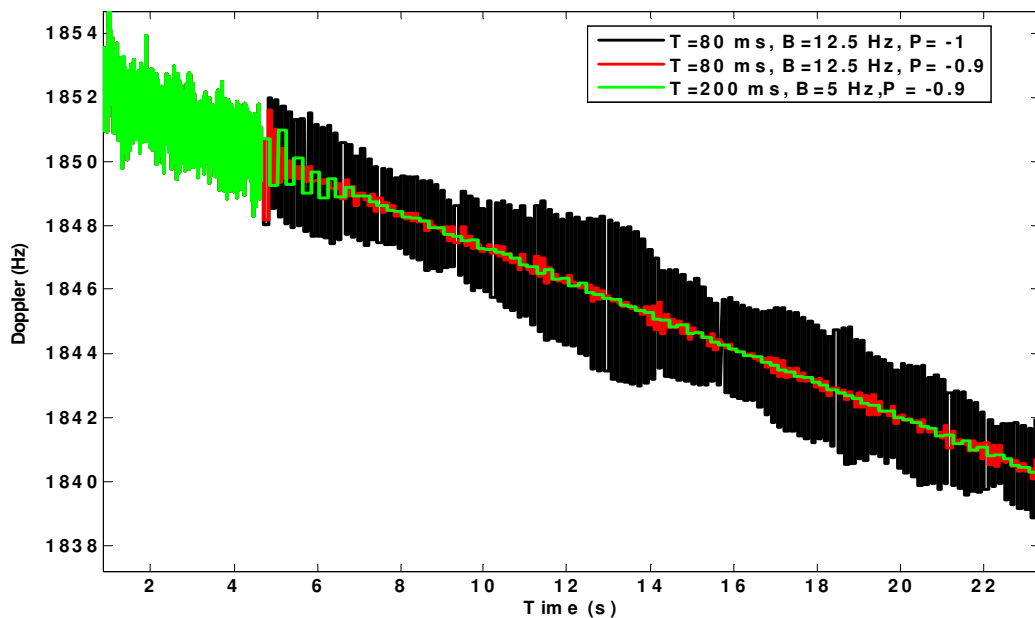
Figure 3-22 Effect of the optimum filter's real left side pole for the rate-only feedback NCO

In Figure 3-23 the Bode plots of three different methods for a third order loop filter design with phase rate only feedback NCO are compared for an integration time of 20 ms and desired noise bandwidth of 15 Hz. The filter structure of Ward (2006) with a digital bilinear transform (boxcar integrators severely degrade the performance for high $B_L T$ values as shown in Figure 2-15) is chosen as an example of the transformation method.

As mentioned earlier, in contrast with the two other methods, the filter coefficients are solely determined by the bandwidth rather than by the bandwidth and update interval of the loop.

From Figures 3-23 and 3-24 it can be inferred that the performance of the optimum loop and the controlled-root loop are near to each other in their comparable region. The deficiency of the transformation method is evident in the magnitude and phase diagrams of Figure 3-23. Although the filter is designed to have a tracking loop with a 15 Hz bandwidth, the actual bandwidth of the loop is 32.8 Hz, where most of the increase in bandwidth is due to the undesired peak of the filter magnitude response rather than the higher 3 dB cutoff frequency. Stability can be obtained for $B_L T$ values less than about 0.55 by this method. However, given the significant deviation of the noise bandwidth from the desired value, the use of this approach is not recommended for $B_L T$ values larger than about 0.1 (Kazemi et al 2009). From Figure 2-15 this value will ensure that the increase in bandwidth is less than 20%.

The optimum filters designed herein for the $B_L T$ can be extended to even more than 10 for the third order loop which is usually used for GNSS signal tracking. However, with the added constraint of having less than a 10 dB peak in the magnitude response, it is recommended to chose a $B_L T$ less than 3 for typical applications.
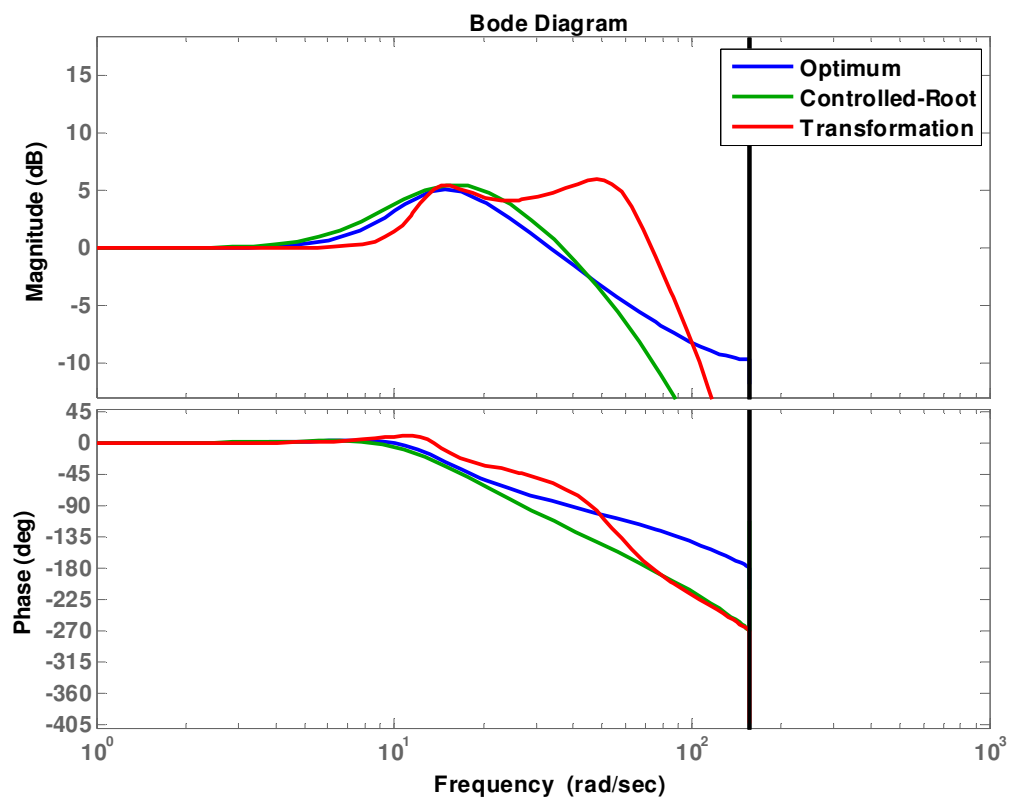
Figure 3-23 Close loop bode diagram of different loop filters design at B$_L$T=0.3
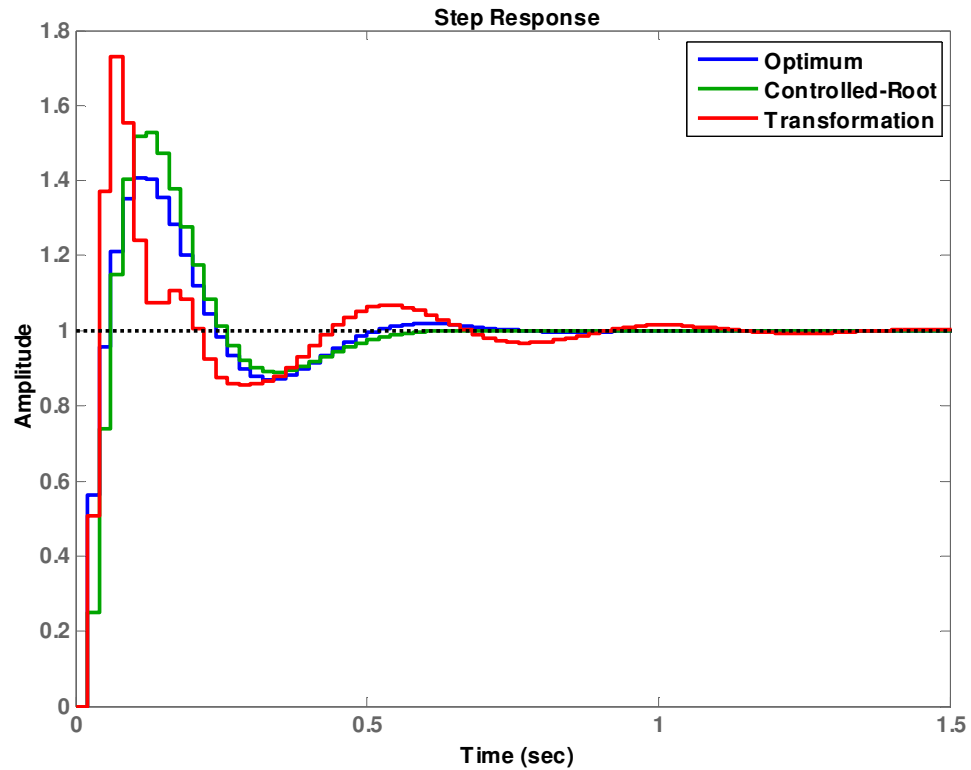
(T=20 ms, B$_L$=15 Hz)

Figure 3-24 Step response of different loop filters design at B_LT =0.3 (T=20 ms, B_L =15 Hz)

Another important point is that the solutions of the set of nonlinear equations such as those of Equation 3-43 should be accurate enough to give an accuracy of approximately four significant digits for the locations of zeros and gain values. Note that the round off errors in the solution of Equation 3-43 may accumulate when computing Equation 3-42. This becomes more significant for the design of higher order loops (Kazemi et al 2009).

3.6 Applications

A series of tests was conducted to assess the performance of the proposed techniques with live GPS signals.

3.6.1 Test Setup I and Test Methodology

To evaluate the designed filters' performance for large B_LT values, two sets of data were used. IF samples were recorded using a NovAtel Euro-3M GPS receiver, modified to extract the raw digitized IF samples. The main objectives of these tests are to show the stability and tracking ability of the designed filters for large B_LT values, in a range where conventional methods cannot operate at all. These tests were conducted using long integration times, where the update rate of the loop is low. The tracking loops discussed above were implemented in the PLAN Group's GSNRx™ (GNSS Software Navigation Receiver) software written entirely in C++. This version of the receiver works in post-mission mode and reads the IF data from a file. The tracking component consists of a DLL, FLL and PLL, all of which were modified based on the optimum configuration discussed above. The test methodology utilized a Spirent 7700 GPS hardware simulator to emulate controlled scenarios of dynamic environments and live GPS signals collected from an open-sky environment for static tests. Since the operational range of the conventional loop design methods is severely limited for the phase rate only feedback NCO, this kind of NCO is used here to demonstrate the advantages of the loops designed herein.

As was mentioned previously, the maximum coherent integration time in a GPS L1 receiver is limited by the presence of a 50 Hz navigation data modulation which typically limits the coherent integration time to less than 20 ms. A reference receiver was used to assist the software receiver to wipe off the navigation data. The test configuration is shown in Figure 3-25.
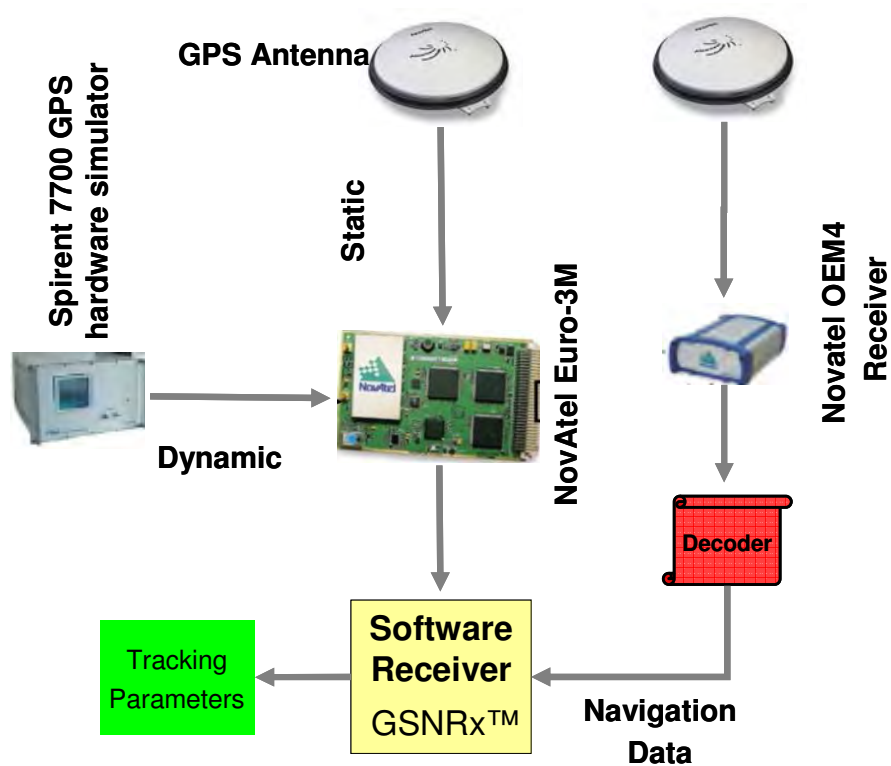
Figure 3-25 Test Setup I

3.6.1.1 Tracking Results I

These tests follow closely the work which was done in Kazemi (2008). An integration time of 200 ms and a noise bandwidth of 10 Hz (resulting in B_LT of 2) were chosen for

the static test using live GPS signals. An OCXO clock was used since a stable clock is required to integrate signal for such a long period. Because of the high $B_L T$ value, the controlled-root and transformation method cannot operate in this configuration. Tracking was initialized with FLL for one second and then switched to PLL with 1 ms of integration time and a bandwidth of 10 Hz. After bit synchronization, the integration time was increased to 200 ms. All six satellites in view were successfully tracked. As shown in Figure 3-26 for PRN 17 (the performance of this satellite is also indicative of other satellites), all the results show successful tracking of the signal and, because of the long integration time, phase and code jitter are consequently reduced.
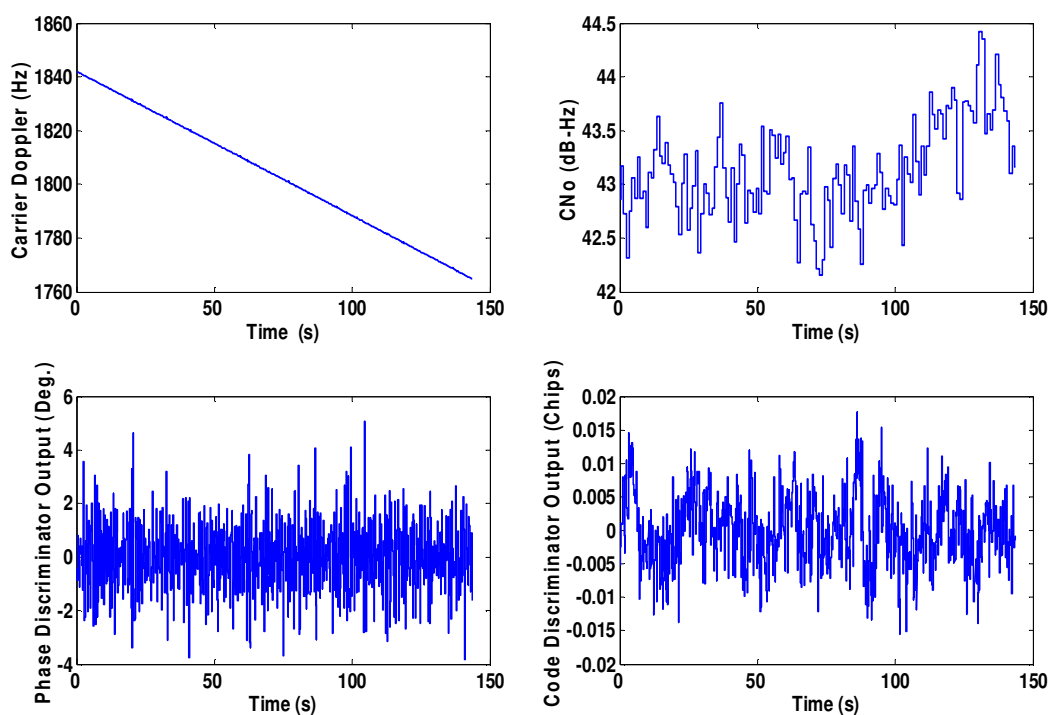
Figure 3-26 All of the tracking metrics show stable loop for T=200 ms and B_L=10 Hz

(B_LT=2)

The second data set tested was collected using a Spirent 7700 GPS hardware simulator. The internal TCXO clock of the Euro-3M card was used and the receiver set to follow a rectangular trajectory. In Figure 3-27 the carrier Doppler frequency of PRN 11 is plotted. The sinusoidal variations in Doppler are caused by the clock, the remaining variations are caused by the motion of the receiver. These sinusoidal variations are due to the clock-steering behaviour of the Euro-3M front-end being enabled. This behaviour puts the tracking loop under the continuous stress of the Doppler and Doppler rate change. As shown in Figure 3-28, the signal was also attenuated down to 30 dB-Hz.
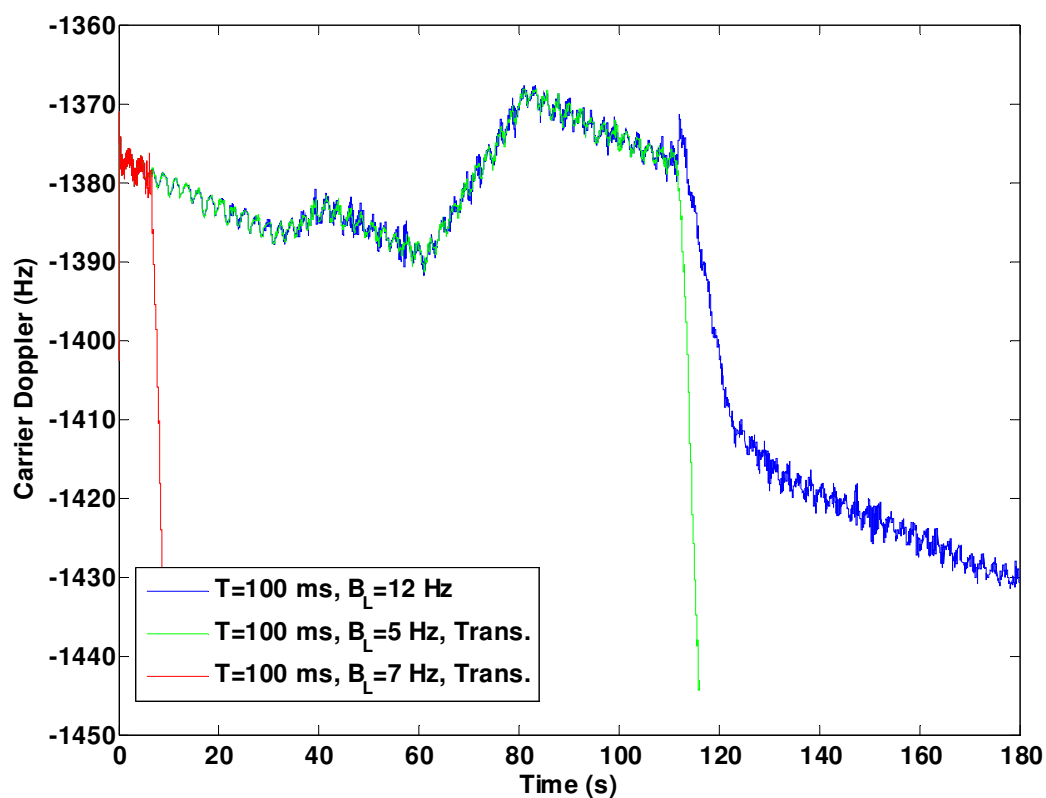
Figure 3-27 Comparison of optimum filter carrier Doppler estimate with conventional design
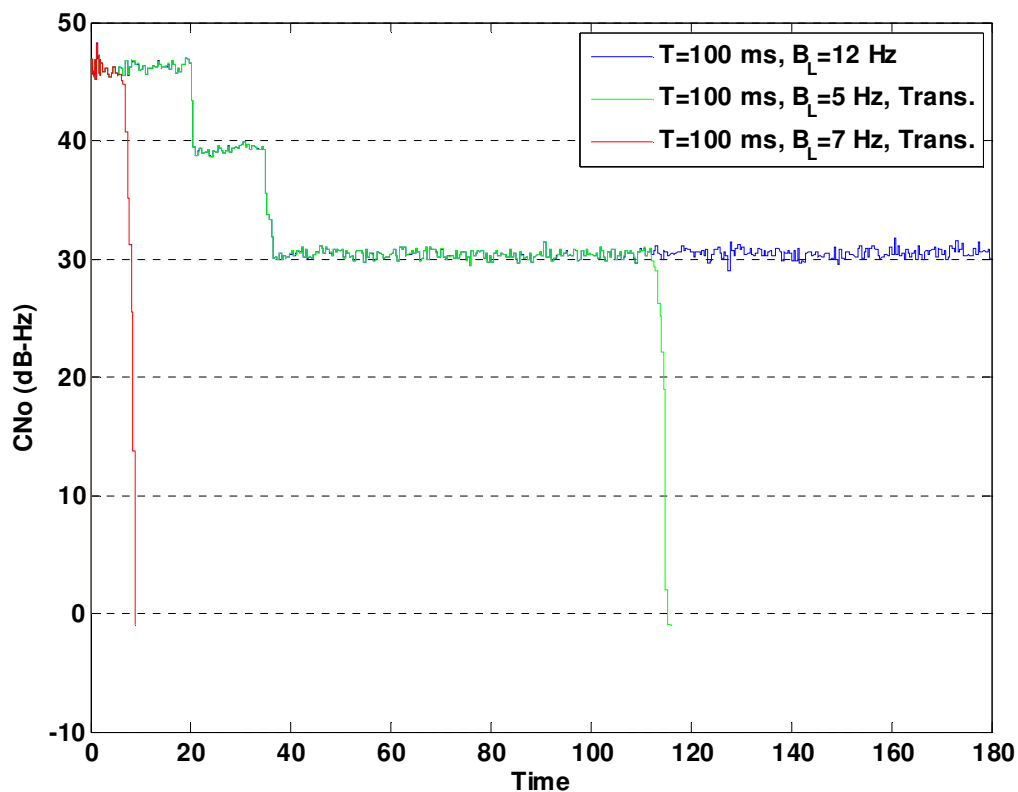
Figure 3-28 CN$_0$ estimates

Because of the continuous variation in the Doppler rate, an integration time of 20 ms is a better choice for tracking this signal, but 100 ms of integration is used to show the ability of the designed filter using high B$_L$T values. This choice also enables the receiver to operate at lower signal levels. The decision feedback stand-alone technique has been used to wipe off the navigation data. Fixing the integration time to 100 ms, the conventional filter structure is analyzed at first. To ensure stability a loop designed by employing the bilinear transformation with a 5 Hz bandwidth was used. As shown in Figure 3-27, there is a rapid change in Doppler at around 100 seconds. The loop was unable to track this

rapid change (where the line of sight acceleration reaches about 0.8 G) and eventually total loss of lock occurs. As a result, a wider bandwidth is required to track this signal successfully. However, by increasing the bandwidth from 5 Hz to 8 Hz ($B_L T$ =0.8), an unstable loop is obtained.

The third order optimum loop with a 12 Hz bandwidth ($B_L T$ =1.2) design based on Equations 3-27 and 3-39 results in a stable loop that successfully tracks the signal which is a significant improvement with respect to conventional loops.

In DPLLs, with each update interval the fixed locally generated carrier frequency is correlated with the incoming signal. The assumption of having a constant frequency over each 100 ms is not valid in this test (changes of the Doppler frequency during integration time is covered in Chapter 4). The performance is compared with an integration time of 20 ms and a bandwidth of 10 Hz. As shown in Figure 3-29, changes in Doppler frequency in each 100 ms cause phase mismatch between the incoming and locally generated signals, which is correctly detected by the phase discriminator. Reducing the update interval to 20 ms could reduce this phase mismatch, however choosing longer integration time becomes inevitable under very weak signal conditions. In this case choosing an integration time of 100 ms as opposed to 20 ms can improve the sensitivity by about 7 dB. Figure 3-29 shows the output of the phase discriminator at the transition time from strong signal power to 30 dB-Hz. It is obvious that the phase error with 100 ms remains approximately at the same level as before (again mainly caused by the dynamics), but the phase error with 20 ms integration time becomes much noisier (Kazemi 2008).
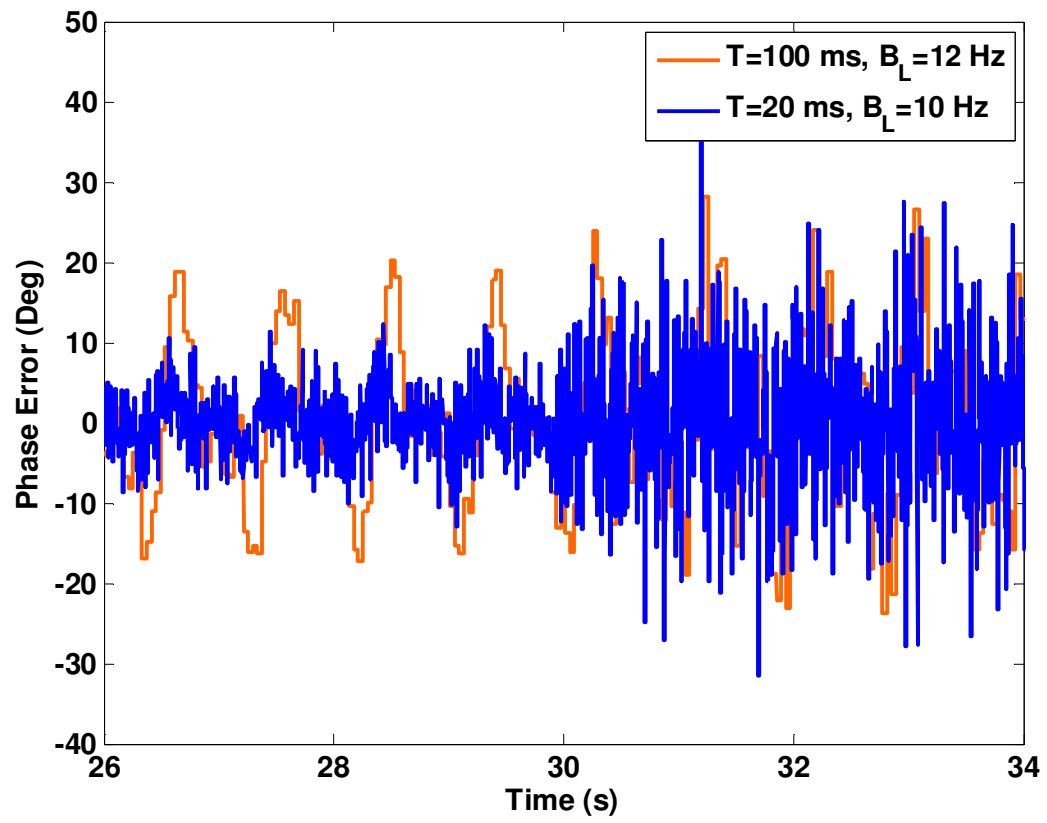
Figure 3-29 Output of the PLL discriminator
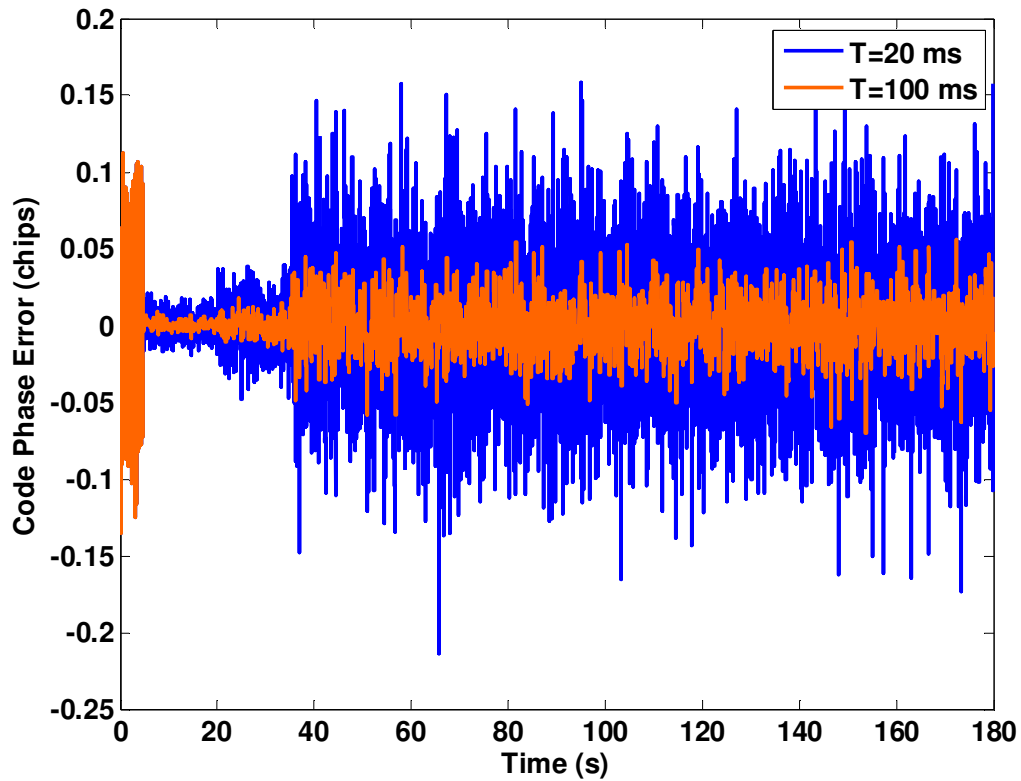
Figure 3-30 Output of the DLL discriminator

As shown in Figure 3-30, the advantage of choosing 100 ms becomes apparent in reducing code jitter since the code does not experience this amount of dynamics especially in aided-DLL scheme.

3.6.2 Test Setup II and Test Methodology

The test setup for the second series of tests is shown in Figure 3-31. Using the National Instrument (NI) frontend, which has a flexible bandwidth and sampling rate, the raw IF

samples are extracted and written to a PC's hard disk. Different data sets are collected using a live line-of-sight (LOS) signal under low multipath conditions.
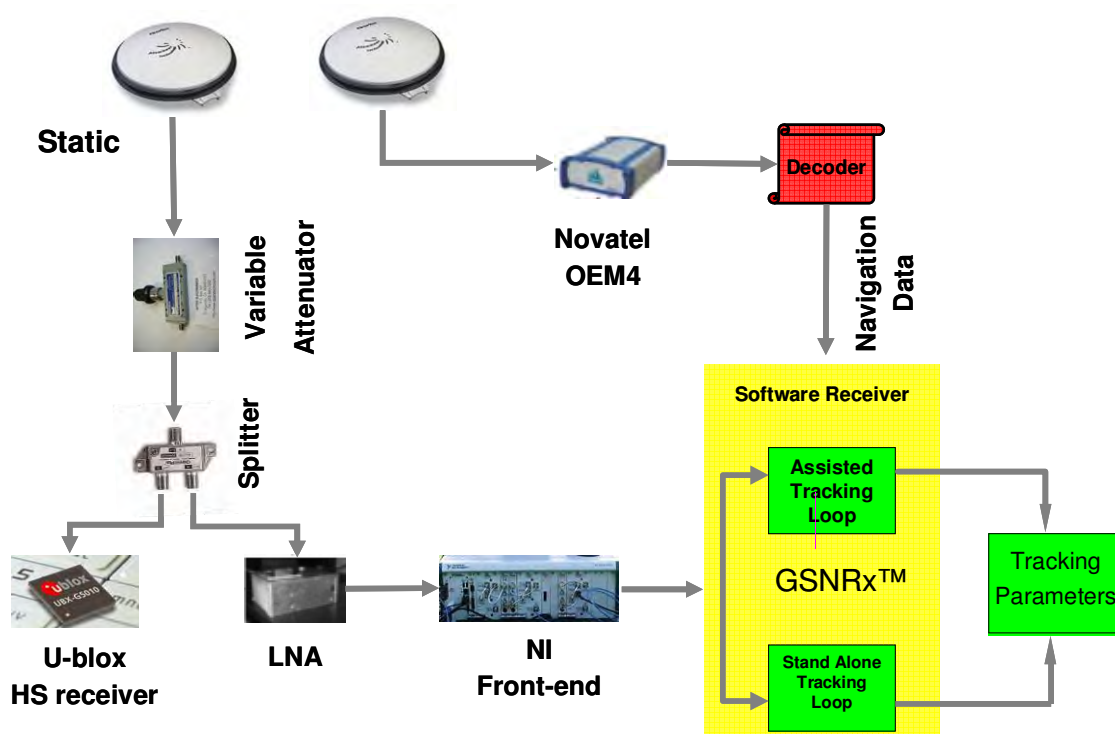
Figure 3-31 Test Setup II

The test methodology utilized attenuated GPS signals to emulate controlled scenarios of weak signal environments. To assess the ability of the receiver to track a certain level of C/N_0 the signal should be kept at that level for a long time. The signal is kept at each C/N_0 level for more than a minute to assess the ability of the tracking architecture to track that level of C/N_0. Different configurations are compared in terms of their ability to track certain levels of C/N_0 in practice.

All of the tracking parameters at very low C/N_0 (say below 15 dB-Hz) are too noisy to assess the ability of the loop to track that level. In order to compensate this effect after attenuating the signal in different steps the level of attenuation is decreased at the end of the test. In this way it can be determined if the tracking loop was able to track the signal at the lowest C/N_0 level.

A NovAtel OEM4 receiver is used as a reference for assisting the software receiver in terms of navigation data for assisted schemes. For signal quality monitoring during the weak real data collection and also comparing the tracking parameters, a hardware U-blox high sensitivity GPS receiver is used. The reacquisition scheme is disabled in the software receiver, in order to test only the signal tracking capability. However, the U-blox receiver reacquires the signal after loss of lock as shown in the tracking results section.

3.6.2.1 Tracking Results II

These tests follow closely the work reported by Kazemi & O'Driscoll (2008). The sensitivity of the tracking loops with different configurations is shown in Figure 3-32 for PRN 23. The performance of this satellite is also indicative of other satellites. The maximum attenuation level which was shown by the variable attenuator was chosen to be 40 dB. This level of attenuation brought down the C/N_0 level to about 10 dB-Hz. Differences in the C/N_0 estimation of the U-blox receiver and the software receiver are caused by the different C/N_0 estimation techniques and different noise figures. The well-

known narrow-band wide-band power estimator (Spilker 1997) with about one second of averaging was used in the software receiver.

The U-blox receiver lost lock at about 12 dB-Hz and reacquired the signal at 24 dB-Hz when the attenuation level decreased again. The assisted scheme with 400 ms of coherent integration was able to track the entire signal without losing lock. One should note that this scheme not only outperforms the U-blox receiver in this static test but, unlike the U-blox receiver, the availability of the phase information makes it a very interesting candidate for precise positioning in adverse conditions. Another important point is that the results for assisted scheme herein can be also extended to dataless channels of newer GNSS signals.
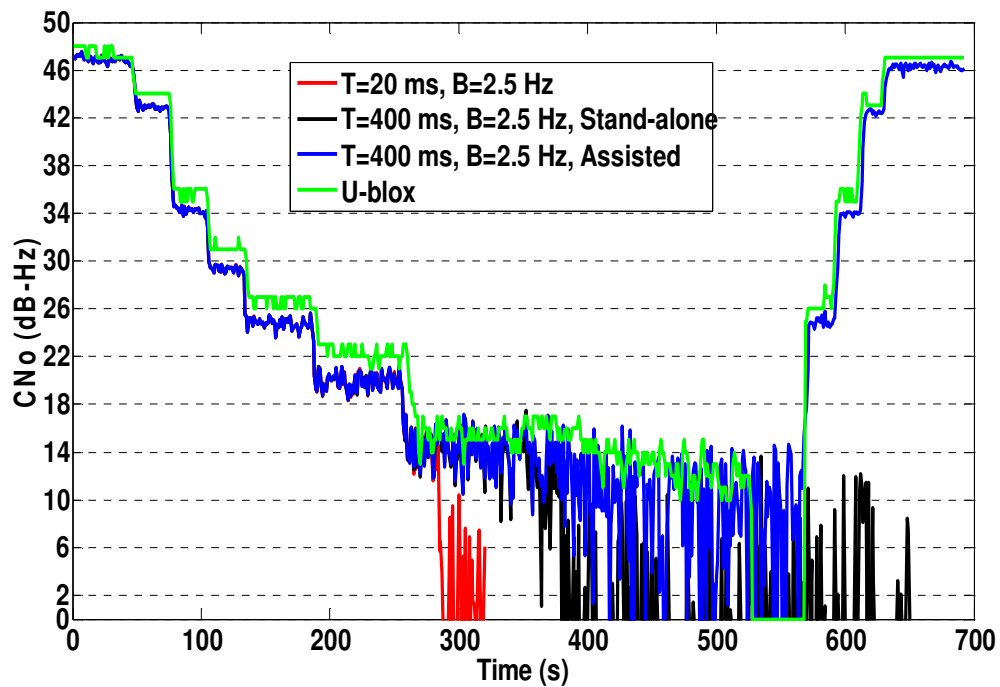
Figure 3-32 Sensitivity analysis for different tracking

The phase lock is shown in Figure 3-33 for 400 ms accumulated in-phase (I) and quadrature channels (Q). The Q channel was kept at the noise level for the entire tracking time showing the proper lock condition.
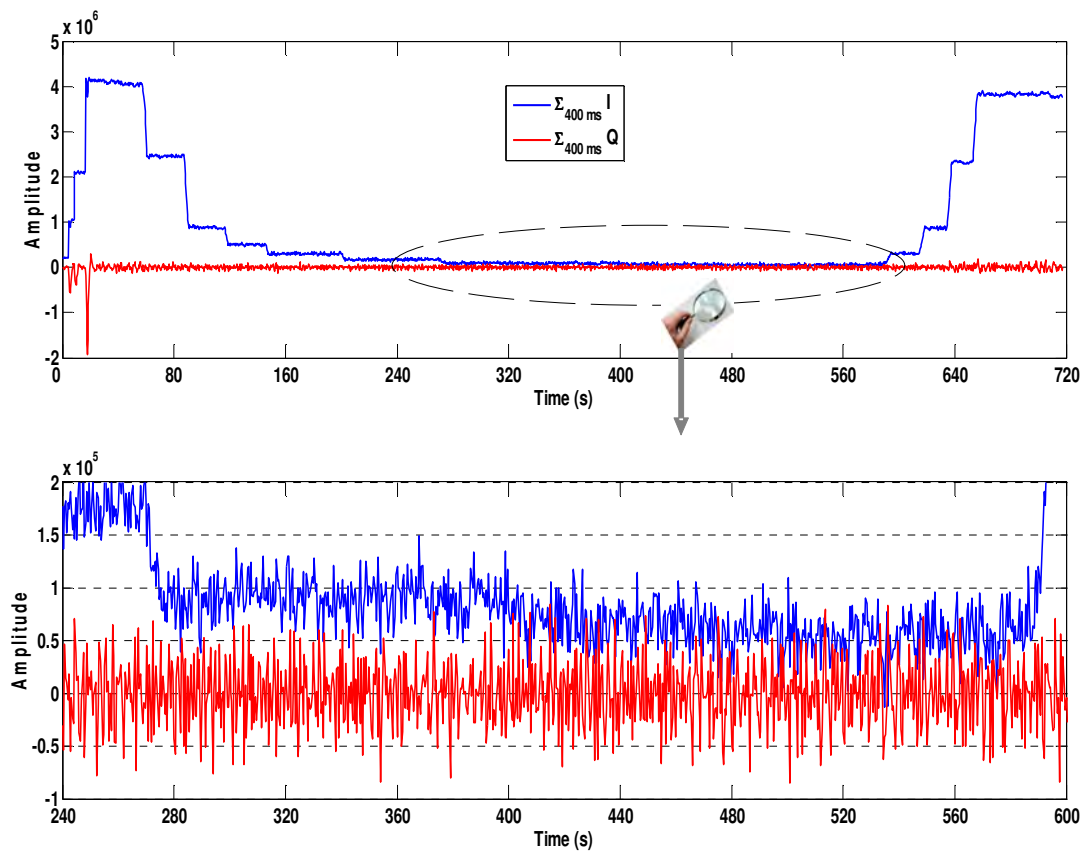
Figure 3-33 Accumulated Is and Qs showing the proper lock condition
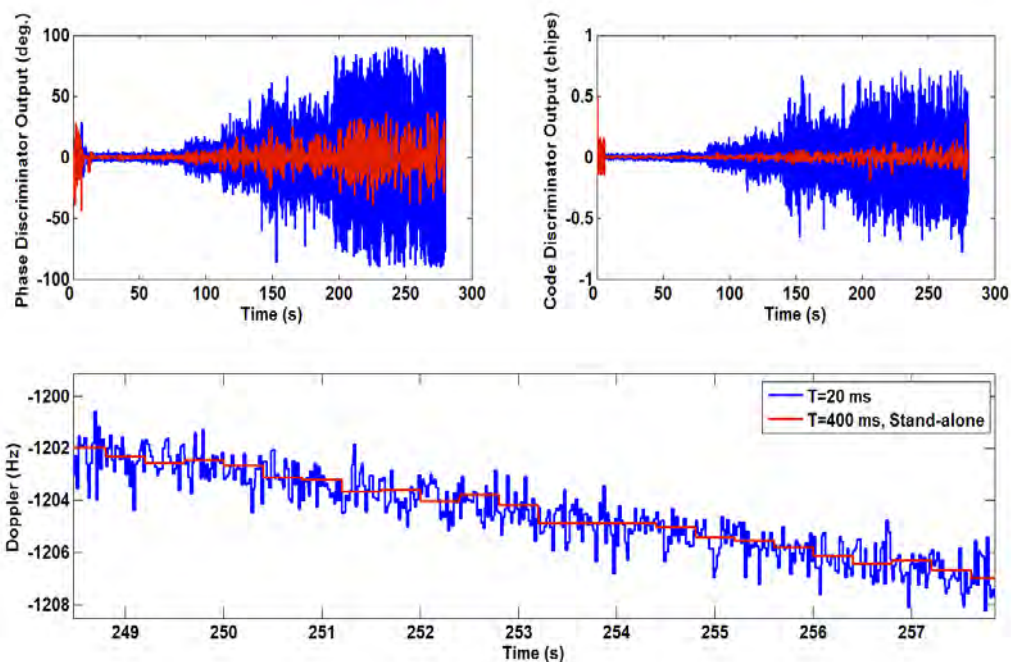
Figure 3-34 Noise reduction of the decision feedback in comparison with a

conventional 20 ms tracking loop

The performance of the decision feedback loop for increasing the integration time is shown in Figure 3-34. The traditional 20 ms loop lost lock as soon as the C/N_0 drops below 18 dB-Hz. The decision feedback loop with 400 ms integration shows more robustness in comparison with the 20 ms loop and lost lock about 40 seconds later but eventually the minimum achievable sensitivity is the same as the 20 ms loop at about 18 dB-Hz.

The main reason is the high BER at low C/N_0s, which causes wrong sign detection of the bits. However, as Figure 3-34 shows, the main advantage of the decision feedback

scheme is in reducing the noise in code and phase error measurements and also in the Doppler estimate.

While the problem of the instability in longer integrations can be circumvented by using the optimum filter structure, there is another important limiting factor in increasing integration time. This main limiting factor is the well known sinc-patterned correlation loss in each integration interval. This correlation loss is caused by the frequency error in each integration interval (Spilker 1997). This issue can be circumvented to some extent by the improved DPLL architecture proposed in Chapter 4.

3.7 Summary

This Chapter presented the optimum filter structure for DPLLs with rate-only feedback NCOs and phase and phase rate feedback NCOs. The filters are optimum in the sense that based on the linear Z-domain model of the loop, the phase noise variance is minimized.

It was shown that the operational range of the conventional loop filters in terms of $B_L T$ values can significantly be extended. Stephens and Thomas (1995) have shown that there are some significant tracking benefits in having a large $B_L T$ value, including reduced cycle slips. Moreover for a fixed update rate, larger bandwidth will reduce the steady state error of the DPLL which results in an improved dynamic performance.

While the $B_L T$ is practically limited to less than 0.4 for controlled-root and transformation methods for third order loops with rate-only feedback NCOs, this number can be extended to more than 10 when the optimum structure derived herein is adopted.

Design curves for first to fourth order loops were given, which enable one to design filters for a selection of normalized loop noise bandwidth. Practical considerations for the design and use of these filters were also given. The stability of the designed loops for large B_LT values was also demonstrated using live GPS signals in both static and dynamic cases. For the first time the performance of a DPLL tracking architecture in very long integration times for weak GPS signal applications was presented. Assisted and stand-alone schemes were considered and it was shown that, by using live GPS L1 signals in an assisted scheme, phase lock can be maintained down to 10 dB-Hz. This shows a 5 dB improvement in comparison with conventional techniques. Since only navigation data were used as assistance to the loop, the results are also relevant for pilot channel tracking of modernized GPS signals.

It was shown that by using the decision feedback principle and the sign detector, significant improvements in phase and code jitter reduction can be obtained in the case of a stand-alone receiver. However, this technique will not necessarily increase the sensitivity because of the high BER in lower signal levels.

Chapter Four: New improved DPLL structure

While the problem of instability in longer integrations and excessive NCO noise can be circumvented by using the optimum filter structure derived in Chapter 3, there is another important limiting factor in increasing integration time. This main limiting factor is the well known sinc-patterned correlation loss in each integration interval. This correlation loss is caused by the frequency error in each integration interval. In order to decrease the phase mismatch between the incoming and locally generated signal and the correlation loss in low update rate loops, an augmented DPLL with frequency rate estimator is proposed in this chapter. A combination of Kalman Filter (KF) and DPLL is used where the KF estimates the frequency rate and feeds this information back to the NCO to change the frequency of the locally generated signal even during each update interval. By this technique it becomes possible to ramp the NCO frequency during each update interval (instead of using the staircase fashion) to reduce the phase error due to the Doppler rate.

The output of the loop filter is used as Doppler measurements for the KF. The additional feedback of the frequency rate to the NCO might raise stability issues. In order to investigate this problem the NCO transfer function and the effect of the frequency rate estimator in Z-domain is modeled precisely and the loop filter is designed based on the results of Chapter 3 to overcome the stability issue raised by high integration time and additional feedback to the loop. The performance of these approaches is demonstrated with live GPS signals and for coherent integration times of up to one second.

4.1 Limitations of linear phase propagation in DPLL

When a digital phase-locked loop with a long loop update time (high integration time) tracks a signal with high Doppler, the demodulation losses due to frequency mismatch can become very significant. This loss is due to frequency mismatch between the locally generated signal and the incoming signal. A frequency error attenuates the apparent received power according to a sinc-squared function, to be henceforth referred to as a power roll-off function. The first null width of the power roll-off function is determined by the integration time T according to the relation f_{null} = 1/T. This relation essentially describes the fact that a 1-Hz error over 1 s causes a 2π phase change between the incoming signal and the locally generated carrier, negating all energy received.

At each loop update epoch in a conventional tracking architecture, the phase error signal is sampled, filtered, and used to set the frequency of the numerically controlled oscillator (NCO) to its new value. So, the continuously changing frequency of the signal tracked is followed by the NCO in a staircase fashion. As a result, it is assumed that the Doppler changes are negligible during each integration time. This assumption is approximately valid when a lower integration time (such as 20 ms) is used. However, by utilizing an integration time of one second for instance, even for the static case the Doppler frequency can change by 1 Hz during this interval, and using a conventional closed-loop tracking architecture will result in zero correlation power.

In conventional NCOs, the Doppler frequency estimated by the loop filter is used to update the NCO rate for the next integration interval. In cases where short integrations are utilized (fast update rate) this frequency can be assumed to be constant during the

integration interval. As a result during each update interval the NCO phase can be propagated linearly without increasing the phase mismatch (Figure 4-1). However, if longer integration is required then linear propagation of the NCO phase will result in increasing the phase mismatch and correlation loss. This situation is depicted in Figure 4-2.
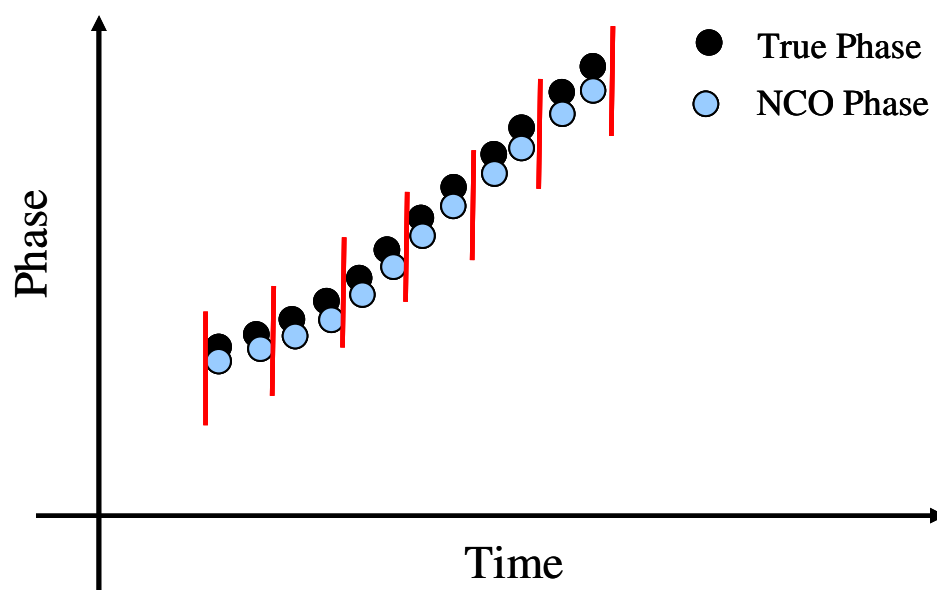
Figure 4-1 Low phase mismatch in case of fast update rate in conventional NCOs

(short integration time)
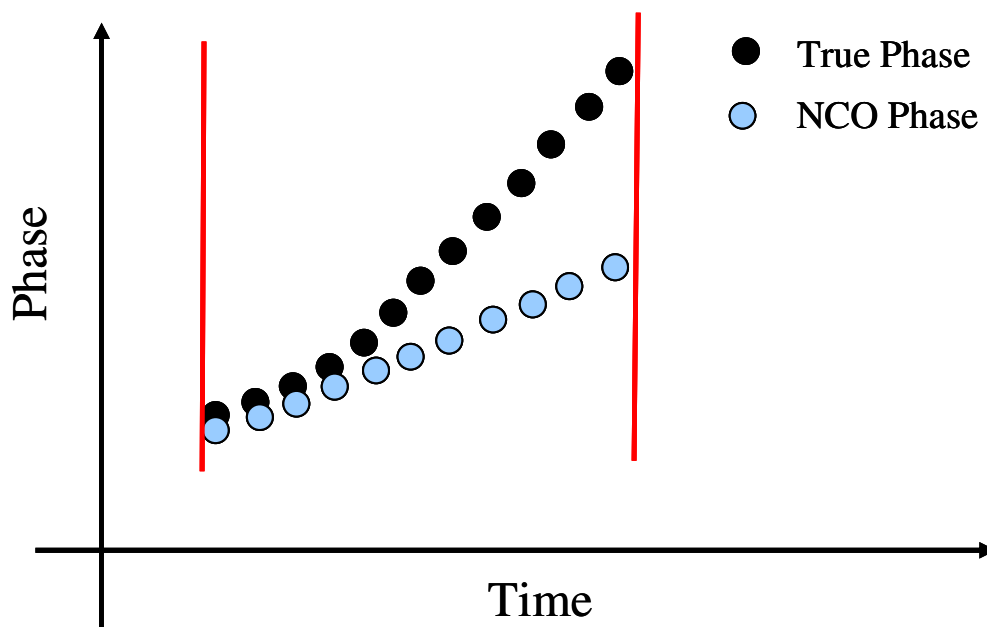
Figure 4-2 High phase mismatch in case of low update rate in conventional NCOs

(long integration time)

This effect is shown in Figure 4-3 based on live GPS signals and for the test in Section 3.6.2. In comparison with the 400 ms integration of Section 3.6.2, the integration time of 800 ms increases the phase mismatch between incoming and generated phase. This effect can be seen by the increase in the Q channel power and also by the increase in the BER as well. Integration times up to about 400 ms can be considered as a good tradeoff between reducing the noise at the discriminator outputs and the increase in phase mismatch because of the frequency change during the integration interval for static conditions.
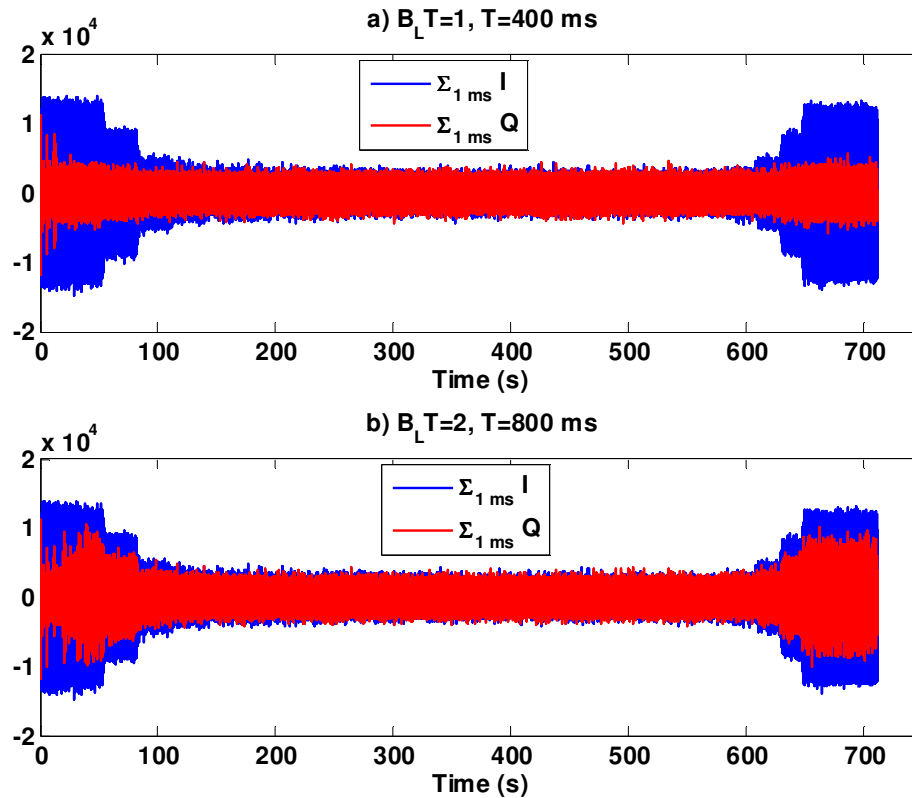
Figure 4-3 Increases in integration time and phase mismatch.

One way of reducing these Doppler-related losses is to compensate for the Doppler effect at each update interval using some kind of frequency-rate estimator. It can be estimated by utilizing the predicted trajectory. In cases in which the trajectory is not available this parameter should be estimated in the tracking loop itself. The performance of the fixed-window least-squares estimator to estimate the frequency rate is shown by Mileant & Simon (1986) who also mention the possibility of combining a DPLL and a Kalman filter for ramping the NCO frequency. However, the designed loop in the above was not completed mainly due to the stability challenges caused by the additional feedback to the

NCO. The modeling and design of the frequency rate estimator follows the work presented in Kazemi et al (2009).

4.2 NCO With Phase Rate and Frequency Rate Feedback

As mentioned previously, additional feedback to the NCO might cause stability issues. Since in this case the estimator becomes part of the loop, the poles of this estimator should be compensated by some means. This requires modeling of the loop precisely in order to design a proper compensator. The transfer function of the NCO significantly impacts the stability of the loop, especially at high $B_L T$ values. Hence, it has to be modeled carefully to determine the operational range of the loop (maximum allowable integration time and bandwidth). To model the NCO in the Z-domain the relationship between the average generated phases in two consecutive update intervals should be derived. By considering sufficiently short integration intervals the frequency rate of the received signal can be assumed constant during this interval.

Assuming that the frequency rate information is available to the loop the generated phase at the nth epoch can be written as

$$\varphi = \frac{1}{2}\dot{f}_n t^2 + f_n^s t + \varphi_0 \qquad \text{4-1}$$

where $\dot{f}_n$ is an estimated frequency rate, f_n^s is the phase rate at the start of the integration interval and φ_0 is the NCO phase at the start of this interval. This scheme is depicted in Figure 4-4.
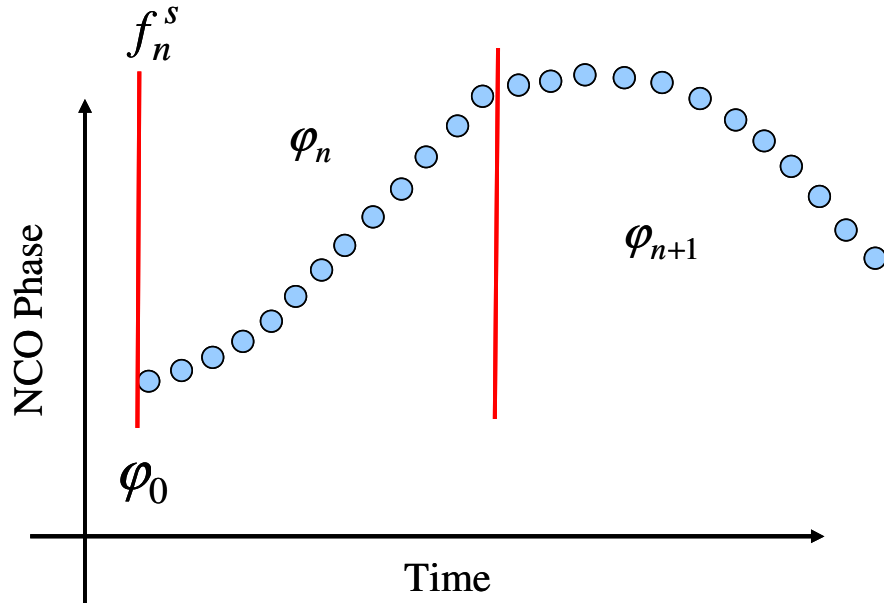
Figure 4-4 Schematic illustration of the NCO phase for the frequency and frequency rate feedback NCO

The average phase rate during each update interval is estimated by the loop filter. By assuming a constant frequency rate at each update interval, the average phase rate will be equal to the phase rate at the middle of the interval. As a result, Equation 4-1 can be written as

$$\varphi = \frac{1}{2}\dot{f}_n t^2 + (f_n - \dot{f}_n \frac{T}{2})t + \varphi_0 \qquad\qquad 4\text{-}2$$

where f_n is the average estimated phase rate by the loop filter. From Equation 4-2 the average generated phase by the NCO at the nth epoch can be derived as

$$\varphi_n = -\frac{T^2}{12}\dot{f}_n + \frac{T}{2}f_n + \varphi_0 \qquad\qquad 4\text{-}3$$

and similarly for the n+1th epoch it can be written as

$$\varphi_{n+1} = -\frac{T^2}{12}\dot{f}_{n+1} + \frac{T}{2}f_{n+1} + \varphi_1$$ 4-4

where φ_1 is the NCO phase at the start of the n+1th epoch. Assuming that the NCO phase is propagated continuously at each update interval, φ_1 can be written as

$$\varphi_1 = f_n T + \varphi_0.$$ 4-5

By substituting Equation 4-5 into Equation 4-4 and subtracting Equation 4-3 from Equation 4-4, the following relation between the average generated phases of the NCO in two consecutive intervals can be derived.

$$\varphi_{n+1} - \varphi_n = \frac{T^2}{12}\dot{f}_n - \frac{T^2}{12}\dot{f}_{n+1} + \frac{T}{2}f_n + \frac{T}{2}f_{n+1}.$$ 4-6

If the frequency rate is available from an external source, for instance from a trajectory file, then the system might be considered with two independent inputs and one output. However, in the scheme adopted here the frequency rate is estimated from the Doppler frequency. These two cases are shown in Figure 4-5. As such, in the Z-domain the relation between frequency rate and the phase rate can be written as

$$Z\left\{\dot{f}_n\right\} = E(z)Z\left\{f_n\right\}$$ 4-7

where $E(z)$ is the transfer function of the frequency rate estimator.
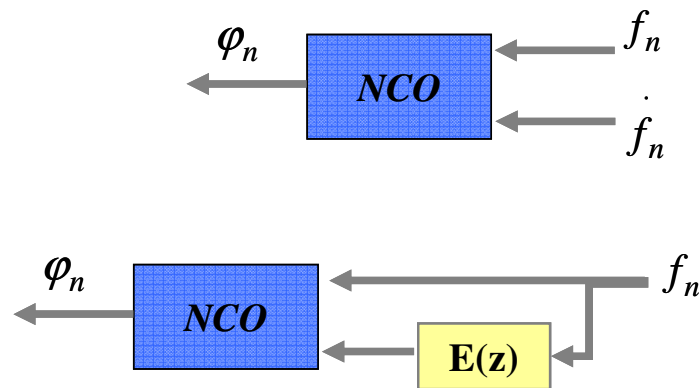
Figure 4-5 Two possible cases for applying the frequency rate to the NCO

By considering the effect of delay and taking the Z-transform of Equation 4-6 the transfer function of the NCO with phase rate and frequency rate feedback can be found as

$$N(z) = \frac{T^2}{12} \frac{E(z)(1-z) + \dfrac{6}{T}z + \dfrac{6}{T}}{z(z-1)}$$

4-8

Note that in comparison with conventional NCOs this transfer function is much more complicated, hence it increases the difficulty involved in designing the loop filter. It is also possible to add phase feedback to this NCO. In this case the NCO phase function is no longer a continuous function and the NCO applies a phase discontinuity at each update. These discontinuities can be determined so as to obtain a simpler transfer function. As a result φ_1 in Equation 4-5 can be modified to achieve a desired relation between the average generated phases in consecutive epochs.

4.3 Frequency Rate Estimator

To estimate the frequency rate, a second order Kalman filter is adopted. The theory and performance analysis of Kalman filter can be found in Simon (2006) and will not be repeated here. In order to determine $E(z)$, the transfer function of the Kalman filter in its steady-state should be derived. The output of the loop filter is used as a measurement for the Kalman filter. Note that the output of the loop filter at the nth epoch is the average predicted phase rate for the $n+1^{th}$ epoch. The state model can be written as

$$\begin{bmatrix} \bar{f}_{n+1} \\ \dot{\bar{f}}_{n+1} \end{bmatrix} = \begin{bmatrix} 1 & T \\ 0 & 1 \end{bmatrix} \begin{bmatrix} \bar{f}_{n} \\ \dot{\bar{f}}_{n} \end{bmatrix} + \omega_n \qquad\qquad 4\text{-}9$$

where $\bar{f}_{n+1}$ is the phase rate and ω_n is a white zero-mean noise process which has a covariance matrix Q which models the uncertainty in the state model. Note that the estimated phase rate is already available from the loop filter and $\bar{f}_{n+1}$ will be a refined estimate of the phase rate. The measurement model can be written as

$$f_{n+1} = \begin{bmatrix} 1 & 0 \end{bmatrix} \begin{bmatrix} \bar{f}_{n+1} \\ \dot{\bar{f}}_{n+1} \end{bmatrix} + \upsilon \qquad\qquad 4\text{-}10$$

where υ is the measurement noise with a variance of R. By using the state estimate update of the Kalman equation, the estimated states can be written as

$$\begin{bmatrix} \hat{f}_{n+1} \\ \dot{\hat{f}}_{n+1} \end{bmatrix} = \begin{bmatrix} 1 & T \\ 0 & 1 \end{bmatrix} \begin{bmatrix} \hat{f}_{n} \\ \dot{\hat{f}}_{n} \end{bmatrix} + \begin{bmatrix} k_1 \\ k_2 \end{bmatrix} (f_{n+1} - \hat{f}_{n} - T\dot{\hat{f}}_{n}) \qquad\qquad 4\text{-}11$$

where k_1 and k_2 are the Kalman gains and they can be assumed constant in a steady state condition and can be found as

$$\begin{bmatrix} k_1 \\ k_2 \end{bmatrix} = P_\infty H^T (H P_\infty H^T + R)^{-1}$$

4-12

where H is the observation matrix and P_∞ is the steady state value of the covariance of the estimation error which can be found by solving the following algebraic Riccati equation:

$$P_\infty = F P_\infty F^T - F P_\infty H^T (H P_\infty H^T + R)^{-1} H P_\infty F^T + Q$$

4-13

where F is the transition matrix defined as $\begin{bmatrix} 1 & T \\ 0 & 1 \end{bmatrix}$. The above equation can be solved numerically to determine the steady state Kalman gains. As can be inferred from Equation 4-13, the Q matrix can be used as a control parameter to change the Kalman gain values. Small Q matrix makes the Kalman filter less sensitive to new measurements which is suitable for weaker signals. Conversely a large Q matrix is desirable for high dynamic situations.

By taking the Z-transform of Equation 4-11, the transfer function of E(z) can be found. Taking the Z transform of (14) results in the following equations:

$$\begin{cases} (z - 1 + k_1)\overline{F}(z) = (T - k_1 T)Y(z) + k_1 X(z) \\ k_2 \overline{F}(z) = -(z - 1 + T k_2)Y(z) + k_2 X(z) \end{cases}$$

4-14

where $\overline{F}(z)$, Y(z) and X(z) are the Z transforms of $\overset{\frown}{f}_{n+1}$, $\overset{\circ}{f}_{n+1}$ and f_{n+1}, respectively.

By solving the above set of equations, the transfer function of the estimator E(z), which represents the relation between the input to the estimator, i.e. f_{n+1}, and its output, i.e. $\overset{\circ}{f}_{n+1}$, can be derived as

$$\frac{Y(z)}{X(z)} = E(z) = \frac{k_2 z(z-1)}{z^2 + (k_1 + k_2 T - 2)z + (1-k_1)}. \qquad 4\text{-}15$$

After finding $E(z)$ the classical tracking architecture of Figure 2-9 can be modified as shown in Figure 4-6.

As mentioned earlier $\hat{f}_{n+1}$ is a refined estimate of the phase rate. This value could be used as a command signal to update the phase rate of the NCO. However this requires another modification to the loop and the effect of the $\frac{\overline{F}(z)}{X(z)}$ estimator should also be considered to ensure the stability of the loop. This approach will not be considered here. Therefore, in this work, the output of the loop filter will be used to update the phase rate of the NCO. However, $\hat{f}_{n+1}$ could be used for velocity estimation. The transfer function of the refined frequency estimator can be found as

$$\frac{\overline{F}(z)}{X(z)} = M(z) = \frac{z(k_1 z + k_2 T - k_1)}{z^2 + (k_1 + k_2 T - 2)z + (1-k_1)}. \qquad 4\text{-}16$$
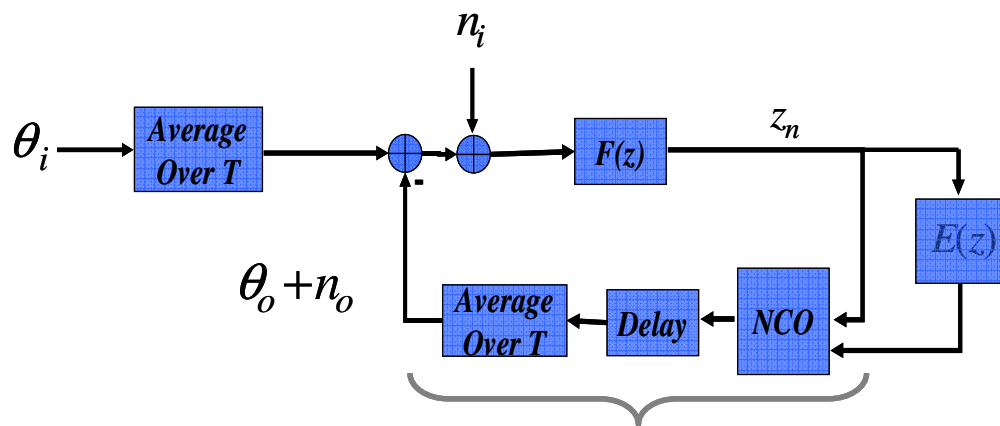
Figure 4-6 Modified DPLL model

In comparison with other denoising techniques such as wavelets, *M(z)* has the advantage that it can denoise the Doppler in real time (instead of post processing with wavelets) and with less computational burden.

Using Equations 4-16 and 4-8 the transfer function of the NCO can be derived. As shown in Chapter 3 this transfer function could be used to optimize the closed loop transfer function. It can be shown that if k_2T remains near zero, Equation 4-8 can be approximated by a transfer function of a rate only feedback NCO, as such, loops designed in Chapter 3 could be directly used without any significant performance degradation.

4.4 Tracking Results

The same test setup as in section 3.6.1 is used here to evaluate the performance of the augmented DPLL. The performance of the KF estimator in estimating the phase rate and frequency rate of a live GPS signal with integration time of 20 ms is shown in Figures 4-7 and 4-8, respectively. In Figure 4-7, f_{n+1} is shown in blue and its refined estimate by the KF, i.e. $\hat{f}_{n+1}$, is shown in red. A much more refined estimate of the phase rate is achieved by using the $M(z)$ estimator. However, as mentioned earlier, the f_{n+1} values are used to update the NCO phase rate. If it is desired to use the refined estimate of the phase rate, the effect of the poles of the $M(z)$ estimator should be taken into account. In Figure 4-9 the denoising effect of this scheme is shown for the same test as in Figure 3-28. Choosing a high bandwidth of 58 Hz and an integration time of 20 ms makes the

Doppler estimate too noisy for a signal which was attenuated to achieve a C/N$_0$ of 30 dB-Hz. Although it is not required to chose such a high bandwidth for this test, it is merely chosen to illustrate the real-time filtering effects of *M(z)*.
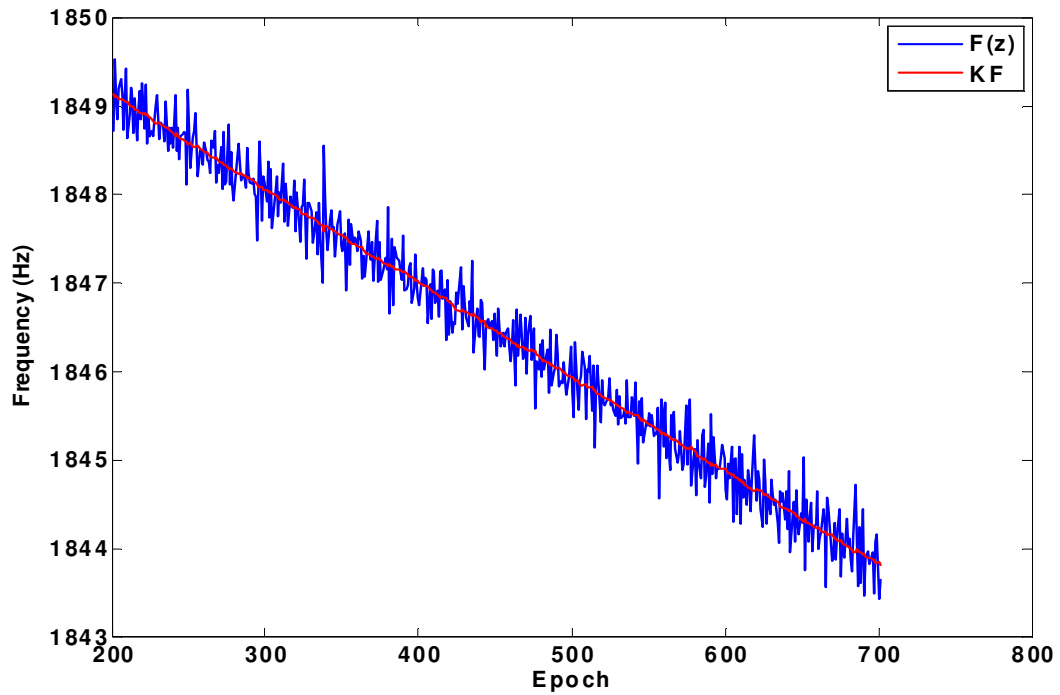
Figure 4-7 Estimated Doppler frequency
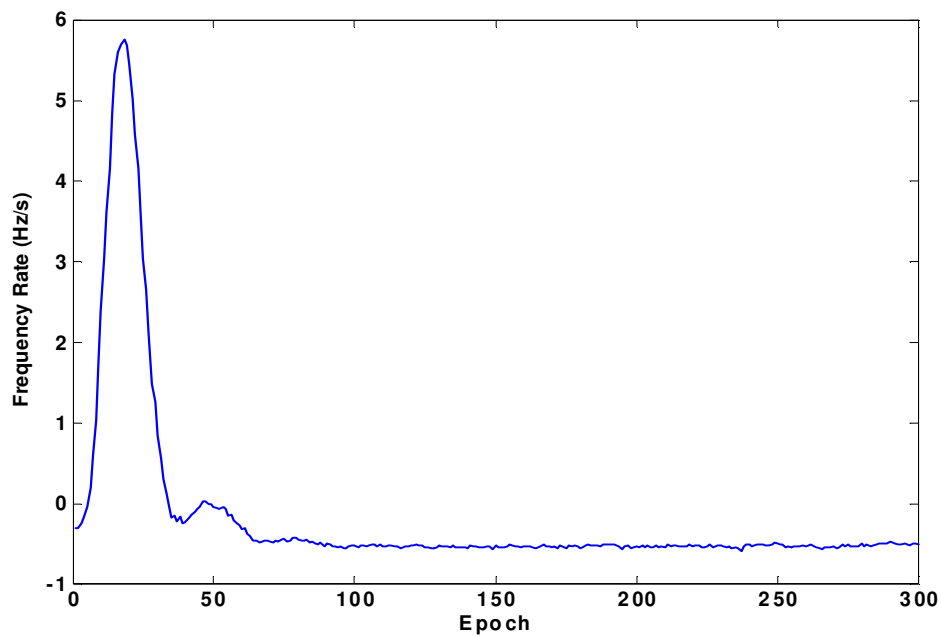
Figure 4-8 Frequency rate estimated by E(z)
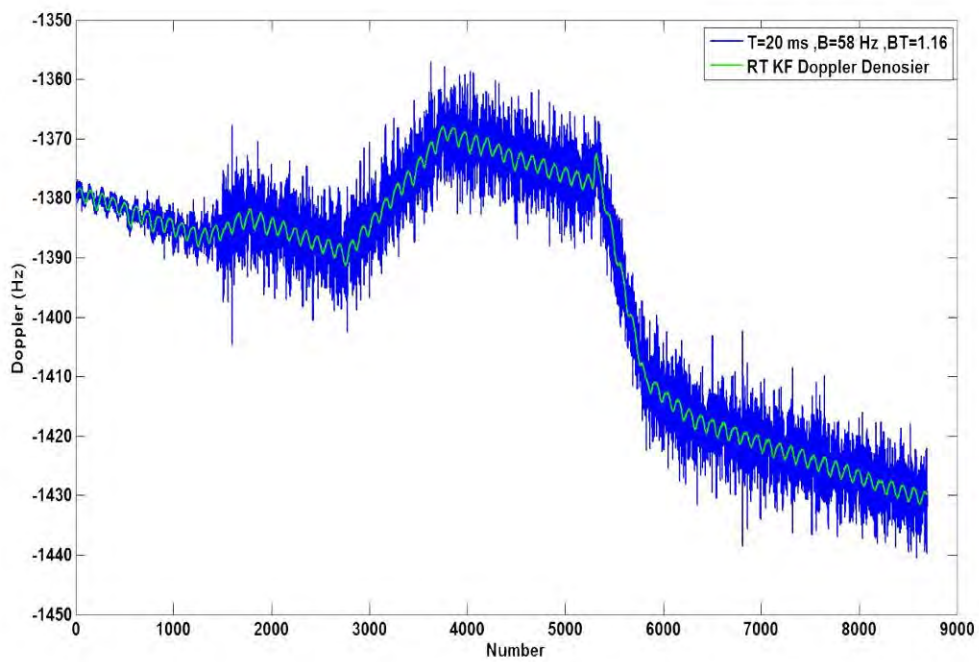
Figure 4-9 Filtering capability of the augmented DPLL

The slow transient response of the frequency rate estimator in Figure 4-8 is due to the small Q matrix chosen in Equation 4-13. If a faster response is required, a larger Q matrix should be chosen, however the system becomes less robust against noise. The corresponding Kalman gains of the chosen Q matrix were 0.3474 and 0.1806 for k_1 and k_2, respectively. By these values the transfer function of the NCO in Equation 4-8 can be approximated by the transfer function of the phase rate only feedback NCO. Therefore the optimum digital loop filter for different bandwidths and loop orders can be easily designed by using the designed curves for the phase rate only feedback NCO.

The importance of this new DPLL architecture becomes evident for long integration times where the correlation loss and increased phase mismatch become significant. The performance of the phase lock indicator is shown in Figure 4-10. This phase lock indicator is calculated based on filtering of the estimated phase error generated every one millisecond. In this case a coherent integration time of one second was used. The value of 1 in phase lock indicator stands for a perfect phase lock. The improvement in reducing the phase mismatch becomes apparent in comparison with a conventional loop. Note that a high elevation satellite with a low Doppler frequency rate is chosen for this comparison. In cases where Doppler frequency rate is higher it becomes impossible to track the signal with a conventional DPLL while one second of integration is utilized. As shown in Figure 4-11, integration time is increased gradually to one second to ensure the convergence of the transient response.

An interesting point is that unlike the PLI output, this phase match improvement is not evident from comparing phase discriminator outputs. As depicted in Figure 4-12 there is no significant difference between the phase discriminators performance. This fact gives

an insight into the operation of the DPLL. The DPLL tries to achieve a zero average phase error operational point regardless of the phase propagation method. This is shown in Figure 4-13. Although both DPLL and augmented DPLL result in nearly the same average phase error in one second, an augmented DPLL follows the incoming signal with less MSE (Mean Square Error) during the integration interval. This improvement results in a better Bit Error Rate (BER) performance, fewer cycle slips and lower correlation loss.
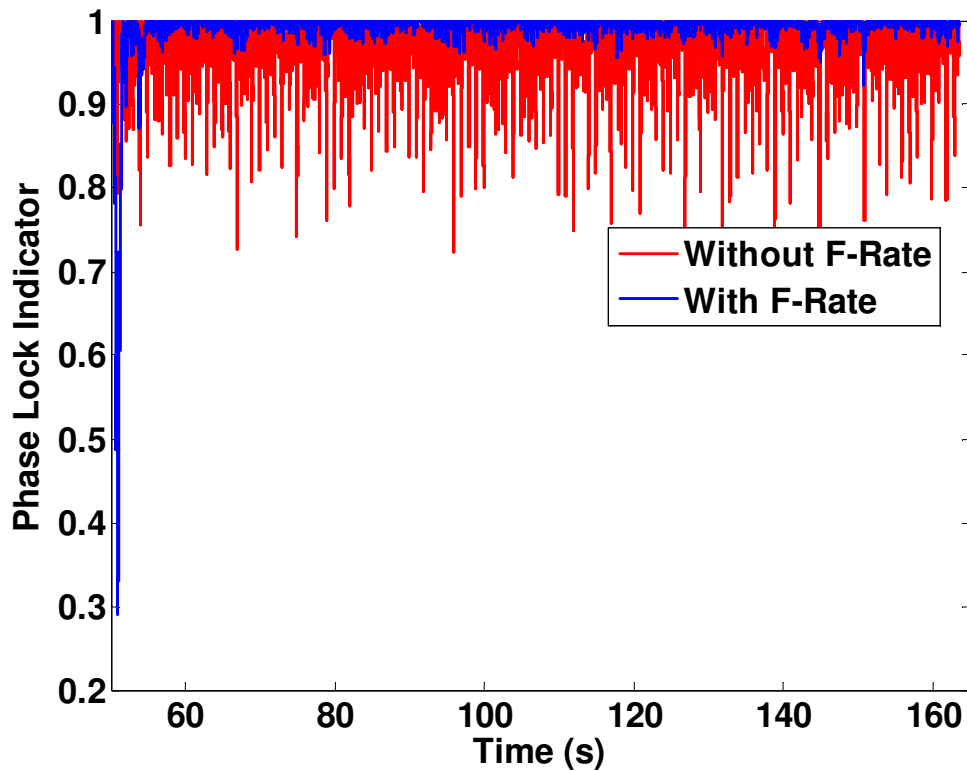
Figure 4-10 Phase lock indicator
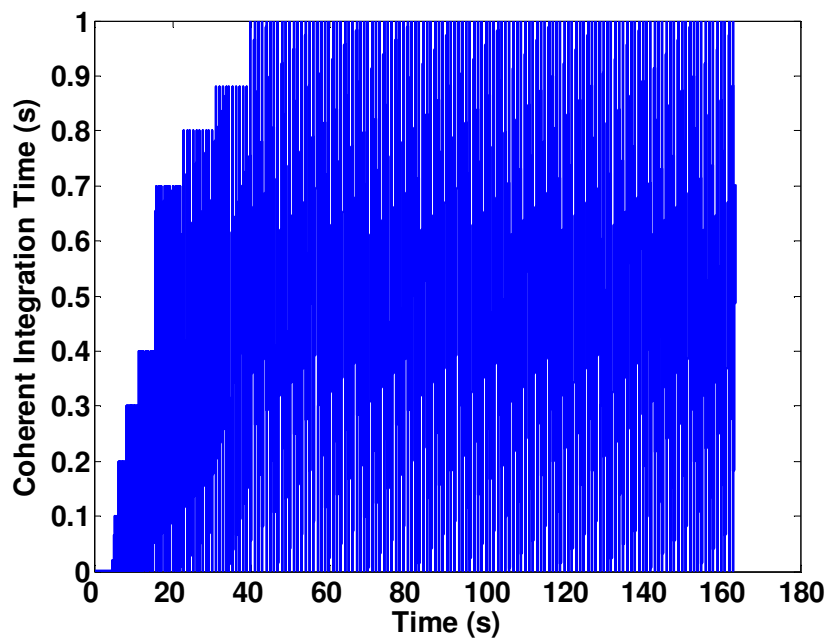
Figure 4-11 Integration time increased gradually
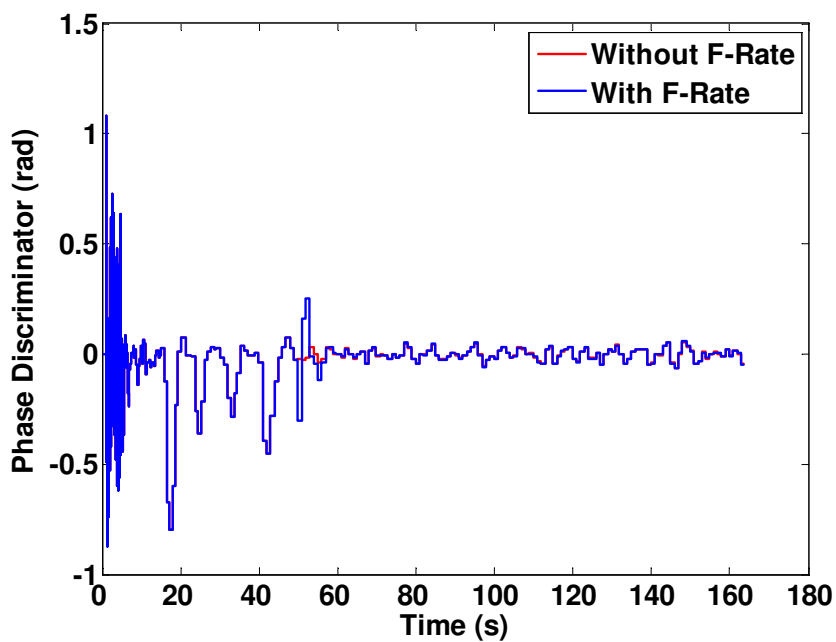
Figure 4-12 Phase discriminator performance
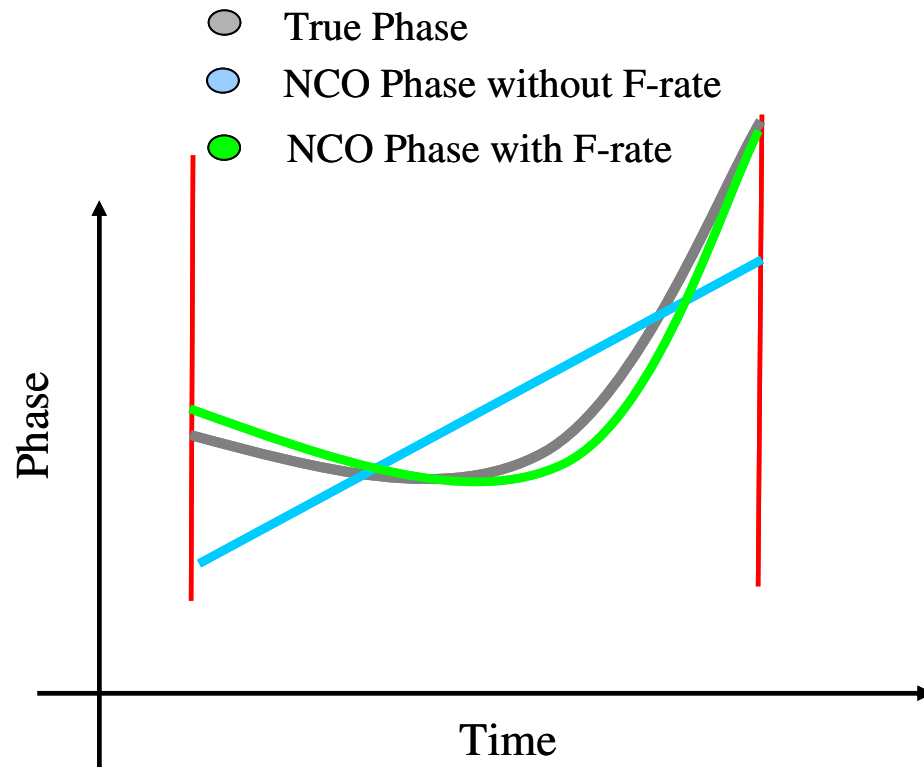
Figure 4-13 Different phase propagation schemes

4.5 Summary

This Chapter presented a digital phase locked loop with a frequency rate estimator. The frequency rate estimator was designed based on a steady state Kalman filter. The NCO with phase rate and frequency rate feedback was introduced and its transfer function was derived precisely. Based on this model for the NCO and the transfer function of the frequency rate estimator the tracking loop was optimized in order to minimize the phase noise variance. The loop filter also acts as a compensator to ensure the stability of the loop.

The performance of these approaches was demonstrated with line of sight live GPS signals and for coherent integration times of up to one second. It was shown that this new tracking architecture can significantly improve the performance of the loop in high integration times. This DPLL reduces the phase mismatch between the locally generated signal and the incoming signal and this reduction in turn results in a better Bit Error Rate (BER) performance, fewer cycle slips and lower correlation loss.

Chapter Five: Seamless Outdoor to Indoor Tracking Using Successive Tracking Scheme

In this chapter a successive tracking scheme is implemented to overcome the problem of tracking weak GPS signals in indoor environments. In this technique several tracking schemes can be cascaded serially. The first tracking scheme is usually chosen to have a low C/N_0 threshold but possibly a high RMS error. The subsequent tracking stages track the remaining error signals from the first stage. Since the overall C/N_0 threshold on carrier frequency estimation is lower than the carrier phase estimation, the first stage is chosen to be a frequency estimator. The carrier phase can be estimated in subsequent stages and since part of the dynamics have been removed by the first estimator, narrower bandwidths and higher integration times can be used at latter stages. The performance and advantages of this technique are shown based on GPS signal simulations and live GPS signals in selected indoor environments. It is shown that the tracking capability of this scheme in some cases is better than the commercially available HSGPS receivers.

5.1 Indoor signal tracking

The E-911 requirements for autonomous cellular phone location has motivated the development of highly specialized GPS receivers in which the use of aiding from communication networks is maximized to avoid the need to read the navigation data or

any other tracking mode that requires continuous satellite tracking (Kaplan & Hegarty 2006).

The common practice for GPS receivers in cellular handsets is to never close any tracking loops but rather to dwell on the GPS signals in a controlled (network-aided) search mode long enough to extract the required information. The methods for obtaining the required measurements in indoor applications are similar to the techniques for acquisition albeit a major difference is that the external aiding typically results in a very narrow window in the two dimensional codephase/Doppler parameter space (Kaplan & Hegarty 2006). Stand-alone high sensitivity GPS receivers mostly rely on having a large number of correlators. For instance, the u-blox 5 receiver utilizes over one million effective correlators (u-blox 2010). However this method is not feasible in software based receivers. Hence a practical approach for closed-loop indoor signal tracking with a limited number of correlators (three in this case) instead of the quasi-acquisition methods is investigated in this Chapter.

Relying solely on extended integration (as in Chapter 4) for indoor carrier phase tracking during antenna movement might not be practical as shown in Figure 5-1. In this test the user was moving from outside towards the building. Rapid changes in Doppler caused by the motion and changes in the antenna tilt require low integration time and high bandwidth. However, as the antenna goes inside usually more than 30 dB signal attenuation is expected. As a result, during this period longer integration time is required in order to prevent loss of lock. Consequently at a transition point the designer faces a dilemma of requiring both low and high integration times. Note that in this case, even the second order phase propagation shown in Chapter 4 might not be sufficient to follow the

carrier phase precisely and a fast update rate loop should be used. Moreover changes in the amplitude caused by severe fading is another limiting factor in increasing the integration time. Eventually deep fading causes loss of lock as can be inferred from the C/N_0 estimator in Figure 5-1.
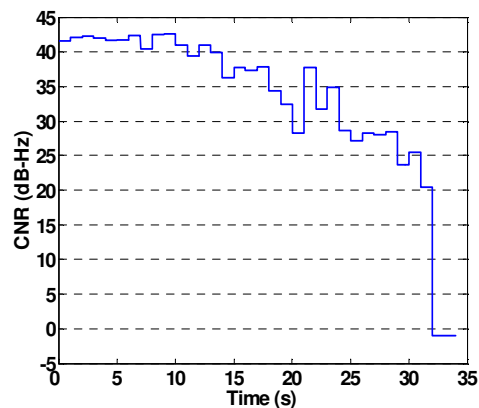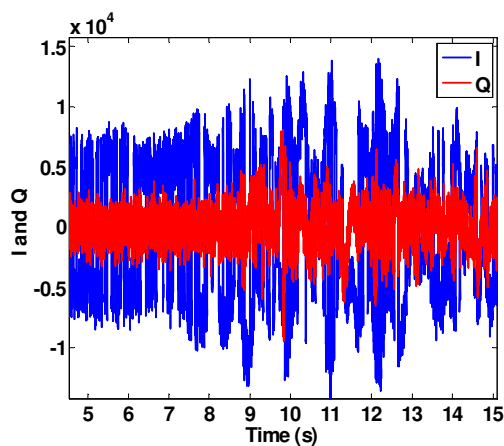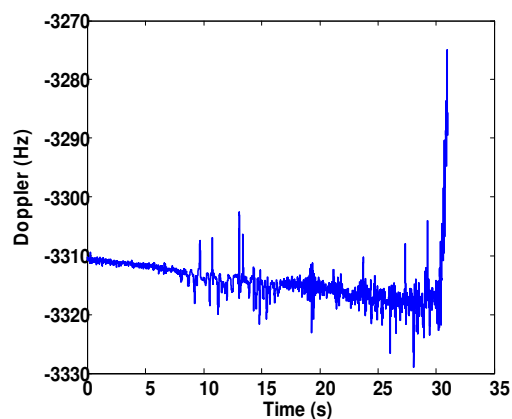
Figure 5-1 Different tracking metrics indoors

If the Doppler changes are known to be limited to some specific orders (for instance if only up to rate of Doppler rate is present and higher orders Doppler derivatives are negligible) then the designed loops in previous chapters can be utilized without further modifications. In order to overcome these difficulties the integration time should be kept

short. The following steps are recommended as a possible solution for tracking GPS signals in severely GPS-degraded environments:

- Successive tracking schemes should be used in which several tracking schemes can be cascaded serially.

- Since carrier frequency estimation is more robust against noise and dynamics in comparison to carrier phase estimation, initial stages should be chosen as frequency estimators. The carrier phase can be estimated in later stages.

- The coherent integration time (T) should be kept short enough to overcome the random changes in Doppler and signal amplitude. Since only T seconds of integration might not be adequate to enhance the signal to ratio in harsh environments, N of these T seconds integrated samples can be used to for a single update of the NCO. Although pure coherent integration (integration time of NT seconds) is considered as an optimum solution it is also a sharp filter which can filter out the useful information in a signal and cause loss of lock.

In order to achieve the above goals a method based on Kumar (1990) is adopted herein for indoor GPS tracking and for the first time in practice it is shown that this technique can be used for seamless outdoor to indoor tracking.

5.2 Successive Tracking Scheme

In the successive scheme, the parameters will be estimated by an algorithm which has a low threshold on SNR but with possibly higher RMS estimation errors. Then an error signal whose parameters are equal to the difference between the true parameters and the above estimates is processed by another algorithm to estimate these error signal parameters. Since the error signal involves much smaller dynamics, the second algorithm can have a smaller bandwidth resulting in a smaller estimation error (Kumar 1990). This scheme is shown in Figure 5-2 where $\theta_I(t)$ is the incoming phase, $\theta_L(t)$ is the first stage estimate, $\theta_0(t) = \theta_I(t) - \theta_L(t)$, $\theta_1(t) = \theta_0(t) - \hat{\theta}_0(t)$, and the estimated incoming phase can be written as $\theta_I(t) \cong \theta_L(t) + \hat{\theta}_0(t) + \hat{\theta}_1(t)$.
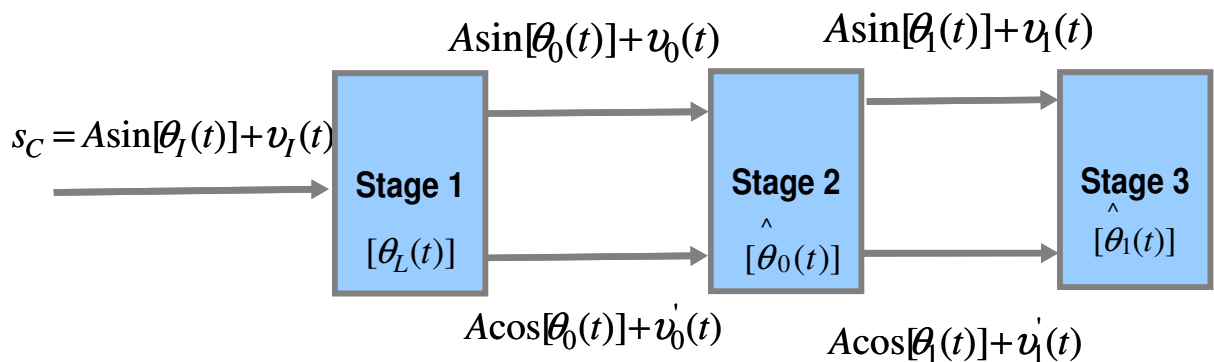
Figure 5-2 Successive tracking scheme

The incoming phase process over a small estimation period can be approximated by

$$\theta_I(t) \cong \varphi_I + \omega_I t + 0.5\dot{\omega}_I t^2 + \frac{\ddot{\omega}_I t^3}{6} \ .$$

5-1

The average sampled version of the phase error process can be written as

$$\theta_0(k) = \theta_I(k) - \theta_L(k) \cong \varphi_0 + \omega_0 kT + 0.5\dot{\omega}_0 (kT)^2 + \frac{\ddot{\omega}_0 (kT)^3}{6} \ ;$$

$$k = 1, 2, ..., N$$

5-2

where φ_0, ω_0, $\dot{\omega}_0$ and $\ddot{\omega}_0$ are the initial phase error, frequency error and corresponding derivatives, respectively.

By estimating the error signal parameters in Equation 5-2, the locally generated signal can be corrected correspondingly at each NCO update interval. In order to eliminate the phase error φ_0 and to derive relatively coarse estimates of the frequency error and its derivatives, the following modification can be applied to the correlator outputs after the first stage:

$$I_d(k) \overset{\Delta}{=} I(k) - I(k-1)$$

$$Q_d(k) \overset{\Delta}{=} Q(k) - Q(k-1)$$

5-3

By expanding the sine and cosine terms in a Taylor series around $t_{k-1} = (k-1)T$, Equation 5-3 can be written as (Kumar 1990)

$$I_d(k) = -T(\omega_0 + \dot{\omega}_0 \tau_k + 0.5\ddot{\omega}_0 \tau_k^2)Q(k-1) + \zeta_i(k)$$

$$Q_d(k) = T(\omega_0 + \dot{\omega}_0 \tau_k + 0.5\ddot{\omega}_0 \tau_k^2)I(k-1) + \zeta_q(k)$$

5-4

where ξ_i and ξ_q are the noise terms and

$$\tau_k = (k - 0.5)T \ .$$

5-5

The measurement model in Equation 5-4 can be written as

$$Z(k) = H(k)x + \xi_k \qquad \qquad \text{5-6}$$

where

$$H(k) = \begin{bmatrix} -TQ(k-1) & -T\tau_k Q(k-1) & -0.5T\tau_k^2 Q(k-1) \\ TI(k-1) & T\tau_k I(k-1) & 0.5T\tau_k^2 I(k-1) \end{bmatrix} \qquad \text{5-7}$$

and

$$Z(k) = \begin{bmatrix} I_d(k) \\ Q_d(k) \end{bmatrix}$$

$$x = \begin{bmatrix} \omega_0 \\ \dot{\omega}_0 \\ \ddot{\omega}_0 \end{bmatrix}. \qquad \text{5-8}$$

The estimated error signal parameters can be derived using the least-squares estimate:

$$\hat{x} = \left\{ \sum_{j=1}^{N} H^T(j)H(j)\lambda^{N-j} \right\}^{-1} \left\{ \sum_{j=1}^{N} H(j)^T Z(j)\lambda^{N-j} \right\} \qquad \text{5-9}$$

where λ is used as a forgetting factor with $0 < \lambda < 1$.

This scheme is illustrated in Figure 5-3. Note that the update rate of the NCO is equal to $T_N = NT$. As shown in Figure 5-3 for N=4, the boundary samples can also contribute in making two differential measurements by overlapping between two consecutive update interval.
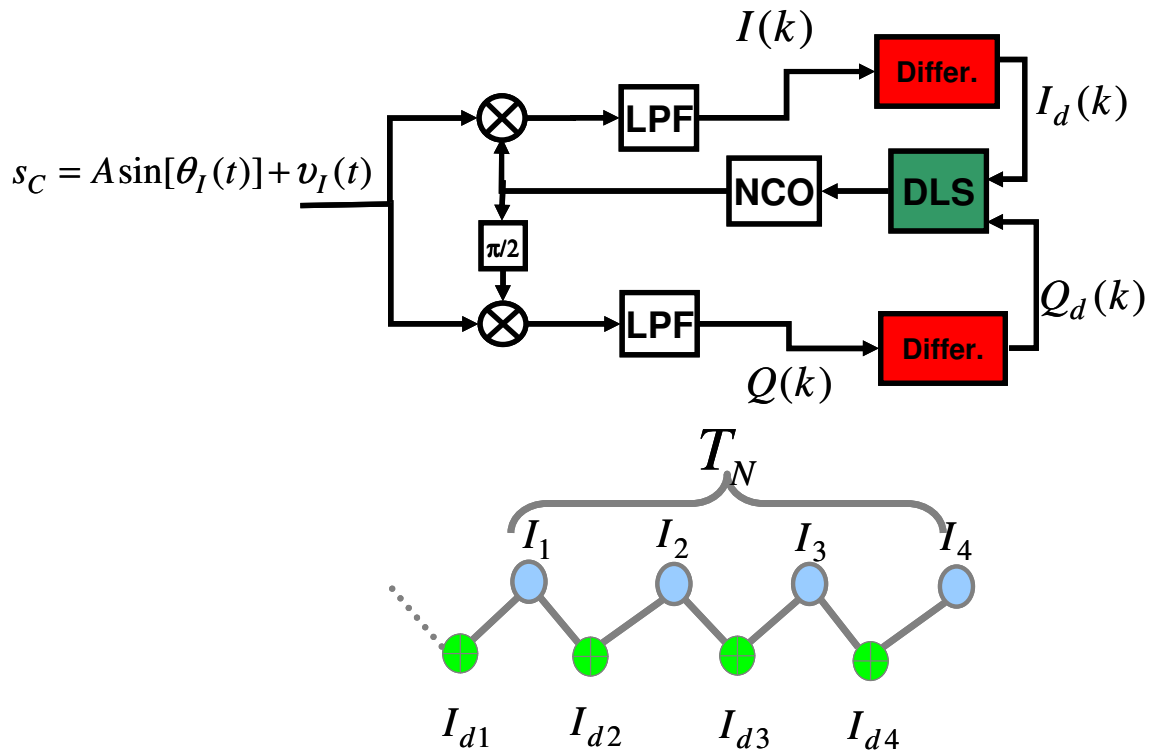
Figure 5-3 LS tracking scheme

Since the noise in Equation 5-4 is coloured there would be a bias in the parameter estimates under low SNRs. To reduce such a bias the noise should be whitened (Kumar 1990) by passing through the transfer function $(1-z^{-1})^{-1}$ as shown in Figure 5-4. Assuming that the algorithm in Equation 5-9 asymptotically approaches a time-invariant system, then the least-squares algorithm might be interchanged with $(1-z^{-1})^{-1}$. This technique corresponds to post-averaging the estimated parameters. An exponentially data-weighted averaging can be performed on the estimated parameters to take into account the time variation of parameters.
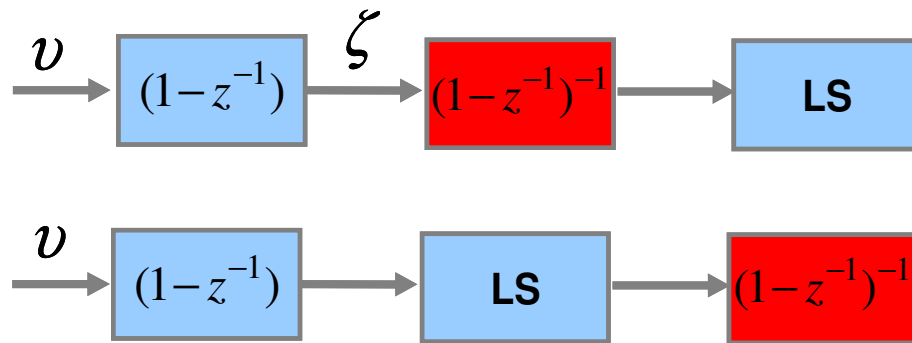
Figure 5-4 Noise whitening scheme

After estimating the error signal parameters the locally generated signal can be corrected accordingly. The next stage is chosen to be a KF which has the duty of estimating the phase in addition to frequency. As shown later, this stage can also act as a bias or cycle slip detector. Note that the first stage NCO needs to operate at the IF frequency and high sampling rate for down conversion; however subsequent stages operate at baseband which has significantly less computational burden. The in-phase and quadrature phase components from the second stage can be computed as

$$
\begin{aligned}
I^{'}(k) &= I(k)Cos(\hat{\theta}_0(k-1)) + Q(k)Sin(\hat{\theta}_0(k-1)) \\
Q^{'}(k) &= Q(k)Cos(\hat{\theta}_0(k-1)) - I(k)Sin(\hat{\theta}_0(k-1))
\end{aligned}
. \qquad \text{5-10}
$$

In the previous method, instead of estimating the incoming signal parameters directly, the error signal parameters $\theta_I - \theta_L$ were estimated. The same approach could be used for the second stage to estimate the error signal $\theta_o - \hat{\theta}_0$ from Equation 5-10 and correspondingly correct the second stage NCO phase, i.e. $\hat{\theta}_0$. However since for the second stage the computations are at baseband, θ_0 can be estimated directly based on $I(k)$ and $Q(k)$. This scheme is shown in Figure 5-5. Nevertheless, Equation 5-10 should be computed if a

third stage is going to be used, since $I'(k)$ and $Q'(k)$ will be considered as input signals

for the third stage.
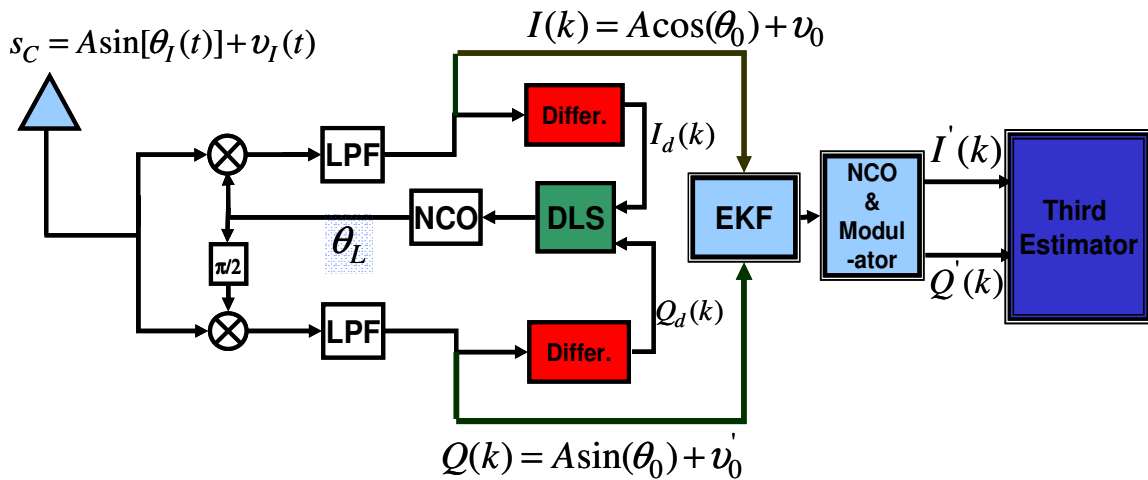
Figure 5-5 Realization of the successive tracking scheme

In order to achieve some processing gain to counter the fact that these are weak signal

samples, the outputs of the first stage are grouped into batches of N samples. Within the

current set of N samples (index by k i.e. $k = 1, \ldots, N$), a new index ℓ is introduced such

that the ℓ th group of N samples is index ℓ and $\ell = 1, 2,\ldots,\infty$.

The incoming phase process for the second stage can be approximated as

$$\theta_{0\ell}(k) \cong \varphi_{0\ell} + \omega_{0\ell}kT + 0.5\dot{\omega}_{0\ell}(kT)^2.$$ 5-11

The phase process parameters at each update interval can be estimated as

$$\hat{\theta}_{0\ell}(k) = H(k)\hat{x}_{0\ell}(k-1)$$

$$x_{0\ell}(k) = \begin{bmatrix} \varphi_{0\ell} \\ \omega_{0\ell} \\ \dot{\omega}_{0\ell} \end{bmatrix} \qquad \text{5-12}$$

$$H(k) = \begin{bmatrix} 1 & kT & 0.5kT^2 \end{bmatrix}$$

The estimate of the vector parameters can be found as

$$\hat{x}_{0\ell}(k) = \hat{x}_{0\ell}(k-1) + K_\ell(k)\chi_\ell(k) . \qquad \text{5-13}$$

where K_ℓ is the Kalman gain and $\chi_\ell(k)$ is the innovation sequence (Simon 2006).

Assuming the incoming phase can be measured directly, the innovation sequence

becomes

$$\chi_\ell(k) = \frac{Q(k)Cos(\hat{\theta}_{0\ell}(k)) - I(k)Sin(\hat{\theta}_{0\ell}(k))}{\sqrt{I(k)^2 + Q(k)^2}} . \qquad \text{5-14}$$

The Kalman gain is updated as

$$K_\ell(k) = P_\ell(k-1)H^T(k)(\sigma^2 + HP_\ell(k-1)H^T(k))^{-1}. \qquad \text{5-15}$$

where σ^2 is the measurement noise variance and P is the estimation error covariance

matrix and for $k = 1,2,...,N$ is updated as

$$P_\ell(k) = (I - K_\ell H(k))(P_\ell(k-1) + Q') . \qquad \text{5-16}$$

where Q' is the covariance matrix of the process noise. In deriving Equation 5-16 the

one-step Kalman filter equation (Simon 2006) with transition matrix equal to the identity

matrix is used.

To take into account the time variations of the signal vector parameter after each N

samples, the covariance matrix is reinitialized again to the steady state value, i.e.

$P_\ell(0) = \overline{P}$ and the initial estimate for the next N sample is taken to be equal to the last

estimate from previous N samples, i.e. $x_{\ell+1}(0) = x_\ell(N)$. This is an appropriate choice for the initial estimate since, if the first stage converges, then the input signal to the next stage would be random and remain close to zero. This scheme is shown in Figure 5-6 for *N=4*.

$\hat{x}_{01}(0) = 0$

$P_1(0) = \overline{P}$

$\ell = 1$

$\hat{x}_{02}(0) = \hat{x}_{01}(N)$

$P_2(0) = \overline{P}$

$\ell = 2$

$\hat{x}_{03}(0) = \hat{x}_{02}(N)$

$P_3(0) = \overline{P}$

$I_1 \quad I_2 \quad I_3 \quad I_4$

$I(1) \quad I(2) \quad I(3) \quad I(4)$

$k = 1,2,...,N$

$T_N = NT$

$N = 4$
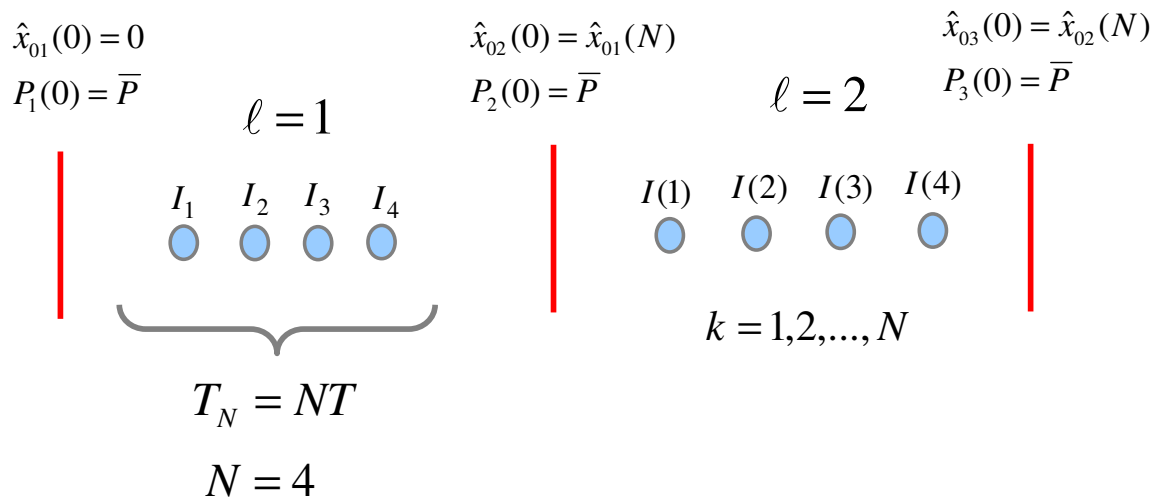
Figure 5-6 Relative timing for the second stage

5.3 Simulations

For filter tuning purposes and to describe some of the advantages of the successive tracking, a GPS signal simulator is implemented. This simulator provides the baseband samples under controlled dynamic conditions. It is assumed that the symbol timing is acquired and the C/A code has been removed.

A sampling rate of 200 samples per second was used. Parameters for one of the typical simulated dynamic trajectory and its corresponding Doppler are shown in Figure 5-7. The signal was attenuated down to 22 dB-Hz. The NCO update rate was chosen to be 200 ms. The estimated Doppler at the end of the simulation time where the Doppler rate is maximum is shown in Figure 5-8. The Doppler error, which is the difference between the incoming signal and locally generated signal frequencies at the first stage, is shown in Figure 5-9. This Doppler error appears as a new incoming signal for the second stage. As shown in Figure 5-9, the Doppler error is correctly detected and tracked by the second stage.
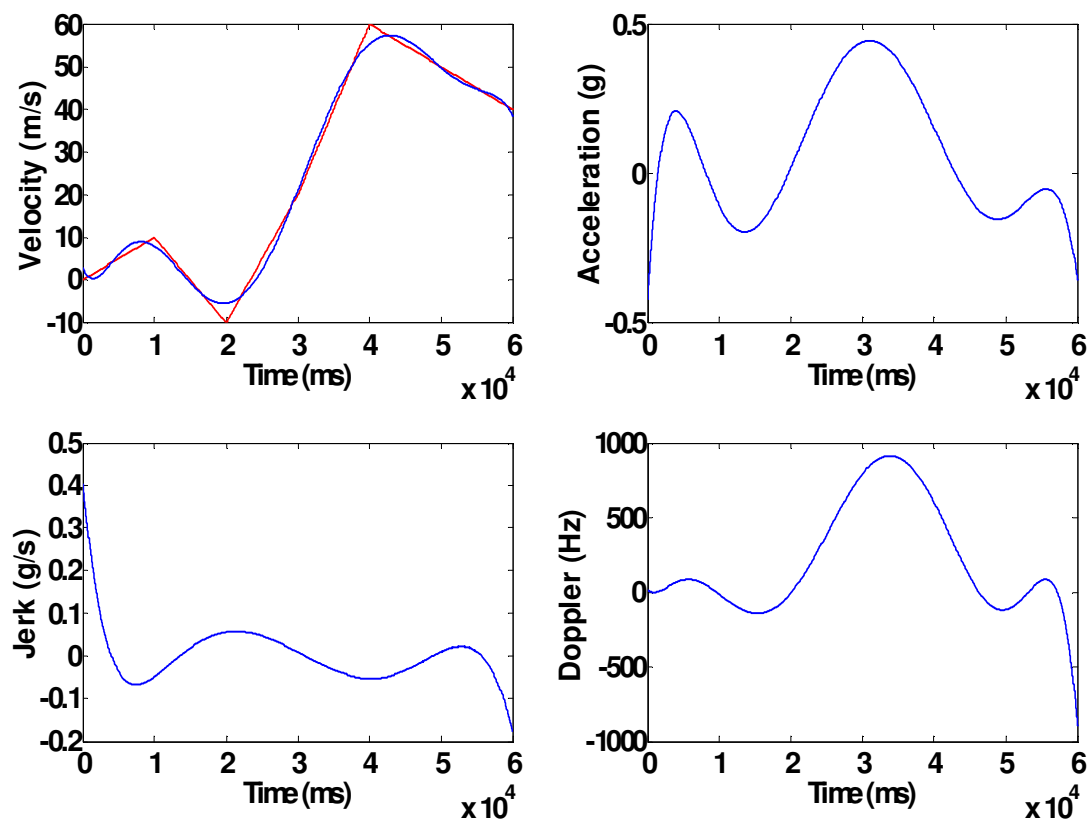
Figure 5-7 Parameters for dynamic trajectory
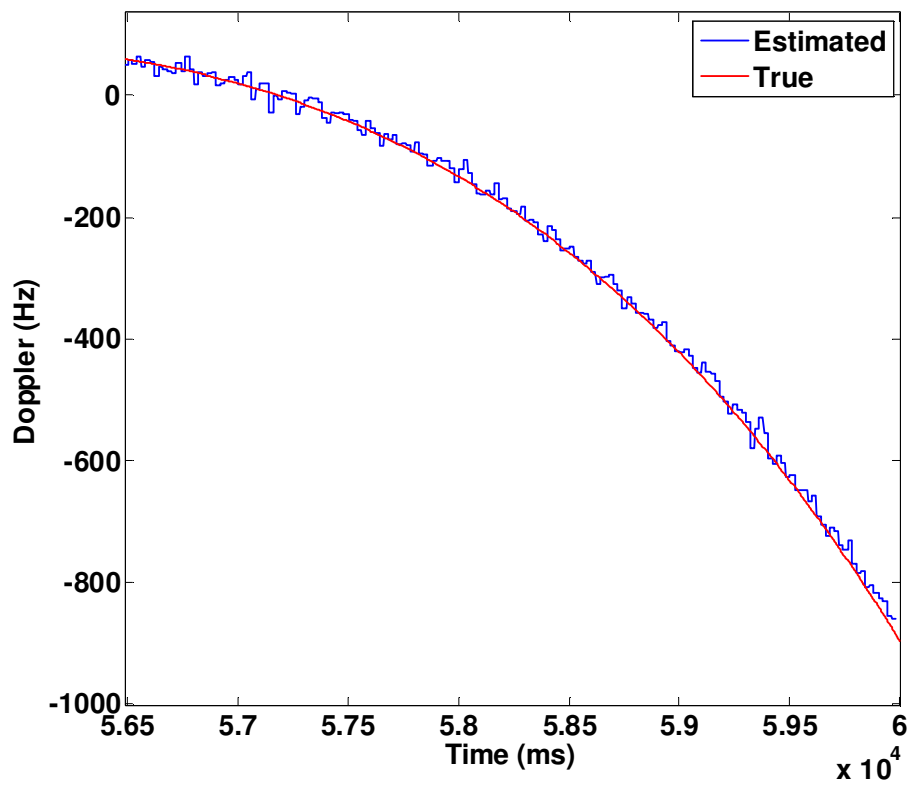
Figure 5-8 True and Estimated Doppler
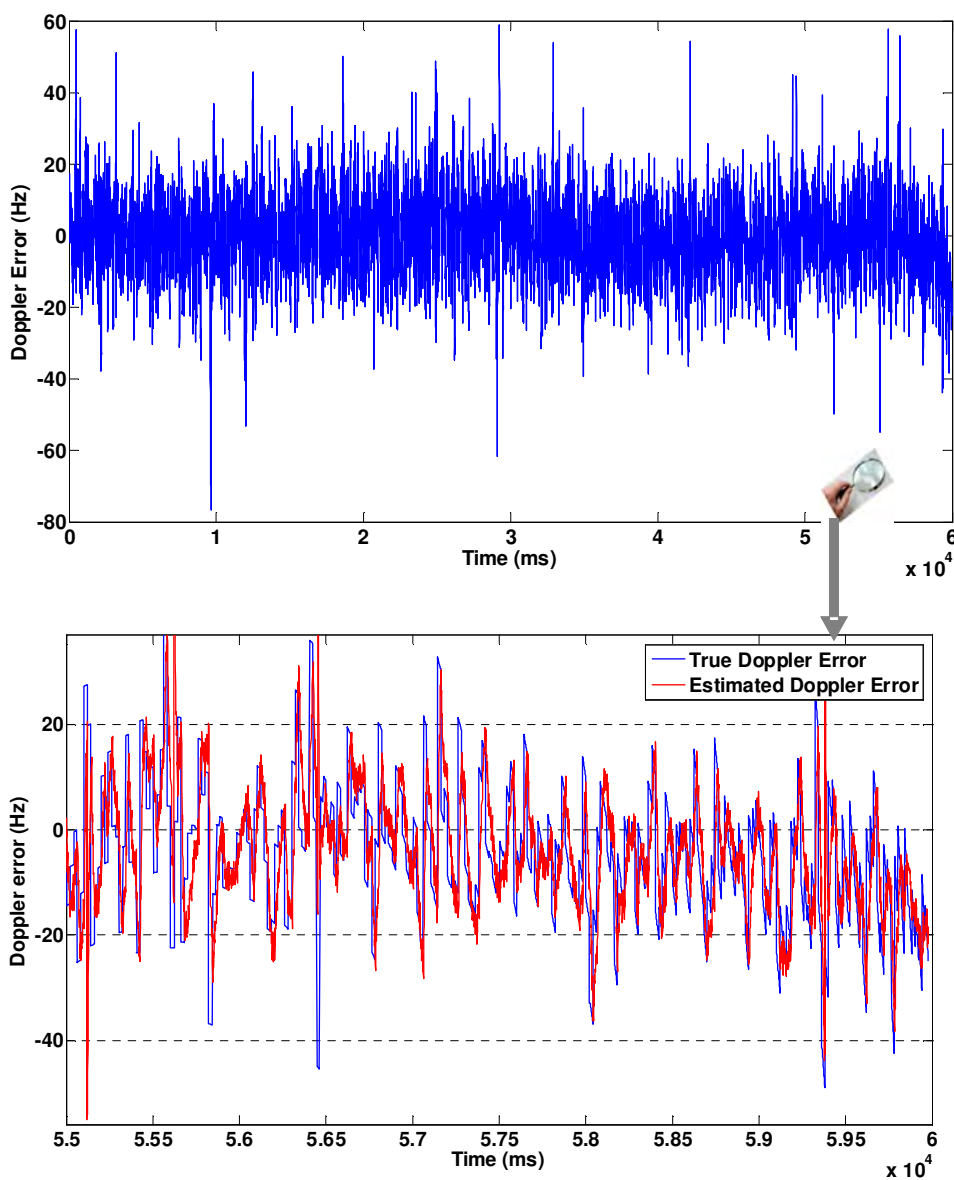
Figure 5-9 Remaining frequency errors from the first stage is detected at the

subsequent stages

Note that in the frequency estimation since the error signals are the same for a frequency

error of Δf Hz and $\Delta f + n/T$ Hz for any integer n, the estimator may make frequency

estimation errors of n/T Hz. By dividing the entire frequency range into 1/T Hz segments

with the first segment extending from *-2/T* to *2/T* Hz, cycle slips in frequency estimation can be defined. Whenever the frequency estimation error jumps from one such segment to an adjacent one, a cycle slip has occurred. The subsequent stages can also track and detect such slip as shown in Figure 5-10. In this case the signal was attenuated down to 17 dB-Hz with T equal to 20 ms and N=10. Figure 5-10(a) shows the frequency tracking performance of the first stage and as it can be inferred after about eight seconds cycle slip has occurred. Figure 5-10(b) shows the performance of the second stage while it successfully detects the slip.
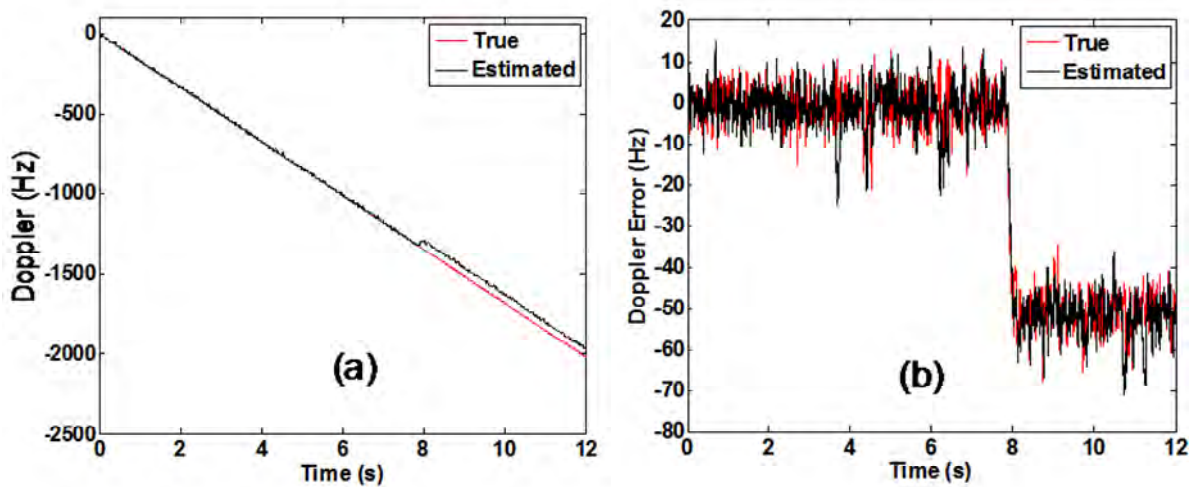
Figure 5-10 Cycle Slip detection during second stage

5.4 Indoor Tracking Results

To evaluate the performance of the above techniques in actual indoor environments several indoor data sets were collected. The main purpose of the tests was to determine

the capability of maintaining lock on GPS signals during deep fades when the signals is typically 30 to 40 dB weaker than the nominal signal strength.

The test setup is basically the same as that of Section 3.6.2, which is shown in Figure 3-32. For signal quality monitoring during the weak real data collection and also comparing the tracking parameters and achievable sensitivity, a U-blox high sensitivity receiver was used. A Novatel GPS–701 antenna mounted on a tripod was used.

To acquire the GPS signal and for bit synchronization the receiver was initialized outside. This scheme also allows for assessing the ability of maintaining lock during the most critical point which is during the transition from outside to inside. At this point the maximum fade is expected while the receiver is in motion.

Indoor data was collected in different environments starting from a relatively benign indoor environment, such as an area with wooden walls and ceilings to a harsh indoor environment with high attenuation and severe multipath. The first data set was collected in the wooden structure shown in Figure 5-11. Note that the ability to maintaining lock can be completely evaluated by the C/N_0 estimator. The utilized C/N_0 estimator is based on a narrow band power versus wide band power ratio (Van Dierendonck 1995). It also acts as a DLL lock indicator. The lock on code is only possible when the lock on carrier signal is achieved. As shown in Figure 5-12 the lock was maintained during the entire data set. However this structure cannot be considered a challenging environment since the maximum attenuation was about 10 dB and for most satellites and the C/N_0 was above 25 dB-Hz. The integration time T was chosen to be 20 ms with N=10.

Figure 5-11 Data collection environment I
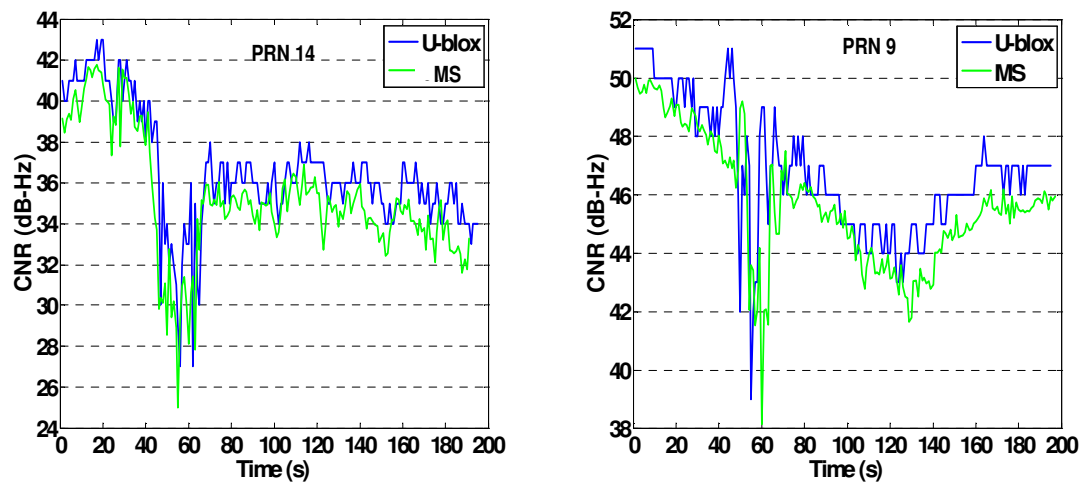
Figure 5-12 C/N$_0$ estimates from u-blox and MS (Multistage) technique

The ICT building of the University of Calgary was chosen for a more challenging environment. The data collection environment is shown in Figure 5-12.
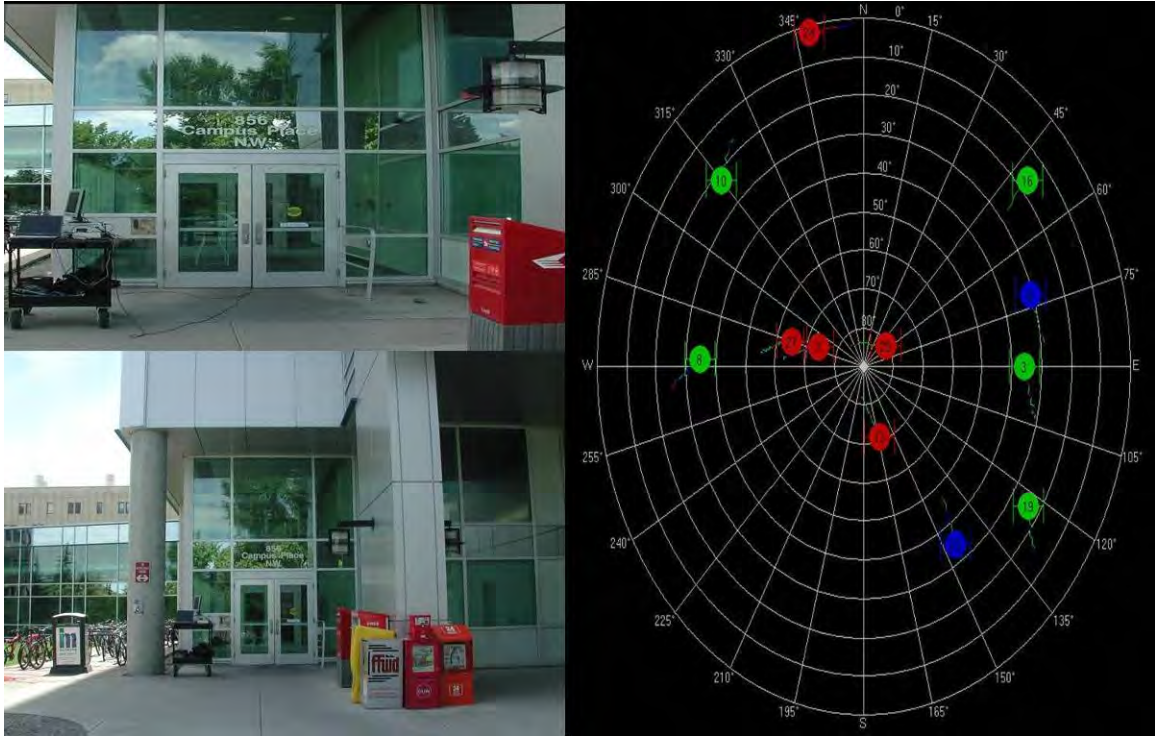
Figure 5-13 Data collection environment II

Since the C/A code Doppler variation is significantly lower than that for carrier Doppler, especially in an aided scheme, an asynchronous DLL-MS (Multi Stage) was designed in which the update rate of the DLL is different from the carrier loops. Due to the lower dynamics and aiding scheme, the integration time can be increased by utilizing the loops developed in previous chapters. However the signal fading and amplitude changes during integration interval should be considered too. An update rate of 2.5 Hz with T=20 ms (N=20) was chosen for the carrier loops whereas a coherent integration time of 140 ms was chosen for the DLL loop.

Even in this challenging environment relatively strong satellites (between 20 and 30 dB-Hz) with low fading could be observed. The strongest satellite (PRN 16) for this test is shown in Figure 5-14. This satellite had a relatively low elevation angle and the signal came directly through the door.
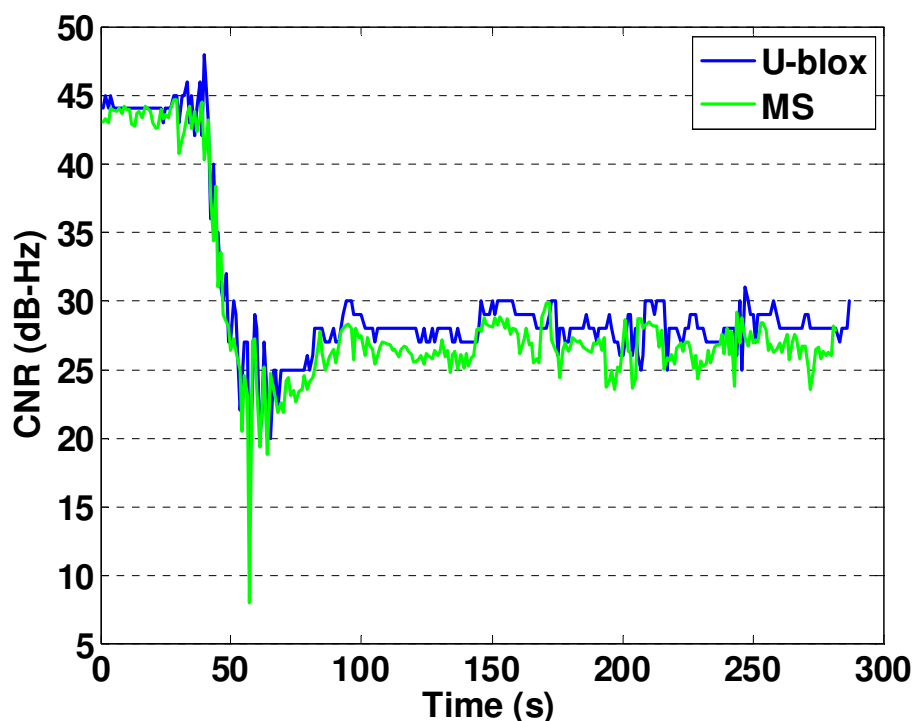
Figure 5-14 C/N$_0$ estimates for PRN 16

A higher elevation satellite (PRN 23) is shown in Figure 5-15. The signal could be as weak as 10 dB-Hz in this case. The asynchronous DLL-MS scheme was able to maintain lock even at the transition point and also when the signal power was about 10 dB-Hz. The same performance was observed among other satellites. The u-blox receiver lost lock at about 155 seconds where the signal power was below 14 dB-Hz and reacquired the signal after this deep fade. The increase in the signal power at the start of the test is due to picking up the antenna to start the motion and changes in the tilt of the antenna.
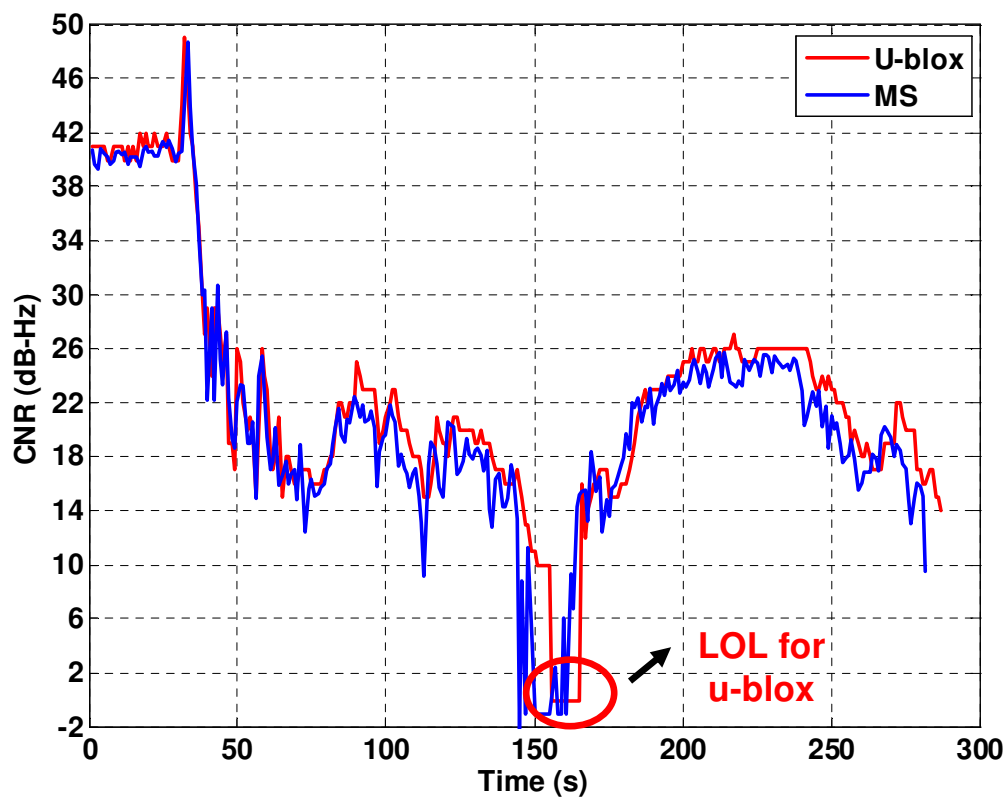
Figure 5-15 C/N$_0$ estimate for PRN 23

The Doppler estimate for PRN 23 is also compared with the one provided by the u-blox in Figure 5-16. A constant value is added to the u-blox Doppler value to compensate for the differences in IF frequencies and clock drifts.
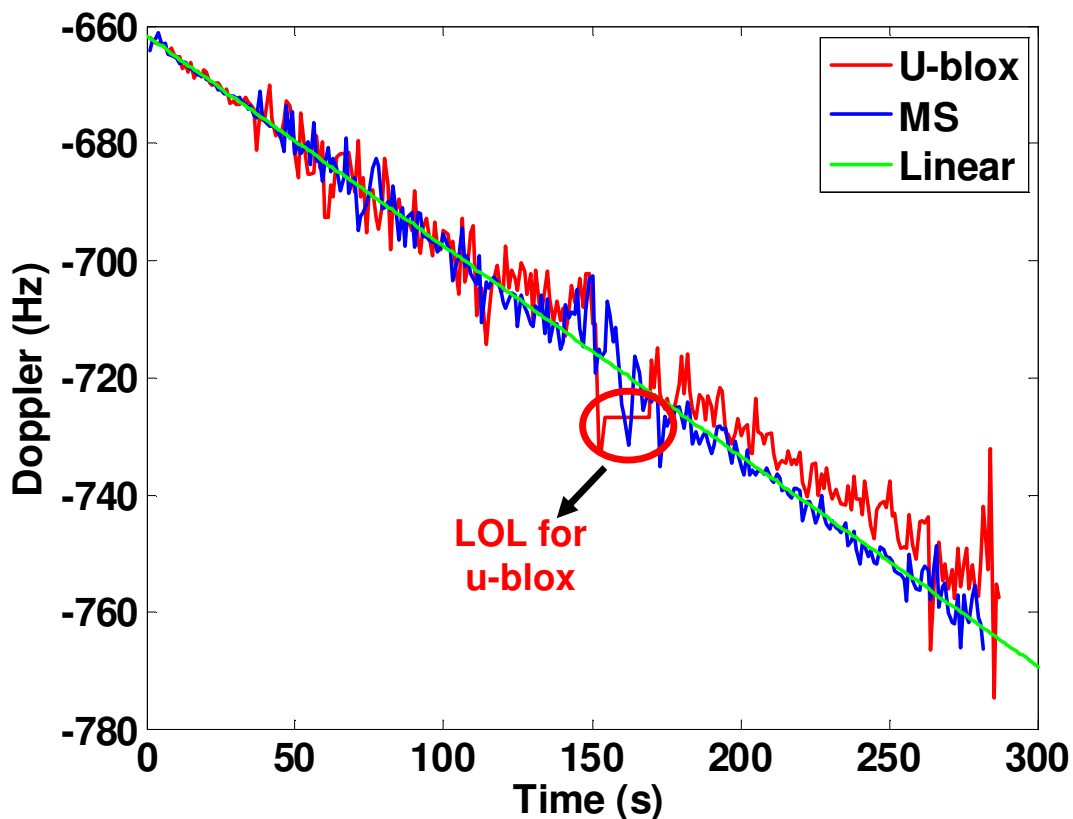
Figure 5-16 Doppler estimate comparison

5.5 Summary

In order to overcome the problem of seamless outdoor to indoor tracking, which is usually followed by deep fading and user motion, it was proposed to divide the NCO update rate into N equal coherent integrated sections. In order to do so a method based on Kumar (1990) was adopted for indoor GPS signal tracking. A successive tracking scheme was implemented to overcome the problem of tracking weak GPS signals in indoor environments. In this technique several tracking schemes can be cascaded serially.

Moreover asynchronous coupled code and carrier tracking were proposed, in which the code tracking can utilize longer integration time and be easily designed using the optimum procedure presented in this thesis. The performance and advantages of this technique are shown based on a developed GPS signal simulator and live GPS signal in selected indoor environments. It is shown that the tracking capability of this scheme in some cases is better than the HSGPS commercially available receivers.

Chapter Six: Conclusions and Recommendations

This Chapter summarizes the various aspects of the research presented in this thesis. Conclusions pertaining to GNSS signal tracking enhancements in adverse conditions are provided and the main contributions toward this goal are discussed. Finally, recommendations for possible future work that can complement the presented results are provided.

6.1 Conclusions

The main objective of this thesis was to gain a deeper understanding of the major limitations of the commonly used tracking architectures in weak signal conditions. By doing so this thesis also endeavoured to propose solutions that can potentially offer performance improvements over conventional techniques. Toward this goal, the following conclusions are drawn.

By establishing a connection between analog and digital tracking loops it was shown that simply transforming designs from the analog domain to the digital domain is not sufficient to analyze tracking loop stability. Proper loop modeling based on the average generated phase of the NCO can sufficiently model the loop for further analysis. Based on these analyses, it is impossible to achieve a B_LT value higher than about 0.6 (The exact value depends on the type of the transformation method) with traditional design methods and for third order loops that are most commonly used for GNSS applications. Moreover in order to prevent performance degradation and unwanted increase in loop

bandwidth the B_LT product should be kept near zero. This constraint severely limits the maximum achievable integration time and bandwidth. The maximum B_LT of 0.1 is recommended if the transformation method is going to be adopted.

Different NCO types were also introduced and their effects on the conventional loops were investigated. Specifically, phase and phase-rate feedback NCOs based on Thomas (1989) were introduced for GNSS applications. By introducing discontinuities in phase propagation in this type of NCO, the deficiency of transformation method can be relatively decreased for higher B_LT values.

Based on a controlled-root method proposed by Stephens & Thomas (1995), the performance degradation caused by the undesired increase in bandwidth can be circumvented. In this case the B_LT is limited to less than 0.4 for third order loops with rate-only feedback NCOs, which are widely used in the design of GNSS and other telecommunication receivers. In this technique the B_LT can be increased to larger numbers by using the phase and phase-rate feedback NCO. However, using the phase and phase-rate NCO tends to increase the phase mismatch for longer integration times. This problem is caused by discontinuities in phase propagation. Moreover, in the controlled root method, loop filter coefficients are determined from loop roots that can each be selectively placed in the S-plane on the basis of loop noise bandwidth, root-specific decay rate, or root specific damping. Different damping factors result in under-damped or critically damped transient responses, hence more emphasis is given to the transient response of the loop, rather than steady state performance. As a result the coefficients given in Stephens & Thomas (1995) are not optimum in any well defined sense.

The main contribution of this thesis was to provide a proven method allowing to synthesize stable tracking loops, without being limited by the usual restrictive condition to keep the loop bandwidth very small as compared with the predetection bandwidth. A method for designing optimum loop filters for digital tracking loops was developed which is an extension of the method presented by Gupta (1968) to fully digital loops and up to fourth order loops. The optimum filter structure for DPLLs with rate-only feedback NCOs and phase and phase rate feedback NCOs were derived. The filters are optimum in the sense that based on the linear Z-domain model of the loop, the phase noise variance is minimized. Moreover, a zero deterministic phase error constraint for a given input is imposed on the loop.

By utilizing the optimum loop structure the operational range of the conventional loop filters, in terms of B_LT values, can significantly be extended for both kinds of NCOs. As a result, one can design stable loops with higher bandwidths or longer integration times. The procedure gives rise to an interesting connection between phase and phase-rate feedback loops and phase-rate only loops by showing that a unique optimum closed loop transfer function exists. While the B_LT is practically limited to less than 0.4 for controlled-root and transformation methods for third order loops with rate-only feedback NCOs, this number can be extended to more than 10 when the optimum structure derived herein is adopted. The proposed method is particularly important in order to synthesize tracking loops that will be able to take advantages of the modernized GNSS signals, which have pilot channels that can be tracked at very low C/N_0 using long coherent integration periods.

The efficacy of the proposed method has been demonstrated both in theoretical and practical ways. For the first time the performance of a DPLL tracking architecture for very long integration times for weak GPS signals was presented. Practical considerations for the design and use of these filters were also given so as to aid designers in choosing proper configurations.

For the phase rate only feedback NCO, since the controlled-root filter does not have the extra pole at -1 it is recommended to use the controlled-root filter for B_LT values less than 0.4 to obtain less noisy Doppler estimates. For B_LT values larger than 0.4, it becomes necessary to use the optimum filter structure derived in this thesis. The extra Doppler noise introduced by the optimum filter is completely negligible for higher integration times (say higher than 100 ms). Alternatively, designers can use a phase and phase rate feedback NCO with the optimum filters derived herein to extend B_LT. In this case the controlled-root design can be used too but the design is not optimum, as discussed previously. The introduced discontinuities in this case can cause extra phase mismatch between the incoming and locally generated signal in practice, especially for high integration times. As such it is recommended to use this kind of NCO for lower integration times (say less than 100 ms).

Assisted and stand-alone schemes were considered and it was shown by using live GPS L1 signals that, in an assisted scheme, phase lock can be maintained down to 10 dB-Hz. This shows an improvement of about 5 dB in comparison with conventional techniques. Since only navigation data were used as assistance to the loop, the results are also relevant for pilot channel tracking in modernized GPS signals.

For the cases when external data aiding is not available, a simple method based on the decision feedback principle was used, in which the data bits are estimated through the tracking process itself to increase the coherent integration time. Obviously the performance of this method is limited by the BER of the BPSK modulation and is reliable down to 24 dB-Hz, where the BER is near 0.001. Note that even in open sky conditions it is common to observe satellites with power levels around 30 dB-Hz. The developed optimum loops followed by the simple navigation data estimation can be utilized instead of the existing loops in commercial receivers to extend the integration time to reduce code and phase jitter and achieve more accurate measurements. For instance instead of a common configuration of 20 ms integration time and 15 Hz bandwidth, a loop with 60 ms integration and 15 Hz bandwidth can be utilized for typical GPS open sky applications, without increasing the computation burdens and requiring external assistance.

An enhanced digital phase locked loop with a frequency rate estimator was also developed. The NCO with phase rate and frequency rate feedback was introduced and its transfer function was derived precisely. Based on this model for the NCO and the transfer function of the frequency rate estimator, the tracking loop was optimized in order to minimize the phase noise variance. By utilizing this loop, the performance of the low update rate loops in terms of phase mismatch and BER can be improved. For the extreme case of a 1 Hz update rate, 20 percent reduction in phase mismatch can be observed for static cases.

In order to overcome the problem of seamless outdoor to indoor tracking, which is usually followed by deep fading and user motion, it was proposed to divide the NCO update rate into N equal coherent integrated sections. In order to do so a method based on

Kumar (1990) was adopted for indoor GPS signal tracking. A successive tracking scheme was implemented to overcome the problem of tracking weak GPS signals in indoor environments. In this technique several tracking schemes can be cascaded serially. The subsequent tracking stages track the remaining error signals from the first stage with possibilities to detect and correct errors and cycle slips from preceding stages. Since the overall C/N_0 threshold on carrier frequency estimation is lower than the carrier phase estimation, the first stage is chosen to be a frequency estimator. Moreover asynchronous coupled code and carrier tracking is proposed, in which the code tracking can utilize longer integration times and be easily designed through the optimum procedure presented in this thesis. The performance and advantages of this technique were shown based on a developed GPS signal simulator and live GPS signal in selected indoor environments. It was shown that the tracking capability of this scheme in some cases was better than the HSGPS commercially available receivers.

6.2 Recommendations

Considering the theoretical and experimental results presented herein, the following recommendations are made to extend the scope of this research and identify the limitations of the proposed methods.

1- The NCO in Chapter 4 can be enhanced for medium range (say less than 100 ms) integration intervals with phase, phase rate and frequency rate feedback. Since the presence of the pole at -1 in the optimum filter structure relatively increases the

noise in the Doppler estimation for loops with low integration intervals, phase discontinuities can be introduced to improve the performance for low integration and high bandwidth loops.

2- Although the main focus of the thesis was on long integration times, the optimum loops can be used for very high bandwidths where conventional loops cannot operate. The benefits of utilizing such scheme for extreme dynamics can be further analyzed.

3- It was found that ionospheric scintillation could cause loss of tracking lock in GPS receivers, potentially endangering critical GPS applications (Humphreys et al 2005). Also there is interest in gaining a better understanding of the effects scintillation has on GPS signal amplitudes and phases. For instance the huge coverage of GPS receivers planned in the POLENET project could represent an unprecedented opportunity to investigate the ionosphere over Antarctica. Either the power fading or the phase variations during ionosphere scintillation may lead to loss of signal lock or increases in measurement errors. Both the power fading and phase variations are similar to effects that can be seen in indoor tracking during motion. As a result the asynchronous DLL-MS scheme could be a possible remedy for tracking GPS signal phase during ionosphere scintillation.

4- In static cases the optimum loops configured in high integration times could be utilized in the indoors to investigate the effect of long integration times on

multipath errors. The amplitude variations during integration intervals can be circumvented by normalizing the signal amplitude in shorter intervals and accumulating these normalized shorter intervals to achieve a desired integration time.

5- As the developed tracking schemes show good potential and performance in tracking live indoor GPS signals, they could be used for characterization of the indoor propagation channel in terms of signal attenuation and its statistical properties. These schemes should be followed by an enhanced C/N_0 estimator in weak signal conditions in order to be used for channel modeling.

6- Design of a novel parallel carrier tracking for weak signal conditions: Two separate loops could be utilized for carrier tracking in which one of them is a frequency estimator, operating with coherent integration time of T and update interval of NT, and the other loop is an optimum DPLL operating with coherent integration time of NT. The frequency estimator would aid the DPLL in a tightly-coupled fashion, and lower bandwidth and higher integration time could be utilized in DPLL to extract the phase information. The drawback of this method is the requirement of two separated NCOs (instead of one in conventional schemes) for carrier tracking. However in modernized GNSS signals because of the presence of data and pilot channels, these two NCOs are already available and each of these loops could operate in one of the channels.

7- New successive tracking scheme utilizing H_∞ filter: Since in successive schemes the subsequent stages should track the error signal, there is large uncertainty in noise variances and system model in later stages, as these parameters depends on a performance of the preceding stage. The use of a H_∞ filter or combined KF- H_∞ is proposed, since $H\infty$ filtering provides a rigorous method for dealing with systems that have model uncertainty. H_∞, filter theory shows the optimal way to make the Kalman filter robust. In H_∞ filtering worst-case estimation performance is a primary consideration rather than RMS estimation performance (Simon 2006).

8- The proposed algorithms were analysed in terms of tracking performance. A detailed performance analysis in the position domain would be valuable.

References

Aghamohammadi A., H. Meyr and G. Ascheid, *Adaptive Synchronization and Channel Parameter Estimation Using an Extended Kalman Filter*, IEEE Transactions on Communications, vol. 37, no. 11, pp. 1212–1219, November, 1989.

Anderson B.D.O. and J.B. Moore, *Optimal Filtering*, Englewood Cliffs, NJ: Prentice-Hall, Inc., 1979.

Best R. E. (1999) *Phase-Locked Loops, Designs Simulation, and Applications,* McGraw-Hill, fourth edition.

Chansarkar, M. M. and L. Garin (2000). *Acquisition of GPS signals at very low signal to noise ratio*, Proceedings of NTM 2000 (Session E1, Anaheim, CA, 26 – 28 January),The Institute of Navigation, Fairfax, VA, pages 731–737.

Charkhandeh, S. (2007) *X86-Based Real Time L1 GPS Software Receiver*, MSc Thesis, Published as Report No. 20253, Department of Geomatics Engineering, The University of Calgary.

Chiou T. , D. Gebre-Egziabher,T. Walter, P. Enge (2007) *Model Analysis on the Performance for an Inertial Aided FLL-Assisted-PLL Carrier Tracking Loop in the Presence of Ionospheric Scintillation*, Proceedings of the 2007 National Technical Meeting of the Institute of Navigation ,January 22 – 24, San Diego, California

Gao, G. (2007) INS-*Assisted High Sensitivity GPS Receivers for Degraded Signal Navigation* PhD Thesis, published as Report No. 20252, Department of Geomatics Engineering, The University of Calgary.

Gardner, F.M. (2005) *Phase Lock Techniques***,** Third Edition, John Wiley & Sons, Inc, USA.

Gebre-Egziabher, D., A. Razavi, P. Enge, J. Gautier, S. Pullen, B.S. Pervan and D. Akos (2005) *Sensitivity and Performance Analysis of Doppler-Aided GPS Carrier-Tracking Loops*, NAVIGATION, 52(2), 49-60.

Gupta, S. C. (1968) *On Optimum Digital Phase-Locked Loop,* IEEE Transactions on Communication Technology, Vol. 16, No. 2, pp. 340-344, April 1968.

Humphreys, E. D., M. L. Psiaki, and P. K. Kinter, Jr., (2005) *GPS Carrier Tracking Loop Performance in the Presence of Ionospheric Scintillation*, in *Proceedings of ION GPS/GNSS*, 13-16 Sept., Long beach CA, pp. 156-166, Institute of Navigation.

Julien, O. (2005) *Design of Galileo L1F Receiver Tracking Loops*, PhD Thesis, published as Report No. 20227, Department of Geomatics Engineering, The University of Calgary.

Jury, E. I. (1964) *Theory and Application of the z-Transform Method*, New York: John Wiley & Sons, 1964.

Kaplan, E. D. and C. J. Hegarty (2006), *Understanding GPS Principles and Applications*, Artech House, Boston, London, 2nd edition.

Kazemi, P.L. (2008), Optimum *Digital Filters for GNSS Tracking Loops*, Proceedings of the ION GNSS 2008, September 16-19, 2008, Savannah, Georgia.

Kazemi, P.L., C. O'Driscoll (2008), *Comparison of Assisted and Stand-Alone Methods for Increasing Coherent Integration Time for Weak GPS Signal Tracking*, Proceedings of the ION GNSS 2008, September 16-19, 2008, Savannah, Georgia.

Kazemi, P.L., C. O'Driscoll, G. Lachapelle (2009), *Optimum Filters for Tracking Loops with Rate-Only Feedback NCO or Phase and Rate Feedback NCO,* submitted for IEEE Transactions on Aerospace and Electronic Systems on January 2009.

Kazemi, P.L., C. O'Driscoll, G. Lachapelle (2009), *Digital Phase Locked Loop with Frequency Rate Feedback*, Proceedings of the ION GNSS 2009, September 2009.

Kumar, R. (1988) *Efficient Detection and Signal Parameter Estimation with Applications to High Dynamic GPS Receivers*, JPL Publication 88-42, National Aeronautics and Space Administration, Jet Propulsion Laboratory, California Institute of Technology, Pasadena, CA, December 1988.

Kumar, R. (1990), *A novel multi-stage estimation of signal parameters,* International Conference on Acoustics, Speech, and Signal Processing, ICASSP-90 ,3-6 Apr 1990 Page(s):2491 - 2494 vol. 5.

Legrand, F. (2002) *Spread Spectrum Signal Tracking Loop Models and Raw Measurements Accuracy Improvement Method*, PhD Thesis, Institut National Polytechnique deToulouse (INPT), France,2002.

Lian, P. (2004) *Improving Tracking Performance of PLL in High Dynamic Applications*, MSc Thesis, published as Report No. 20208, Department of Geomatics Engineering, The University of Calgary.

Lindsey, W. C. and C. M. Chie (1981) *A Survey of Digital Phase-Locked Loops*, in *Proceedings of the IEEE,* Vol. 69, No. 4, pp 410-431, April.

Ma, C., G. Lachapelle, and M.E. Cannon (2004) *Implementation of a Software GPS Receiver*, Proceedings of GNSS 2004 (Session A3, Long Beach, CA, 21-24 September), The Institute of Navigation, Fairfax, VA.

MacGougan G. , *High Sensitivity GPS Performance Analysis in Degraded Signal Environments*, (M.Sc. thesis), June 2003, UCGE Report No. 20176.

Misra, P. and P. Enge (2001) *Global Positioning System Signals, Measurement, and Performance*, Lincoln, MA, Ganga-Jamuna Press.

Mitelman A., Normark P., Martin R. (2006) http://www.fmv.se/upload/Bilder%20och%20dokument/Publikationer/rapporter/13%2020060929_FINAL.pdf, last accessed March 2010.

Ogata K., *Modern Control Engineering*, Englewood Cliffs, NJ: Prentice-Hall, Inc., 2001, Fourth Edition.

Oppenheim A. V. , Schafer R. W. and Buck J. R. (1999), *Discrete-Time Signal Processing*, Prentice Hall Signal Processing Series, Second Edition.

Papoulis, *Probability*, *Random Variables*, *and Stochastic Processes*, New York: McGraw–Hill, Inc., 1965.

Petovello, M, C. O'Driscoll and G. Lachapelle (2008a) *Weak Signal Carrier Tracking of Weak Using Using Coherent Integration with an Ultra-Tight GNSS/IMU Receiver*, Proceedings of European Navigation Conference (Toulouse, 23-25 April), 11 pages.

Petovello, M., C. O'Driscoll and G. Lachapelle (2008b) *Carrier Phase Tracking of Weak Signals Using Different Receiver Architectures*, Proceedings of ION NTM08 (San Diego, 28-30 Jan, Session A4). The Institute of Navigation,11 pages.

Polk D.R. and S.C. Gupta, *Quasi-Optimum Digital Phase-Locked Loops*, IEEE Transactions on Communications, vol. COM-21, no. 1, pp. 75–82, January, 1973.

Progri I., Kelly C., Gao G., Michalson W., Wang J., Lavrakas J. (2007) *Discrete Vs. Continuous Carrier Tracking Loop Theory,Implementation,and Testing with Large BT* (2007) ,in proceedings of ION GNSS,25-28 Sep., Fort Worth, TX.

Proakis J.G. (1989), *Digital Communications*, 2nd Ed., New York, McGraw–Hill, Inc., 1989.

Psiaki, M. L. (2001) *Smoother-Based GPS Signal Tracking in a Software Receiver*, in *Proceedings of ION GPS/GNSS.*, 11-14 September, Salt Lake City, UT, pp 2900-2913

Psiaki, M. L. and H. Jung (2002) *Extended Kalman Filter Methods for Tracking Weak GPS Signals*, in the *Proceedings of ION GPS/GNSS*, 24-27 September, Portland OR, pp. 2539-2553, the Institute of Navigation.

Simon D. and H. El–Sherief (1994), *Hybrid H2/H∞ Estimator for Phase–Locked Loop Filter Design*, Proceedings of the American Control Conference (ACC '94), vol. 3, pp. 2212–2216, Baltimore, MD, USA, 29 June–1 July, 1994.

Simon D. (2006) *Optimal State Estimation: Kalman, H Infinity, and Nonlinear Approaches*, Wiley-Interscience (June 23, 2006)

Shanmugam, S. (2008) *New Enhanced Sensitivity Detection Techniques for GPS L1 C/A and Modernized Signal Acquisition*, PhD Thesis, published as Report No. 20264, Department of Geomatics Engineering, The University of Calgary.

Singh, S. (2006) *Comparison of Assisted GPS and High Sensitivity GPS in Weak Signal Conditions*, MSc Thesis, published as Report No. 20247, Department of Geomatics Engineering, The University of Calgary.

Skone, S., G. Lachapelle, D. Yao, W. Yu, and R. Watson (2005) *Investigating the Impact of Ionospheric Scintillation using a Software Receiver*, in *Proceedings of ION GPS/GNSS*, 13-16 Sept, Long Beach CA, pp 1126-1137.

Soloviev, A., F. van Grass and S. Gunawardena (2004) *Implementation of Deeply Integrated GPS/Low-Cost IMU for Reacquisition and Tracking of Low CNR GPS Signals*, ION National Technical Meeting, San Diego, CA, Institute of Navigation, 923-935.

Spilker, J.J. (1997) *Fundamentals of Signal Tracking Theory* in *Global Positioning System: Theory and Applications Volume I*, Progress in Astronautics and Aeronautics Volume 164.

Stephens D. R. (2002) *Phase-Locked Loops for Wireless Communications: Digital, Analog and Optical Implementations*, Kulwer Academic Publishers; 2nd edition, 2002.

Stephens, S.A. and J.B. Thomas (1995*) Controlled-Root Formulation for Digital Phase-Locked Loops* in IEEE Transactions on Aerospace and Electronic Systems, Vol.31, No. 1 pp 78-95.

Thomas, J. B. (1989) *An Analysis of digital phase-locked Loops,* Publication 89-2, Jet Propulsion Laboratory, Pasadena, CA, Feb. 1989.

Tsui, James B-Y. (2000) *Fundamentals of Global Positioning System Receivers: A Software Approach*, John Wiley & Sons Inc.

Van Dierendonck, A.J. (1997) *GPS Receivers* in *Global Positioning System: Theory and Application Volume I*, Progress in Astronautics and Aeronautics Volume 164.

U-blox (2010) http://www.u-blox.com/en/u-blox-6.html, last accessed March 2010.

Ward, P.W., J.W. Betz and C.J. Hegarty (2006) *Satellite Signal Acquisition, Tracking, and Data Demodulation*, Understanding GPS Principles and Applications, E. D. Kaplan and C. J. Hegarty, Norwood, MA, Artech House, Inc., 153-241.

Watson, R., (2005) *High-Sensitivity GPS L1 Signal Analysis for Indoor Channel Modelling*, MSc Thesis, published as Report No. 20215, Department of Geomatics Engineering, The University of Calgary.

Watson, R., M.G. Petovello, G. Lachapelle and R. Klukas (2007) *Impact of Oscillator Errors on IMU-Aided GPS Tracking Loop Performance*, European Navigation Conference, Geneva, Swizterland.

Wei, Y. (2007) *Selected GPS Receiver Enhancements for Weak Signal Acquisition and Tracking*, MSc Thesis, published as Report No. 20249, Department of Geomatics Engineering, The University of Calgary.

Ziedan, N.I. and J.L. Garrison (2004) *Extended Kalman Filter-Based Tracking of Weak GPS Signals under High Dynamic Conditions*, ION GNSS 2004, Long Beach, CA, Institute of Navigation, 20-31.